Development of electrochemical antibody-based and enzymatic assays for mycotoxin analysis in food

Dissertation

zur Erlangung des akademischen Grades

„doctor rerum naturalium“

(Dr. rer. nat.)

in der Wissenschaftsdisziplin „Bioanalytik“

eingereicht an der

Mathematisch-Naturwissenschaftlichen Fakultät

Institut für Biochemie und Biologie

der Universität Potsdam

und

der Bundesanstalt für Materialforschung und -prüfung (BAM)

von

Soraya Lisanne Riedel (geb. Höfs)

Potsdam, 13. Juni 2023

Soweit nicht anders gekennzeichnet, ist dieses Werk unter einem Creative-Commons-Lizenzvertrag Namensnennung 4.0 lizenziert.
Dies gilt nicht für Zitate und Werke, die aufgrund einer anderen Erlaubnis genutzt werden. Um die Bedingungen der Lizenz einzusehen, folgen Sie bitte dem Hyperlink:
https://creativecommons.org/licenses/by/4.0/legalcode.de

Ort und Tag der Disputation:	Potsdam, 08.09.2023
Hauptbetreuer:	Prof. Dr. Frank F. Bier
Betreuer:	PD Dr. Rudolf J. Schneider
Gutachter*innen:	Prof. Dr. Frank F. Bier PD Dr. Rudolf J. Schneider Prof. Dr. Ulla Wollenberger

Online veröffentlicht auf dem
Publikationsserver der Universität Potsdam:
https://doi.org/10.25932/publishup-60747
https://nbn-resolving.org/urn:nbn:de:kobv:517-opus4-607477

Table of Contents

Danksagung

An dieser Stelle möchte ich mich bei allen Personen bedanken, welche mich während meiner Doktorarbeit unterstützt und motiviert haben.

Als Erstes möchte ich Dr. Rudolf Schneider meinen besonderen Dank aussprechen. Ich möchte mich nicht nur für die hilfreichen Anregungen und Ratschläge zur Anfertigung dieser Arbeit bedanken, sondern vor allem für die stete Unterstützung und Förderung während meiner Zeit in seinem Fachbereich.

Herrn Prof. Dr. Frank Bier danke ich für das Interesse an meiner Arbeit, sowie für die Unterstützung zur Anfertigung dieser Arbeit und der Vorbereitung auf die Disputation.

Frau Prof. Dr. Ulla Wollenberger möchte ich ebenso für das Interesse an meiner Arbeit, sowie der Begutachtung danken.

Des Weiteren gilt mein Dank dem gesamten Fachbereich 1.8 Umweltanalytik der BAM, sowie meinen Kolleg*Innen aus dem MamaLoCA-Projekt und allen, die mir während der Doktorarbeit zur Seite gestanden haben.

Ein besonderer Dank gilt Alexander Ecke, der mich nicht nur hervorragend an meinem neuen Arbeitsplatz eingearbeitet, sondern auch jederzeit mit wissenschaftlichen und persönlichen Ratschlägen zur Seite stand.

Außerdem möchte ich Rabia Bayram, Valerie Jaut, Ange Tekazam und Chantal Vergin danken, die mich während ihrer Abschlussarbeiten und Praktika unterstützt haben.

Ebenso möchte ich Dr. Zoltán Konthur für die Zusammenarbeit mit zahlreichen interessanten Debatten und Ideen danken, wodurch ich viel Neues lernen konnte.

Besonders möchte ich mich bei Sarah Döring für den wissenschaftlichen und persönlichen Austausch bedanken, der mir sehr geholfen hat, Herausforderungen während meiner Doktorarbeit zu überwinden.

Ohne die Unterstützung von Sabine Flemig, Kristin Hoffmann, Nadine Scheel und Shireen Ewald wären mir die Arbeiten im Labor, welche zu den Ergebnissen in dieser Arbeit geführt haben, in dieser Form nicht möglich gewesen. Dafür möchte ich an dieser Stelle Danke sagen.

Ich bedanke mich ebenso bei Sigrid Benemann, Dr. Deniz Hülagü, Dr. Francesca Bennet und Dr. Thomas Schmid für die spannende Zusammenarbeit und Unterstützung.

Auch Dr. Vasile-Dan Hodoroaba möchte ich sowohl für den wissenschaftlichen Austausch als auch für die motivierenden Worte danken.

Mein Dank gilt auch Jörg Schenk von der Firma Hybrotec GmbH für zuverlässige Zusammenarbeit und die Bereitstellung von Antikörpern.

Ich bedanke mich nachdrücklich bei Dr. Peter Carl von der SAFIA Technologies GmbH für die hilfreichen Anregungen zur Anfertigung dieser Arbeit, sowie der wissenschaftlichen Zusammenarbeit und Unterstützung.

Ebenfalls danke ich Dr. Jérémy Bell für die wissenschaftliche Unterstützung und die zahlreichen Ratschläge, welche mir bei der Anfertigung dieser Arbeit geholfen haben.

Danken möchte ich auch Robert Tannenberg. Vor allem für die persönlichen Ratschläge und den wissenschaftlichen Austausch, aber auch für die Anfertigung der Fotos der Fließzelle, welche in dieser Arbeit verwendet wurden.

Gerne möchte ich mich auch bei der BAM für die Bereitstellung der Infrastruktur sowie die finanzielle Unterstützung bedanken.

Mein ganz besonderer Dank gilt meiner ganzen Familie. Besonders danken möchte ich meinen Eltern Sabine und Marcus Höfs, für die Unterstützung während meines gesamten Studiums. Meinem Verlobten, Dr. Marc Riedel, möchte ich für die vielen lieben Worte, den Zuspruch, sowie die alltägliche Unterstützung, aber auch für das Korrekturlesen dieser Arbeit danken.

Abstract

Electrochemical methods are promising to meet the demand for easy-to-use devices monitoring key parameters in the food industry. Many companies run own lab procedures for mycotoxin analysis, but it is a major goal to simplify the analysis. The enzyme-linked immunosorbent assay using horseradish peroxidase as enzymatic label, together with 3,3',5,5'-tetramethylbenzidine (TMB)/H_2O_2 as substrates allows sensitive mycotoxin detection with optical detection methods. For the miniaturization of the detection step, an electrochemical system for mycotoxin analysis was developed. To this end, the electrochemical detection of TMB was studied by cyclic voltammetry on different screen-printed electrodes (carbon and gold) and at different pH values (pH 1 and pH 4). A stable electrode reaction, which is the basis for the further construction of the electrochemical detection system, could be achieved at pH 1 on gold electrodes. An amperometric detection method for oxidized TMB, using a custom-made flow cell for screen-printed electrodes, was established and applied for a competitive magnetic bead-based immunoassay for the mycotoxin ochratoxin A. A limit of detection of 150 pM (60 ng L^{-1}) could be obtained and the results were verified with optical detection. The applicability of the magnetic bead-based immunoassay was tested in spiked beer using a handheld potentiostat connected via Bluetooth to a smartphone for amperometric detection allowing to quantify ochratoxin A down to 1.2 nM (0.5 µg L^{-1}).

Based on the developed electrochemical detection system for TMB, the applicability of the approach was demonstrated with a magnetic bead-based immunoassay for the ergot alkaloid, ergometrine. Under optimized assay conditions a limit of detection of 3 nM (1 µg L^{-1}) was achieved and in spiked rye flour samples ergometrine levels in a range from 25 to 250 µg kg^{-1} could be quantified. All results were verified with optical detection. The developed electrochemical detection method for TMB gives great promise for the detection of TMB in many other HRP-based assays.

A new sensing approach, based on an enzymatic electrochemical detection system for the mycotoxin fumonisin B_1 was established using an *Aspergillus niger* fumonisin amine oxidase (AnFAO). AnFAO was produced recombinantly in *E. coli* as maltose-binding protein fusion protein and catalyzes the oxidative deamination of fumonisins, producing hydrogen peroxide. It was found that AnFAO has a high storage and temperature stability. The enzyme was coupled

covalently to magnetic particles, and the enzymatically produced H_2O_2 in the reaction with fumonisin B_1 was detected amperometrically in a flow injection system using Prussian blue/carbon electrodes and the custom-made wall-jet flow cell. Fumonisin B_1 could be quantified down to 1.5 µM (≈ 1 mg L^{-1}). The developed system represents a new approach to detect mycotoxins using enzymes and electrochemical methods.

Kurzzusammenfassung

Zur Entwicklung von einfach zu bedienenden Vor-Ort-Geräten, welche für die Analytik von wichtigen Parametern in der Lebensmittelindustrie eingesetzt werden können, sind elektrochemische Methoden besonders vielversprechend. Viele Unternehmen führen bereits Mykotoxinanalytik in eigenen Laboren am Produktionsstandort durch, dennoch gibt es große Bestrebungen Analysenmethoden weiter zu vereinfachen. Der Enzyme-linked Immunosorbent Assay (ELISA), welcher häufig mit der Meerrettichperoxidase als enzymatischem Label und 3,3',5,5'-Tetramethylbenzidine (TMB)/H_2O_2 als Enzymsubstraten arbeitet, ermöglicht den sensitiven Mykotoxinnachweis mithilfe optischer Detektionsmethoden. Zur Miniaturisierung des Detektionsschrittes wurde in dieser Arbeit der Aufbau von elektrochemischen Detektionssystemen für die Mykotoxinanalytik untersucht. Dazu wurde zunächst die elektrochemische Reaktion von TMB an verschiedenen Materialien siebgedruckter Elektroden (Kohlenstoff und Gold) sowie bei verschiedenen pH-Werten (pH 1 und pH 4) untersucht. Eine stabile Elektrodenreaktion, welche die Grundlage für den weiteren Aufbau des elektrochemischen Detektionssystems darstellt, konnte bei pH 1 an Goldelektroden erzielt werden. Basierend darauf wurde eine amperometrische Detektionsmethode für oxidiertes TMB entwickelt, wofür eine maßgefertigte Durchflusszelle verwendet wurde. Die amperometrische TMB-Detektion wurde für einen kompetitiven Magnetpartikel-basierten Immunoassay für Ochratoxin A eingesetzt. Mit diesem Assay wurde eine Nachweisgrenze von 150 pM (60 ng L^{-1}) erreicht und die Ergebnisse konnten durch optische Detektion verifiziert werden. Die Anwendbarkeit des Assays konnte in Ochratoxin A dotiertem Bier demonstriert werden, wobei für die Detektion ein tragbarer Potentiostat verwendet wurde, welcher über Bluetooth mit einem Smartphone verbunden war. Hiermit konnten niedrige Ochratoxin A Konzentration von bis zu 1.2 nM (0.5 µg L^{-1}) bestimmt werden.

Aufbauend auf dem entwickelten elektrochemischen Detektionssystem für TMB wurde die Anwendbarkeit des Ansatzes auf einen Magnetpartikel-basierten Immunoassay für das Ergotalkaloid Ergometrine, evaluiert. Unter optimierten Bedingungen konnte mit dem Assay eine Nachweisgrenze von 3 nM (1 µg L^{-1}) erreicht werden. In mit Ergometrin versetztem Roggenmehl konnten Konzentrationen von 25 bis 250 µg kg^{-1} nachgewiesen werden. Die entwickelte elektrochemische Nachweismethode für TMB bietet einen vielversprechenden Ansatz für den Einsatz in vielen anderen Meerrettichperoxidase-basierten Assays.

Für das Mykotoxin Fumonisin B_1, wurde ein neues sensorisches System entwickelt, welches auf einem enzymatischen elektrochemischen Nachweis basiert. Hierfür wurde eine *Aspergillus niger* Fumonisin Aminoxidase (AnFAO) rekombinant als Fusionsprotein mit dem Maltose-bindenden Protein exprimiert. AnFAO katalysiert die oxidative Deaminierung von Fumonisinen, wobei H_2O_2 gebildet wird. Es konnte gezeigt werden, dass AnFAO eine hohe Lagerungs- und Temperaturstabilität hat. Für den Nachweis von Fumonisin B_1 wurde das Enzym kovalent an Magnetpartikel gekoppelt. Das enzymatisch produzierte H_2O_2 konnte anschließend amperometrisch mithilfe von Preußisch Blau/Kohlenstoff-Elektroden in der maßgefertigten Durchflusszelle detektiert werden. Fumonisin B_1 konnte bis zu einer Konzentration von 1,5 µM ($\approx$ 1 mg L^{-1}) quantifiziert werden. Das entwickelte System stellt einen neuen Ansatz dar, um Mykotoxine unter Nutzung von Enzymen und elektrochemischen Methoden zu detektieren.

Vorwort

Teilergebnisse der vorliegenden Arbeit wurden in folgenden Artikeln vorab publiziert:

Höfs, S.; Hülagü, D.; Bennet, F.; Carl, P.; Flemig, S.; Schmid, T.; Schenk, J. A.; Hodoroaba, V. D.; Schneider, R. J., Electrochemical immunomagnetic ochratoxin A sensing: Steps forward in the application of 3,3',5,5'-tetramethylbenzidine in amperometric assays. *ChemElectroChem* **2021,** *8* (13), 2597-2606.

Höfs, S.; Jaut, V.; Schneider, R. J., Ergometrine sensing in rye flour by a magnetic bead-based immunoassay followed by flow injection analysis with amperometric detection. *Talanta* **2023,** *254*, 124172.

List of Abbreviations

Ab	antibody
Ab – Ag	immunocomplex of antibody and antigen
ABTS	2,2'-azino-bis(3-ethylbenzthiazoline-6-sulfonic acid)
Ag	antigen
AnFAO	*Aspergillus niger* fumonisin amine oxidase
APS	Ammonium persulfate
CAD	computer-aided design
CV	cyclic voltammetry
DCC	N,N-dicyclohexylcarbodiimide
DHAP	2',4'-dihydroxyacetophenone
DMA	N,N-dimethylacetamide
DMF	N,N-dimethylformamide
dNTP	deoxynucleotide
DSC	N,N-disuccinimidyl carbonate
GC	gas chromatography
GOx	glucose oxidase
EDS	energy dispersive X-ray spectroscopy
EIS	electrochemical impedance spectroscopy
ELISA	enzyme-linked immunosorbent assay
FAD	flavine adenine dinucleotide
FAD-GDH	flavine adenine dinucleotide dependent glucose dehydrogenase
FAO	Food and Agriculture Organization of the United Nations

FB_1	fumonisin B_1
FB_2	fumonisin B_2
FB_3	fumonisin B_3
HGPRT	hypoxanthine-guanine phosphoribosyl transferase
His-tag	polyhistidine tag
HRP	horseradish peroxidase
HRP C	horseradish peroxidase, isoenzyme C
IAC	immunoaffinity column
IgA	immunoglobulin A
IgG	immunoglobulin G
IgM	immunoglobulin M
IgD	immunoglobulin D
IgE	immunoglobulin E
IMAC	immobilized metal affinity chromatography
IPTG	isopropyl β-D-1-thiogalactopyranoside
K_A	association constant
K_D	dissociation constant
KLH	keyhole limpet hemocyanin
LB	lysogeny broth
LC	liquid chromatography
LOD	limit of detection
MALDI-ToF-MS	matrix-assisted laser desorption/ionization time-of-flight mass spectrometry

MBP	maltose-binding protein
MES	2-(N-morpholino)ethanesulfonic acid
NHS	N-hydroxysuccinimide
Ni-NTA	nickel-nitrilotriacetic acid
OD	optical density
OPD	o-phenylenediamine
OTA	ochratoxin A
OTB	ochratoxin B
OTC	ochratoxin C
OTα	ochratoxin α
OTβ	ochratoxin β
OVA	ovalbumin
PBS	phosphate-buffered saline
PBST	phosphate-buffered saline with 0.05% Tween®
RIA	radio immunoassay
RT	room temperature
SEM	scanning electron microscopy
SDS	sodium dodecyl sulfate
SDS-PAGE	sodium dodecyl sulfate-polyacrylamide gel electrophoresis
SOC medium	super optimal broth with catabolic repressor
TAE	TRIS-acetate-EDTA
TBABH	tetrabutylammonium borohydride
TB	terrific broth

TEMED	N,N,N',N'-tetramethylethylendiamin
TMB	3,3',5,5'-tetramethylbenzidine
ToF-SIMS	Time-of-Flight–Secondary Ion Mass Spectrometry
TRIS	tris(hydroxymethyl) aminomethane

1 Introduction

Since time immemorial humans and animals are exposed to harmful contaminants in food and feed. Mycotoxins are a group of severely harmful food contaminants, which are formed as toxic secondary metabolites of mold fungi. Countless deaths have been caused by epidemic-like outbreaks of mycotoxicosis throughout human history, of which still well over a hundred cases of fatal poisoning have occurred in the last few decades[1, 2]. Beyond acute fatal poisoning, the dietary intake of mycotoxins can also cause long-term health effects such as cancer[3], encephalopathies[4] or fetal malformation[4].

Even though modern farming methods can prevent the mycotoxin contamination of foodstuff such as grain products to a certain extent, highly contaminated crops still occur and need to be excluded from the food production for human consumption. The Food and Agriculture Organization of the United Nations (FAO) estimates that 25% of the world crops are contaminated with mycotoxins, while only considering the occurrence above detectable limits[5]. Since the contamination is inevitable and mycotoxins usually cannot be destroyed by heat or food processing[6, 7], regulation on maximum levels of mycotoxins in foodstuffs is required. In Europe, the European Commission sets legal limits on mycotoxins in various foodstuffs[8-11]. The control of the mycotoxin content of food raw materials is thus a routine analysis in the food industry to guarantee food safety. Mycotoxin analysis commonly involves comprehensive methods such as chromatography, requires trained personnel and is routinely performed by external laboratories. These methods provide reliable results, but at the same time produce significant costs for food companies. The key problem is, the analysis often takes a few days and meanwhile, crops, must be quarantined in separate silos to prevent the potential further contamination of other grain and of the production line. Consequently, not only the analysis itself but also the long storage time of the grain causes immense costs.

On-site analysis of mycotoxins with inexpensive rapid methods would be the next big revolution in the food industry. This would allow the rejection of highly contaminated food raw materials upon arrival of goods and could thus prevent the lengthy quarantine times of the crops.

In contrast to the food industry, point-of-care testing of relevant parameters in the medical context is already far more advanced. The most notable example is the monitoring of blood glucose levels in diabetes patients by enzymatic biosensors with electrochemical detection devices. Today,

wearable miniaturized sensor patches with a size of a 5 cent coin can be connected via Bluetooth to the patient's smartphone[12]. The potential of electrochemical technologies for other applications in miniaturized systems is therefore enormous and gives great promise for the food industry.

Screen-printed enzyme electrodes are usually applied in blood glucose meters [13-15], in which an enzyme acts as the recognition element and as signaling entity[15, 16]. The detection of the enzymatic redox reaction is typically performed by a chronoamperometric measurement[16]. However, up till now, this type of sensor could not be developed for many other small molecules including mycotoxins, since there is often no enzyme available which can recognize the analyte. Furthermore, some mycotoxins, such as aflatoxins and ochratoxin A, require very sensitive detection methods due to their high toxicity and very low legal limits in food. For this purpose, antibody-based methods, such as competitive immunoassays, offer great promise.

Here, the analyte and a "tracer", which is most commonly an enzyme-labeled analyte analogue, compete for the binding sites at an analyte-specific antibody and subsequently the tracer label generates the signal allowing the quantification of the analyte.

Today, already a few rapid antibody-based detection methods for mycotoxins such as enzyme-linked immunosorbent assay (ELISA) with optical detection are applied in the food industry, providing a good basis for sensitive and rapid detection. However, also ELISAs require trained personnel and relatively expensive optical detection devices. The combination of antibody-based techniques with electrochemical methods provides a promising approach to meet the demand for sensitive and cost-effective on-site detection at food production sites.

2 Aim of this work

The aim of this study is to develop a mycotoxin-sensing module for food samples, based on electrochemical detection methods and different biological recognition elements (antibodies and an enzyme). A central aim was to develop a user-friendly inexpensive system that can be applied on-site at production sites in the food industry, as for example, in mills. To fulfill the criteria required by the food industry one of the largest organic mills in Germany, the Elbland Biomühle in Göddenstedt as well as a German association for the grain, milling and starch industry, the VGMS (Verband der Getreide-, Mühlen- und Stärkewirtschaft VGMS e.V.) have been visited and the prerequisites for an analytical mycotoxin test which can be applied at the production site have been defined.

The following aims were fulfilled in the present work:

- Magnetic bead-based competitive immunoassays for two mycotoxins, ochratoxin A and ergometrine, were developed.
- A universal approach for the electrochemical detection in immunoassays, which can be also applied for many further mycotoxins was established.
- A custom-made detection platform, which can be used for the electrochemical measurements was developed.
- The application of an enzyme as recognition element for mycotoxins in combination with electrochemical sensing was demonstrated, using the enzyme *Aspergillus niger* fumonisin amine oxidase (AnFAO) for the detection of the mycotoxin fumonisin B_1.

3 Theoretical Background

3.1 Mycotoxins in food

3.1.1 Occurrence and importance of mycotoxins

Mycotoxins are secondary metabolites produced by fungi (molds) with harmful effects to vertebrates. Molds are ubiquitous in soil since decomposing plant- and animal-based substrates provide ideal growing conditions. They play a key role in the biological material cycle of the ecosystem, since they contribute to the formation of humus and the mineralization[17]. However, their secondary metabolites not only do harm to humans and animals, but some metabolites are also of tremendous importance for pharmaceutical applications, such as the prominent antibiotic penicillin[18-20]. As typical for fungi, they form a mycelium. For the propagation of the fungus, often large amounts of spores are released into the air, which can be transported over hundreds of kilometers[21]. Since they can also grow on wood and paper, they are sometimes found in indoor areas and often on food.

Mycotoxins occur in food and agricultural products all over the world and are considered as inevitable contaminants. Their function for the fungus has not been clearly identified, but it is assumed, that they play a role in the defense of competing microorganisms in the same environment[7, 22-24]. There are many different fungal species producing mycotoxins of which the most important genera involved in the human food chain are *Aspergillus*, *Penicillium*, *Fusarium and Claviceps*[7, 25, 26]. While *Fusarium* and *Claviceps* grow pre-harvest on the plants, *Aspergillus* and *Penicillium* predominately grow post-harvest during storage of food[25].

Today more than 300 mycotoxins are known, but only a few of them have great impact on public health and economy which include aflatoxins, ochratoxin A, trichothecenes, zearalenone, fumonisins, patulin and ergot alkaloids[27, 28]. The exposure of humans to these mycotoxins occurs mainly by dietary intake of contaminated plant-based foods but also by ingestion of animal-based food containing metabolites and residues of mycotoxins[25, 29]. Typical food and feed products susceptible to mycotoxin contamination include maize[25, 28, 30], cereals[25, 28, 30], nuts[25, 28], spices[25, 28], fruit juice[25, 28], and milk[28, 29].

The consumption of mycotoxin-infested food not only can cause acute poisoning but can also have for example teratogenic[31], cancerogenic[3, 32-34], mutagenic[35], neurotoxic[36] or

immunosuppressive effects[37]. Mycotoxin poisoning is also referred to as mycotoxicosis, with various mycotoxins having specific health consequences. Certain mycotoxins are therefore of particular importance as they can cause serious illnesses including death. Mycotoxins which are well-known for their high-abundance and serious health implications for humans and animals include, for example, aflatoxins, trichothecenes, ochratoxin A, ergot alkaloids, zearalenone, fumonisins, or patulin[7, 27, 28]. Most countries, therefore, have regulations for maximum levels of important mycotoxins in food and feed.

3.1.2 Analytical methods, sampling, and sample preparation for mycotoxin analysis

The chemical diversity of mycotoxins and the diversity of food commodities poses a challenge for the development of analytical methods for mycotoxin analysis[38]. Further the concentration of mycotoxins in a complex sample matrix can be as low as a few micrograms per kilogram. Therefore, analytical methods must be tailored for each toxin or toxin class. But not only the development of analytical methods poses a challenge in mycotoxin analysis, also the sample preparation and predominately the sampling, plays a crucial role in mycotoxin analysis.

The analysis of mycotoxins in solid food matrices routinely involves the following three steps: (1) sampling, (2) sample preparation, and (3) analytical detection [28, 39, 40]. The uncertainty of the test result is determined by the uncertainty of each step[41, 42]. The analytical method commonly provides a very low level of uncertainty, whereas the sampling accounts for the highest uncertainty, followed by sample preparation[38, 41].

Especially for very unevenly distributed mycotoxins, occurring in very low concentrations, the sampling uncertainty is high, since only a small percentage of the total quantity is contaminated[41]. In liquid samples, such as milk, it can be assumed, that mycotoxins are evenly distributed, but in solid food commodities such as grain, certain mycotoxins might be concentrated in so-called "hot-spots"[43]. This occurs in particular for mycotoxins produced by *Aspergillus* species, such as aflatoxins[43]. Hence, it is crucial to take many incremental samples from a grain batch[42]. The European Commission has therefore established sampling plans for official controls, which will be further discussed below (see 3.1.3)[44]. Also, for routine analysis in the food industry, several samples are usually taken for mycotoxin analysis. For this, a sampling device is used, which allows to take samples from a grain truck upon its arrival at the production site (see Figure 1). A sample spear allows to take cross-sectional samples, which can be automatically transported by an air flow

system to an in-house laboratory at the production site, where the sample is further prepared for analysis.

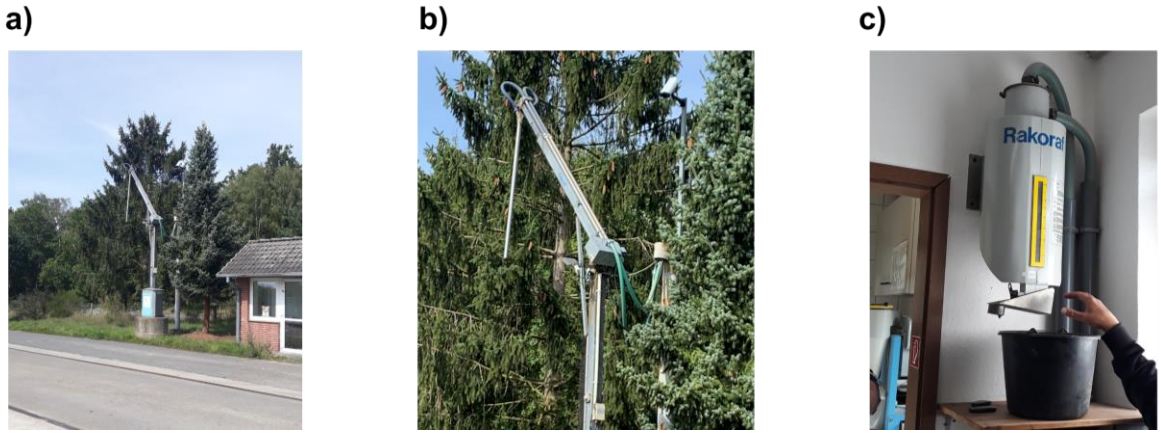

Figure 1 a) Sampling device for grain used for vehicles upon arrival, which is connected to the in-house laboratory at the production site of a mill. **b)** Spear of the sampling device. **c)** Part of the transport system in the in-house laboratory where the grain arrives after sampling. (Pictures were taken in 2021 at the Elbland Biomühle in Göddenstedt, which is one of the biggest organic mills in Germany.)

For analytical methods (chromatography and immunoassays) utilized for mycotoxin analysis, an extraction of mycotoxins from solid food matrices with solvents is required[43]. Before extraction, samples such as grain are typically coarsely ground. The choice of the solvent or mixture of solvents with modifiers (e.g., acids or bases) depends on the mycotoxin and its physicochemical properties, the food matrix and the detection method[28, 43, 45]. For chromatographic methods, the purification of the extract with solid phase extraction or an immunoaffinity columns (IAC) is widely established[39]. Both methods allow the enrichment of the analyte and the removal of matrix compounds. For solid phase extraction the surface of the columns is tailored by different surface chemistries for specific mycotoxins[39]. In IACs the analyte binds to the column via specific antibodies.

Analytical methods for mycotoxin detection can be divided into qualitative and quantitative methods. A qualitative method is the antibody-based lateral flow immunoassay and quantitative methods include predominantly immunoassays and chromatographic methods such as gas chromatography (GC) and liquid chromatography (LC) with fluorescence, UV, or mass spectrometry detection[28, 39, 40]. However, LC is much more frequently applied than GC and is currently considered as the state-of-art in mycotoxin analysis[40]. Also, validated official methods are commonly based on chromatography. For developing countries, such sophisticated methods are beyond the resources[39] and also worldwide the food industry has a major interest in rapid and

inexpensive analytical methods for mycotoxin analysis. In literature many different types of rapid methods have been reported, including lateral flow tests[46], amperometric lab-on-a-chip biosensors[47], impedimetric[48] or conductometric sensors[49] in which typically antibodies[46, 47, 50] but also molecular imprinted polymers (MIPs)[50], aptamers[48, 50] or enzymes[49] were applied as recognition elements. For all mycotoxins, regulated by the European Commission, various sensing approaches have been developed, including aflatoxins[46, 47], ochratoxin A[48, 51], patulin[49], deoxynivalenol[46, 52], zearalenone[46, 53], fumonisins[46, 54], T-2[46] and HT-2 toxin[55], and ergot alkaloids[56]. Those developments give great promise for future developments of on-site analysis methods[50, 57]. However, while sensor-based methods are, so far, rarely used outside of academic research, microplate-based immunoassays (ELISA kits) and lateral flow tests dominate the market. Compared to sophisticated methods, ELISAs are fast, sensitive, have a high sample throughput and usually no further purification step of the extract is required but they are often highly sensitive to the matrix.

3.1.3 European Commission regulations on maximum levels and methods of sampling and analysis of mycotoxins

Most nations distributed on all continents have established regulations on the maximum levels of mycotoxins in certain foodstuffs (for example the US[58], the European Union member states[8-11], Canada or the MERCOSUR member states in Latin America[59]).

The European regulations are among the strictest worldwide[60]. The European Commission sets legal limits for aflatoxins, ochratoxin A, patulin, deoxynivalenol, zearalenone, fumonisins, citrinin and ergot alkaloids[8-10]. The legal limits for different foodstuffs range from 0.1 µg kg^{-1} for aflatoxin B_1 in processed cereal-based foods for babies to 4,000 µg kg^{-1} for fumonisins in unprocessed maize[8-10].

Table 1 shows the maximum levels of the currently regulated mycotoxins in a selection of certain foodstuffs. Further information can be found in the corresponding regulations (COMMISSION REGULATION (EC) No 1881/2006, COMMISSION REGULATION (EC) No 1126/2007, COMMISSION REGULATION (EU) 2021/1399)[8-10]. Owing to their different toxicological properties, the legal limits are adapted to each type of toxin to toxicologically acceptable levels. To protect consumers, foods that exceed the maximum levels of mycotoxins, should not be placed on the market, even after mixing with other foods[8].

Table 1- Permittable maximum levels of mycotoxins in certain foodstuffs according to the European Commission[8-11, 61]

mycotoxin	foodstuffs	maximum levels (µg kg^{-1})
aflatoxins	cereals and products derived from cereals	aflatoxin B_1: 2 [8] sum of aflatoxin B_1, B_2, G_1, G_2: 4 [8]
	processed cereal-based food for babies and young children	aflatoxin B_1: 0.1 [8]
ochratoxin A	unprocessed cereals	5 [8]
	processed cereal-based food for babies and young children	0.5 [8]
patulin	fruit juices	50 [8]
	apple juice for infants and young children	10 [8]
deoxynivalenol	unprocessed cereals (other than durum wheat, oats, maize)	1,250 [9]
	processed cereal-based food for babies and young children	200 [9]
zearalenone	unprocessed cereals (other than maize)	100 [9]
	processed cereal-based food for babies and young children	20 [9]
fumonisins	unprocessed maize	sum of fumonisin B_1 and B_2: 4,000 [9]
	processed maize-based food for babies and young children	200 [9]
T-2 and HT-2 toxin	wheat, rye, and other cereals (except oats, wheat, and maize)	sum of T-2 and HT-2 toxin 100 (indicative level)[61]
citrinin	food supplements based on rice fermented with red yeast *Monascus purpureus*	100 [11]
ergot alkaloids	rye milling products	500 until 30.6.2024 250 as from 1.7.2024
	processed cereal-based food for babies and young children	20 [10]

The sampling of food commodities plays a vital role in the determination of mycotoxin levels regarding the precision, since it is challenging to obtain a representative sample[38, 62]. As discussed above, mycotoxins are often heterogeneously distributed in food commodities[38, 63] especially in food raw materials and therefore the European Commission defines general criteria for official sampling methods for certain mycotoxins[44]. For different mycotoxins and food commodities specific sampling provisions apply[44]. Further also, the particle size of the food commodity influences the sampling[44]. To achieve a similar representativeness for food products of different particle size, a higher sample weight has to be analyzed, for food products with a large particle size (such as figs or nuts), than for products with a small particle size (e.g., flour)[44]. From a “lot”,

which is a food commodity delivered at one time, "sublots" are used for the sampling[44]. Different samples ("incremental samples") must be taken at different positions of the lot or sublot, which are then combined to an "aggregate sample" which is then further processed to obtain the "laboratory sample" used for the analysis[44]. For example, for the control of aflatoxin B_1, total aflatoxins, ochratoxin A and *Fusarium*-toxin levels, a cereal commodity with a lot weight of more than 1,500 tonnes must be divided into sublots of 500 tonnes[44]. From a sublot 100 incremental samples, each weighing about 100 g, must be taken and combined to the aggregate sample with a weight of 10 kg[44].

The complete samples are finely grinded to obtain complete homogenization and subsequently they are analysed[44]. Also, for analytical methods certain requirements were defined, which must be applied by control laboratories to obtain reliable and comparable results[44]. The following criteria are generally used to characterize the analysis methods used for food control: accuracy, applicability (matrix and concentration range), limit of detection, limit of determination, precision, repeatability, reproducibility, recovery, selectivity, sensitivity, linearity and measurement uncertainty[44, 64]. The precision values can be obtained either from a collaborative trial using an internationally recognized protocol (ISO 5725:1994 or IUPAC International Harmonised Protocol) or performance criteria of the method have been established on the basis of criteria compliance tests[64]. Values of repeatability and reproducibility should be represented in an internationally recognized form (as defined by ISO 5725:1994 or IUPAC)[64]. For most of the regulated mycotoxins specific performance criteria, for analytical measurements are required, predominantly regarding their recovery rates and precision in the relevant concentration range[64]. Generally, for most of the regulated mycotoxins, higher concentrations which are closer to the legal limits, require a higher precision of the analytical method and recovery rates closer to 100%[44]. Performance criteria of analytical methods for mycotoxins with regulated maximum levels in comparatively high mycotoxin concentrations regarding their maximum limits are shown in Table 2. Further information can be found in the COMMISSION REGULATION (EC) No 401/2006[44].

Official controls of the mycotoxin levels in foodstuffs can only be performed by official laboratories designated by the competent authority, that fulfills certain European Standards reported in REGULATION (EC) No 882/2004[44, 64]. The requirements on analytical methods for official methods described above can be best fulfilled by chromatographic methods with previous sample preparation and therefore they are mainly applied for official controls[65]. However, in

routine analysis in the food industry which must be carried out daily to provide consumer-safety, official methods are not practical and cost-effective. For this purpose, screening methods such as immunoassays or biosensors provide an inexpensive alternative[65].

Table 2 - Performance criteria of the European Commission for mycotoxin analysis methods used for official controls in a certain concentration range[44]

mycotoxin	concentration range µg kg^{-1}	recovery %	RSD_r *a %	RSD_R *b %
aflatoxins B_1, B_2, G_1, G_2	>10	80 - 110	as derived from Horwitz equation*c	2 × value resulting from Horwitz equation
ochratoxin A	1-10	70 - 110	≤ 20	≤ 30
patulin	>50	75 - 105	≤ 15	≤ 25
deoxynivalenol	>500	70 - 120	≤ 20	≤ 40
zearalenone	>50	70 - 120	≤ 25	≤ 40
fumonisin B_1 and B_2	>500	70 - 110	≤ 20	≤ 30
T-2 toxin	>250	60 - 130	≤ 30	≤ 50
HT-2 toxin	>200	60 - 130	≤ 30	≤ 30

*a RSD_r: relative standard deviation under repeatability conditions
*b RSD_R: relative standard deviation calculated under reproducibility conditions
*c $RSD_R = 2^{(1 - 0.5 \log C)}$ (C is the concentration ratio)
(according to REGULATION (EC) No 401/2006[44])

3.1.4 Ochratoxin A

Ochratoxin A (OTA) was first identified in 1965 by van der Merve et al., as a toxic metabolite of *Aspergillus ochraceus*, a fungus which frequently grows on stored cereals such as wheat[66]. Today it is known that many different *Aspergillus* and *Penicillium* species can produce OTA[67-71] and it is one of the most abundant and toxic mycotoxins[68]. It can be found on many different commodities all over the world such as coffee beans[72], maize products[73], pork products[74], wine[75] or beer[75] but it is primarily found in the north temperate zones on wheat and barley[68, 76].

OTA is a crystalline, white, odorless solid with a molecular weight of 403.8 g mol^{-1} [77]. Many different structurally similar compounds and naturally formed derivates are known[68], particularly ochratoxin B (OTB), an analogue of OTA lacking the chlorine, ochratoxin C (OTC) an ethyl ester of OTA, ochratoxin α (OTα) the isocoumaric derivative of OTA and ochratoxin β (OTβ) the dechloro analogue of OTα[67] (see Figure 1). However, only OTA is regulated by the European Commission as it is the most toxic compared to the others, of which only OTB occurs naturally[7].

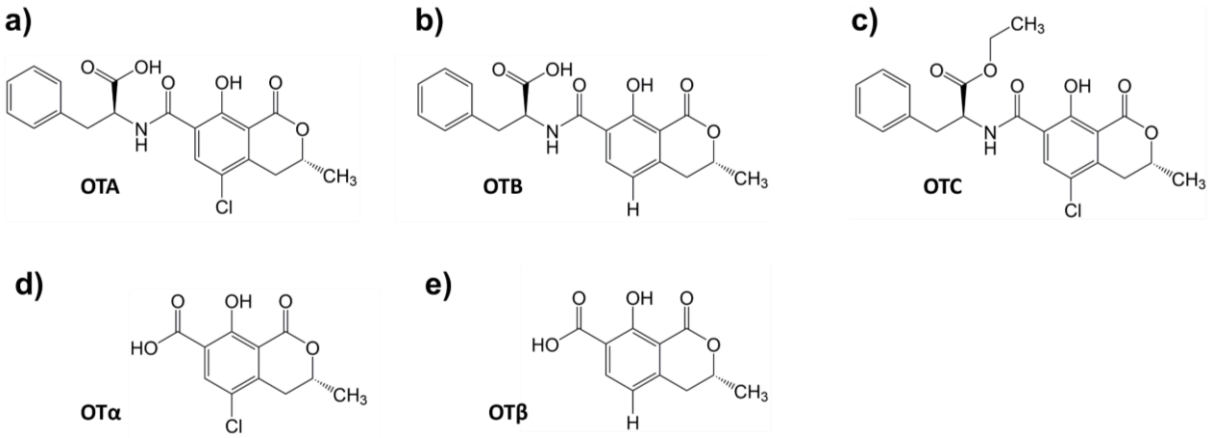

Figure 2 Structure of **a)** ochratoxin A (OTA), **b)** ochratoxin B (OTB), **c)** ochratoxin C (OTC), **d)** ochratoxin α (OTα) and **e)** ochratoxin β (OTβ).

Multiple toxic effects for OTA were demonstrated in animal experiments, such as nephrotoxicity[34], carcinogenicity[34, 78], embryotoxicity[79], teratogenicity[31], neurotoxicity[36] and immunotoxicty[80]. For humans, a correlation between OTA exposure and Balkan endemic nephropathy and urothelial urinary tract tumors is suggested[76]. The International Agency for Research on Cancer (IARC) classifies OTA as possibly carcinogenic to humans (group 2B)[76]. However, the mode of action of OTA is still unclear[81]. Human exposure occurs predominantly by consumption of contaminated grain and pork products[76]. Due to the high toxicity of OTA the maximum permittable levels in foodstuffs are as low as a few µg kg^{-1} [8].

3.1.5 Ergot alkaloids

In human history, the ergot alkaloids, a group of mycotoxins, have repetitively provoked epidemic-like outbreaks, claiming tens of thousands of lives in Europe in the Middle Ages[82]. Parasitic Fungi of the *Claviceps* genus[83], predominantly *Claviceps purpurea*[83, 84] are the most prominent producers of ergot alkaloids, but also fungi from the *Aspergillus* and *Penicillium* genera can produce them[83]. Fungus-infected plants, such as grasses and grains, develop so called sclerotia, which grow in place of the grain in the ear as dark, hardened mycelium[85]. They are the wintering bodies of the fungus and contain the ergot alkaloids[85]. Typically, the highest levels of ergot alkaloids occur in rye and rye products[84, 86], however *Claviceps purpurea* can also infect millet, wheat, triticale, barley and oat[84].

To date, more than 50 different ergot alkaloids have been reported[84]. Owing to their high abundance in sclerotia, ergometrine, ergotamine, ergosine, ergocristine ergocornine, ergocryptine

(α- and β-isomers) and their -inine (S)-epimers are particularly important[84]. Their composition and content in sclerotia are highly variable[84, 87-89]. For Canadian rye, triticale, wheat, and barley, a relative composition of ergot alkaloids of ergocristine 31% – ergocristinine 13%, ergotamine 17% – ergotaminine 8%, α-ergo-cryptine 5% – α-ergocryptinine 3%, ergometrine 5% – ergometrinine 2%, ergosine 4% – ergosinine 2%, ergocornine 4% – ergocorninine 2% has been reported[90]. The common structural feature of these ergot alkaloids is the ergoline moiety, methylated at the N6 nitrogen and has a C9-C10 double bond with various substituents at the C8 position (see Figure 3)[83]. Ergotamine, ergosine, ergocristine ergocornine, ergocryptine (α- and β-isomers) and their -inine epimers are peptide alkaloids (ergopeptines), whereas ergometrine and ergometrininine are simple lysergic acid derivatives[91].

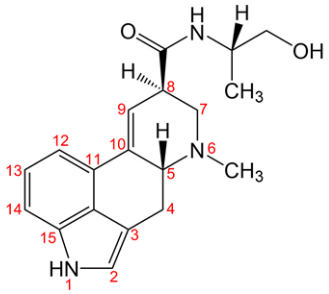

Figure 3 Structure of ergometrine (figure reproduced from Höfs et al.[56])

Poisoning with ergot alkaloids causes ergotism which is also called St. Anthony's fire[26]. A characteristic symptom is the vasoconstriction causing gangrene, which can lead to the loss of fingers, hands, feet and limbs[26]. Further symptoms comprise nausea and vomiting abdominal pain, insomnia or hallucinations[92]. Today color sorting machines in the food industry can efficiently remove sclerotia and therefore fatal ergot poisonings have become rare. Until 2021, the European Commission regulated only the maximum content of ergot sclerotia in certain food products. Even though the presence of ergot sclerotia is a good indicator for ergot alkaloids, their absence does not assure the absence of ergot alkaloids[86]. Broken sclerotia can still contaminate other grains during food processing[10]. Consequently, a new European Commission regulation on the maximum levels of the sum of the six major ergot alkaloids and their corresponding epimers came into force in 2021[10].

3.1.6 Fumonisins

Fumonisins are a group of mycotoxins that belong to the fusarium toxins, since they are mainly produced by various species of this genus[93]. They were first discovered in 1988 by Gelderblom et al.[32]. The most prominent producers are *F. verticillioides* and *F. proliferatum*, since they have a wide geographical distribution, frequently occur on maize and they can produce high levels of fumonisins[93]. Furthermore, these species are associated with known animal mycotoxicosis[93]. Beside Fusarium species, it was also reported that *Aspergillus niger*[94, 95] and *Alternaria alternata f. sp. lycopersici* can produce fumonisins[96].

Fumonisins are polyketides containing two propane-1,2,3-tricarboxylic acid side chains esterified to an aminopolyol backbone (see Figure 4)[97]. Today many different compounds are known of which fumonisin B_1 (FB_1), fumonisin B_2 (FB_2) and fumonisin B_3 (FB_3) are the most prominent. FB_1 is the dominant fumonisin compared to FB_2 and FB_3 [98-101]. The European Commission only regulates the maximum levels of the sum of FB_1 and FB_2 in certain foodstuffs[8, 9].

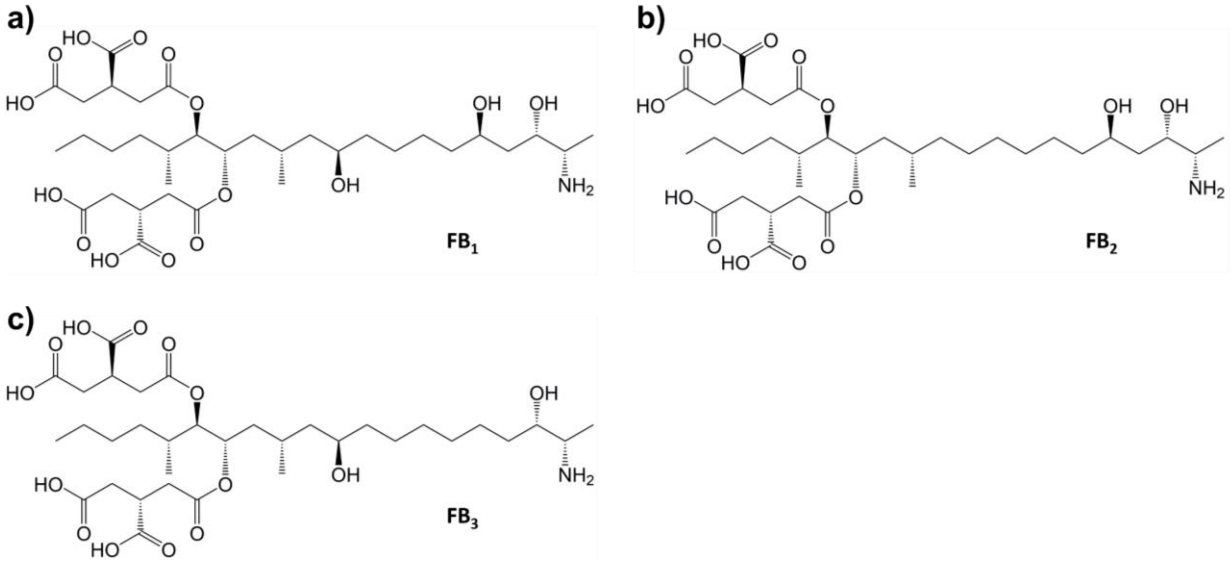

Figure 4 Structure of **a)** fumonisin B_1 (FB_1), **b)** fumonisin B_2 (FB_2) and **c)** fumonisin B_3 (FB_3).

FB_1 is known to cause diseases of farm and laboratory animals, which include equine leukoencephalomalacia[102, 103], porcine pulmonary oedema[104] or cancer in rats[105]. Furthermore, it is hepatotoxic[7] and in humans it is associated with esophageal cancer[33, 106] and neural tube defects[107]. The IARC, therefore, classifies toxins derived from *Fusarium verticillioides* as possibly carcinogenic to humans (Group 2B)[108].

The main source of human exposure is maize and maize-based products which can be contaminated by very high amounts of fumonisins[97, 109]. However, fumonisins were also reported in other foodstuffs such as millet[110], soy beans[110], beer[110], asparagus[110], oats[109, 111], wheat[109, 112], barley[109], rice[109, 113].

3.2 Immunoassays and biosensors for mycotoxin detection

3.2.1 Antibodies

Antibodies, also known as immunoglobulins, are glycoproteins synthesized in the serum of vertebrates. They play a key role in the humoral immune response for the defense against certain antigens but are also widely used as therapeutics or recognition element in bioanalytical assays or sensors for diagnostic applications or in the food industry.

Two types of polypeptide chains, the light chain and the heavy chain form the structure of immunoglobulins. The light and the heavy chain have a molecular weight of about 25,000 Da and 50,000 Da, respectively[114]. There are different classes of immunoglobulins, namely IgA, IgG, IgM, IgD and IgE, each of them with a different underlying structure. IgG is the most abundant in serum[114] and the most widely used in immunoanalytical techniques. IgGs are Y-shaped proteins consisting of two identical heavy and two identical light chains, connected by two disulfide bonds in the so-called “hinge” region of the antibody and two disulfide bonds link the light chains with the heavy chains (see Figure 5)[114-117]. The amino acid sequence of these chains can be divided into a constant and a variable region, with the heavy chains consisting of three constant (C_H1, C_H2, C_H3) and one variable domain (V_H), whereas the light chain has one variable (V_L) and one constant domain (C_L)[115, 118, 119].

Antibodies can be cleaved at the interchain disulfide bonds in the hinge region using proteolytic enzymes (e.g. trypsin, papain or pepsin)[115, 120, 121]. The two kinds of fragments produced by the cleavage are called Fab fragment and Fc fragment[115]. Each of the two Fab fragments consists of the whole light chain (C_L and V_L) and the two N-terminal domains of the heavy chains (C_H1 and V_H). The Fab fragment also contains the antigen-binding site, also called paratope. The paratope is directed against a specific region of an antigen, called epitope. The Fc fragment contains both C-terminal heavy chains with each consisting of two constant domains (C_H2 and C_H3). In contrast to the Fab fragments, the Fc fragments were found to be crystallizable[121].

The variable regions of the antibodies are of essential importance, since they determine the specificity towards an antigen[115]. The Fab fragment contains a region of hypervariable amino acid sequences, also referred to as Fv region[117]. This region forms the antigen-binding site and determines the specificity of the antibody towards an antigen[117].

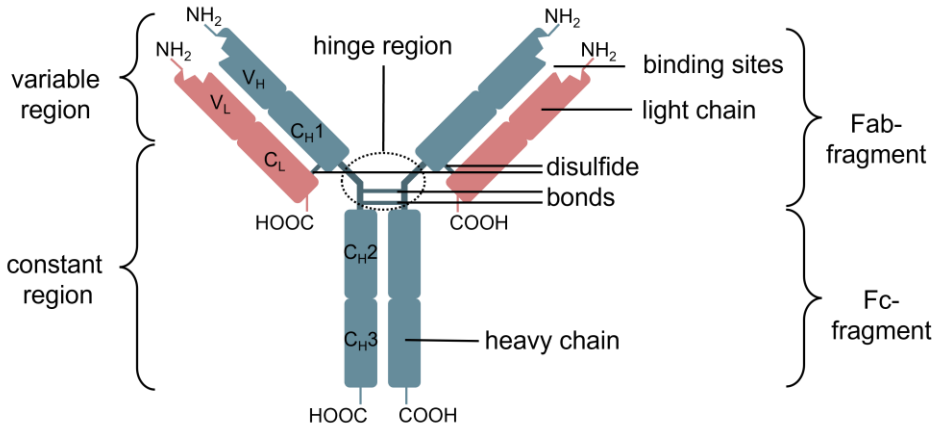

Figure 5 Schematic illustration of the structure of an IgG antibody

B-lymphocytes, also known as B cells, produce IgGs after an antigen has entered the organism. Physiologically formed antibodies in response to an antigen are always polyclonal, which means they are secreted by different B cells and typically have specificities against different epitopes of the antigen. For their production, an antigen is injected into an animal (often sheep, rabbit, or mouse) to immunize the animal, and the antibodies can be obtained from the serum. However, monoclonal antibodies are used more frequently for analytical and diagnostic applications or as therapeutic agents. They are produced by a single B-cell line and are accordingly directed against a single epitope of an antigen. The hybridoma technology, developed in 1975 by Köhler and Milstein, allows the efficient in vitro production of monoclonal antibodies[122].

For the hybridoma technology, isolated B cells from the spleen of an immunized animal, most frequently a mouse, are fused with myeloma cells lacking the hypoxanthine-guanine phosphoribosyl transferase (HGPRT) gene to produce hybridoma cells[122, 123]. Fused cells are selected from unfused cells by their cultivation on HAT medium, containing hypoxanthine aminopterin and thymidine[122, 123]. The aminopterin inhibits the *de novo* synthesis of DNA by blocking the synthetic pathway for the purine and pyrimidine bases, which therefore prevents the growth of the cells. In contrast to the myeloma cells the B cells hold the HGPRT, allowing the synthesis of purines from hypoxanthine, therefore also the DNA synthesis. Since the aminopterin

also blocks the pyrimidine synthesis, thymidine is also added to the media, to allow the production of essential thymine. The unfused B cells die by natural cell death and myeloma cells cannot survive on HAT-medium, since they are lacking the hypoxanthine-guanine phosphoribosyl transferase (HGPRT) gene[123]. Hence, only fused hybridoma cells can survive on the HAT medium. Those hybridoma cells can produce monoclonal antibodies, such as the B cells, but additionally have immortal properties of the myeloma cells, allowing their cultivation[122].

Low-molecular weight compounds, in this context called "haptens", are too small to cause an immune response in vertebrates[124]. To produce monoclonal antibodies against haptens, such as mycotoxins, they must be coupled to a carrier protein to induce an immune response. Frequently, bovine serum albumin (BSA) is used as a carrier protein but also other proteins, such as ovalbumin (OVA) or keyhole limpet hemocyanin (KLH) are applied[124, 125].

The choice of the functional group for coupling the hapten to the protein used for immunization is crucial. The antibodies produced with hapten-protein conjugates used as immunogen are specific to the portion of the hapten that is distal to the carrier protein. For this reason, molecular spacers are sometimes used to create a distance between the carrier and the hapten.

The affinity of an antibody (Ab) towards an antigen (Ag) to form an immunocomplex (Ab – Ag) can be described by the association constant (K_A), or by its reciprocal, the dissociation constant (K_D). Typical K_D values are in the low micromolar (10^{-6} M) to nanomolar range (10^{-9} M), but also antibodies with remarkably low K_D values, in the picomolar range, can be achieved[126-128].

K_D can be described by the following equation:

$$K_D = \frac{[Ab][Ag]}{[Ab-Ag]} = \frac{k_{off}}{k_{on}} \quad (1)$$

with:

$$Ab + Ag \rightleftharpoons Ab - Ag \quad (2)$$

k_{on}: association rate constant

k_{off}: dissociation rate constant

3.2.2 Immunoassays

Immunoassays are bioanalytical methods for the quantification of analytes by their recognition of highly specific antibodies. Compared to comprehensive instrumental analytical methods, such as

chromatography and mass spectrometry, providing a high sensitivity and reliability, immunoassays are used as a rapid but also highly sensitive screening tool.

Immunoassays can be divided into homogeneous and heterogeneous assays. In homogeneous assays the antibody-analyte binding takes place in one liquid phase, whereas in heterogeneous assays either the antibody or the antigen/hapten conjugate is immobilized onto a surface, most frequently to a microplate. In the present work, only heterogeneous immunoassays will be discussed.

To detect the binding event of the antibody and analyte, a labeling of the antibody or analyte is required, most frequently enzymes such as horseradish peroxidase or alkaline phosphatase are used, but also fluorescence[129-131], nanomaterial[132] or radioisotope[133, 134] labeling can be applied. The first immunoassays were the radio immunoassays (RIA), developed in 1960, by Yalow and Berson[134]. Radioimmunoassays allow sensitive detection, but also pose health risks to the operator due to the radioactivity of the label. Therefore, a harmless alternative was sought. Today the most frequent used immunoassay is the ELISA (enzyme-linked immunosorbent assay)[128], which was developed in 1971 by two groups independently, Van Weemen and Schurs[135] and Engvall and Perlmann[136]. Using enzymes as labels often enables similar sensitivities as obtained with RIA[136, 137], since enzymes can react with a high number of substrate molecules to detectable products, enabling a significant signal amplification.

There are different ELISA formats, which can be divided into direct, indirect, sandwich and competitive ELISA (see Figure 6)[138]. In direct ELISAs an antigen is attached to the surface of a microplate and an enzyme-labeled antibody, specific for the antigen (primary antibody), binds the antigen on the surface of the microplate (see Figure 6 a). After each binding step a washing step is required to remove any unbound species. Finally, a suitable enzyme substrate is added which can be quantified after its enzymatic turnover. Most often chromogenic, fluorescent, or redox active substrates are used. The indirect ELISA works quite similar, here the primary antibody, which binds the antigen on the surface is not labeled and thus a secondary labeled antibody is required, which can bind the primary antibody (see Figure 6 b). Since the primary antibody is often a monoclonal mouse antibody, rabbit or sheep anti-mouse antibodies are frequently used as secondary antibodies. In the sandwich ELISA, one antibody, called capture antibody, is attached to the plate binding the antigen and another labeled antibody called detection antibody, also binds

the antigen Also, here an unlabeled detection antibody may be used instead of a labeled one, together with a secondary labeled antibody (see Figure 6 c). In competitive immunoassays a primary antibody is attached directly or via a secondary antibody to the microplate (see Figure 6 d). The analyte (antigen or hapten) competes with a tracer, which is an analyte-enzyme conjugate, for the binding sites at the antibody. In another arrangement, the antigen or a hapten conjugate is attached to the plate and a primary antibody and analyte (antigen or hapten) are added to the solution, leading to the competition between surface bound antigen/hapten and the analyte in solution. In competitive ELISAs, the generated signal is thus generally inversely proportional to the analyte concentration. The sandwich and competitive ELISA can be further divided into direct and indirect, as depicted in Figure 6 a and b.

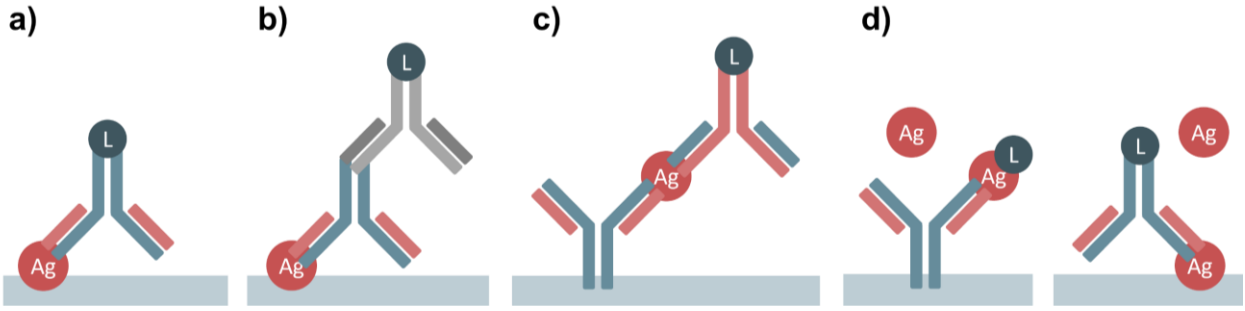

Figure 6 ELISA formats. **a)** Direct ELISA, with an antigen (Ag, red) attached to the surface and a bound antigen-specific primary antibody with an enzyme label (L). **b)** Indirect ELISA, with Ag attached to the surface and a specifically bound primary antibody to which a labeled secondary antibody (grey) binds. **c)** Sandwich ELISA with the capture antibody bound to the surface, which binds the Ag and the labeled detection antibody also binding the Ag. **d)** Two arrangements of competitive ELISAs, with either the primary antibody attached to the surface and a labeled Ag or with the Ag attached to the surface and a labeled primary antibody.

3.2.3 TMB/HRP-based assays

Today, the most frequently used enzymatic label in ELISAs is horseradish peroxidase (HRP). Furthermore, most of the commercially available ELISA kits make use of this enzyme and for many important analytes, HRP conjugates or HRP-labeled antibodies exist on the market. HRP is a heme-containing enzyme[139, 140], which catalyzes the reduction of peroxides, such as hydrogen peroxide. It is one of the most important reporter enzymes, not only for immunoassay, but also for other diagnostic assays and has been studied for over a century[140]. The roots of the horseradish, *Armoracia rusticana,* are a rich source of peroxidases, containing several isoenzymes of peroxidases[139], of which the most abundant one is the C isoenzyme (HRP C)[140]. HRP C consists of a polypeptide chain of 308 amino acids, with 8 neutral carbohydrate side chains attached through

asparagine residues and has a total molecular weight of 44 kDa[141, 142]. Two different types of metal centers are essential for the catalytic activity and its structure[140]. One is the heme group and the other are two Ca^{2+} ions[140, 143]. The heme group is attached to the enzyme via the central iron ion to a histidine residue forming a coordination bond[140]. The second coordination site of the iron is unoccupied but available to hydrogen peroxide during the enzymatic catalysis[140].

The HRP-catalyzed reduction of H_2O_2 in the presence of an electron donor (XH_2) follows for most reagents the following equation (3)[140]:

$$H_2O_2 + 2XH_2 \rightarrow 2H_2O + 2XH^{\bullet} \quad (3)$$

The first step of the catalytic reaction is the reaction between H_2O_2 and the Fe(III) resting state, generating compound I, which is a high oxidation state intermediate of an Fe(IV) oxoferryl center and a porphyrin-based radical cation[140, 144, 145]. In the presence of a reducing substrate, the first one-electron reduction step occurs and leads to the formation of an Fe(IV) oxoferryl species, called compound II[140, 144]. After another one-electron reduction, the resting state is reached again[140, 144].

Reducing substrates are amines, aromatic phenols, phenolic acids, sulfonates, or indoles[140, 146]. By far the most frequently used substrate in ELISA is the chromogenic 3,3',5,5'-tetramethylbenzidine (TMB) in combination with H_2O_2, since TMB is non-mutagenic[147], virtually non-carcinogenic[148] and HRP has a high turnover rate for TMB allowing high sensitivities in HRP-based assays[147, 149]. In the past also frequently 2,2'-azino-bis(3-ethylbenzthiazoline-6-sulfonic acid) (ABTS) or o-phenylenediamine (OPD) have been used as HRP substrates for colorimetric detection, but they do not only have higher detection limits, but are also mutagenic[150].

The oxidation mechanism of TMB has been described by Josephy et al. (see also Figure 7)[151]. After enzymatic oxidation of TMB by HRP in the presence of H_2O_2, a blue-colored charge-transfer complex is formed, which exists in a rapid equilibrium with a radical cation, which forms the yellow diimine after further oxidation[151]. Strong acids such as H_2SO_4 can accelerate the formation of the yellow diimine[152], which is highly stable at acidic pHs[151]. It has been also described for other aromatic amines of the benzidine series, that they can form stable redox systems at highly acidic pHs in which the oxidation and reduction occur in a simple bivalent process, while at weakly

acidic conditions, the redox reaction involves free radical intermediates and follows an univalent course[153].

Before addition of a strong acid, three absorption peaks may be observed at 370 nm, 450 nm and 655 nm allowing its photometric detection[147, 154]. After addition of a strong acid only one absorption maximum for the yellow-colored diimine can be observed at a wavelength of 450 nm[147, 154]. For the analytical quantification in ELISAs, most frequently the absorption is measured at 450 nm after enzymatic oxidation and the subsequent addition of a strong acid (usually H_2SO_4) at 450 nm. However, due to its electroactive properties, it can be also detected electrochemically by voltammetry and amperometry[155-161]. By cyclic voltammetry (CV) it could be demonstrated that TMB undergoes a two-step oxidation and reduction at neutral pH values on carbon electrodes, whereas a single two-step oxidation and reduction occur in the presence of a strong acid (H_2SO_4)[156, 158, 161]. Consequently, for the analytical detection, electrochemical measurements could be either performed before the addition of H_2SO_4[162, 163] or afterwards, when the fully oxidized diimine is obtained[158, 161, 164, 165].

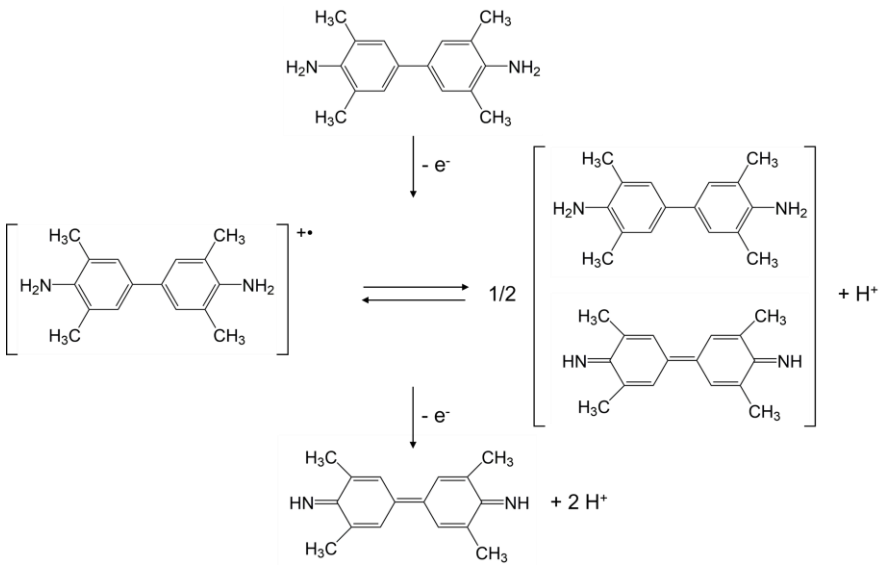

Figure 7 Oxidation of TMB (according to Josephy et al.[151])

However, only limited research has been focused on the comparison of the electrochemistry of TMB at different pH values or on the pitfalls in amperometric TMB detection, although it is generally known that electroactive precipitates can be formed on electrode surfaces after oxidation of TMB[163, 166, 167]. For analytical electrochemical measurements, the reproducibility of the electrode response is of high importance, especially if one electrode is used for sequential

measurements. Thus, the electrochemistry of TMB at different pH values (pH 1, pH 4) and different electrode materials, will be discussed in the present work.

3.2.4 Electrochemical immunoassays and -sensors

For the application of immunoassays and immunosensors in the food industry hand-held electrochemical detection devices are promising alternatives to optical detection methods. In comparison to other transducers, electrochemical devices can be miniaturized, are inexpensive and they do not require a high-level energy source[168]. Moreover, the electrodes can be produced at low cost by using the screen-printing technology, which can produce electrodes intended for single use. Therefore, three electrodes, working, counter and reference electrodes, required for most common electrochemical methods, are often printed on one disposable chip.

Electrochemical immunosensing strategies have been reported for many different mycotoxins, such as OTA[51, 169-171], aflatoxins[47], zearalenone[53], fumonisins[54, 172, 173], deoxynivalenol[52, 173] or citrinin[174]. For immunosensors, an immunoreactant is located in proximity of the transducer or associated within the transducer such as an electrode surface[168], whereas in immunoassays with electrochemical detection the immunoreaction and the detection of electroactive products are spatially separated[175]. Frequently, potentiometric, amperometric or capacitive transducers are used for electrochemical immunosensing[168]. Essentially, electrochemical immunoassays and -sensors can be divided into methods using labels and label-free methods, see also Figure 8 [175].

When labels are used, either the antibody or the antigen/hapten is labeled, as also typical for conventional plate-based immunoassays with optical read-out. Most often enzymes, such as alkaline phosphatase, glucose oxidase, HRP or catalase are used as labels, allowing the generation of an electroactive product upon addition of a suitable substrate[168, 175]. Enzymes used for this purpose should have high turnover numbers, electrochemically active products, stable enzyme substrates and products in buffer, and the enzymatic products should have low side reactions[168]. The electroactive product can be detected by amperometry or voltammetry. In principle all the assay formats depicted in Figure 6, are suitable for electrochemical detection. The immunoreactants can either be immobilized on the transducer surface or another surface such as a microplate or on magnetic particles. Immunosensors are commonly used for a single measurement, since the regeneration of the sensor is difficult[168]. Thus, many sensors are required to obtain enough data for calibration. Immunoassays have the advantage of a higher throughput, when performed in a

microplate of 96 wells. The read-out of immunoassays can be either performed by sequential injection of the content of the microplate wells to a flow system, or by several electrodes inserted into the microplate wells[168, 175].

In label-free immunosensors, the binding event can be measured directly, without the need of an auxiliary reaction[168]. Electrochemical impedance spectroscopy (EIS) is a widely used method for label-free affinity sensors. The transduction is based on an increased interfacial electron transfer resistance related to the antibody-antigen intercation[175, 176]. However, the major drawback of label-free immunosensors is, that false positive results can occur due to unspecific binding[177] and moreover, EIS immunosensors are better suited for large molecules such as proteins than for small molecules as mycotoxins.

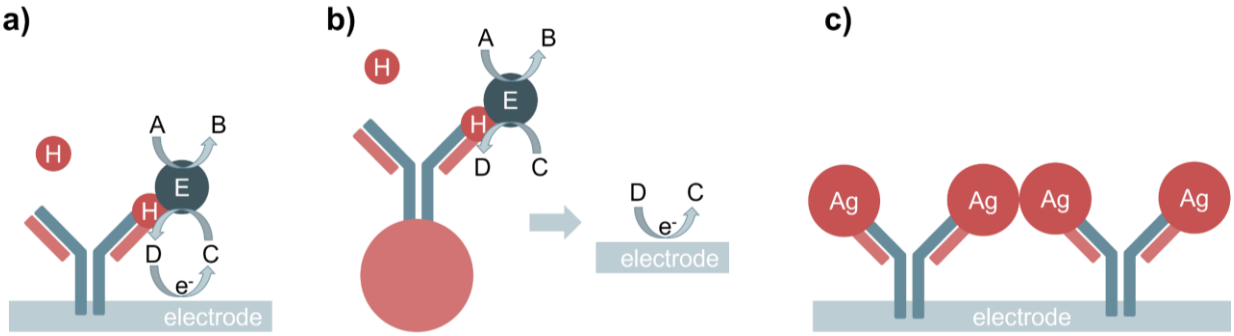

Figure 8 a) A competitive immunosensor using an enzyme (E) labeled hapten (H) with the antibody immobilized to an electrode surface. The enzymatic reaction with suitable substrates (A and C) generates an electroactive product (D) which can be detected at an electrode. **b)** Competitive immunoassay on a particle with electrochemical detection. **c)** Label-free immunosensor for an antigen (Ag), with the antibody immobilized to the electrode surface in which the interfacial electron transfer resistance increases after the binding event.

For OTA many different electrochemical immunosensing approaches have been reported in literature[169-171, 174, 178], of which most are based on competitive assay formats. For example, Jodra et al. described a magnetic bead-based OTA immunosensor for coffee samples, in which protein G-modified magnetic beads were decorated with polyclonal anti-OTA antibodies[170]. An OTA-HRP tracer was used, competing for the binding sites with OTA. The magnetic beads were captured on the surface of a screen-printed carbon electrode, and the detection was performed upon addition of H_2O_2 and hydroquinone by electrochemical reduction of enzymatically produced benzoquinone. A limit of detection of 0.32 µg L^{-1} was obtained. A similar sensor could be developed for fumonisins (FB_1, FB_2, FB_3) by the same group, reaching a detection limit of 0.33 µg L^{-1} [54].

Although OTA has a low molecular weight, several label-free approaches of immunosensors have been reported[178, 179]. For example, Radi et al. developed an impedimetric immunosensor[178]. Here, a gold electrode was functionalized with a 4-carboxyphenyl monolayer, to which anti-OTA antibodies were bound covalently by carbodiimide chemistry. The interaction of OTA with the antibodies induced an impedance change and a linear increase of the electron transfer resistance with OTA concentrations ranging from 1 to 20 ng ml^{-1}, with a limit of detection of 0.5 µg L^{-1}.

In the 1990s, substantial work on ergot alkaloid ELISAs has been reported by Shelby et al.[180-183]. However, in contrast to all the other regulated mycotoxins, hardly any immunosensing approaches have been developed for ergot alkaloids to date, which might be attributed to the fact, that legal limits have only been in force since 2022[10]. To the best of knowledge, only one immunoassay with electrochemical detection for one of the 12 major ergot alkaloids, ergometrine, has been reported so far by Höfs et al.[56], which will be further presented in this work.

3.2.5 Enzymes

Enzymes are biocatalysts which can enhance the reaction rate of biochemical reactions, without being consumed in the reaction. They can catalyze a wide range of important processes with great commercial importance, as for the production of sweetening agents, modification of antibiotics and they are used in washing powders and cleaning products[184]. Beyond these applications they play a key role for analytical devices and assays for clinical, forensic, and environmental applications[184]. The word enzyme has first been used in 1876 by Wilhem Kühne[185, 186], which is derived from the Greek words “en” (meaning within) and “zume” (meaning yeast)[184]. In the 1920s it has been discovered that the catalytic activity of enzymes is associated with their protein structure[184, 187].

Enzymes catalyze the conversion of substrate molecules to products and are usually highly specific towards their substrates. Whereas some enzymes are rather group specific, such as the alkaline phosphatase, which catalyzes the hydrolysis of phosphate monoesters[188], other enzymes provide absolute specificity towards their substrates, such as glucose oxidase catalyzing the oxidation of β-D-glucose[184, 189]. A high specificity is of particular importance for their use in analytical assays or biosensors[184].

Enzymes are typically globular proteins, consisting of 100-2,000 amino acid residues forming a specific three-dimensional structure[184]. The active site of the enzyme, where the substrate binds, is essential for the catalytic activity and can involve less than 10 amino acids[184, 190]. The shape and charge of the active site determine the specificity of the enzyme towards its substrate, whereas the rest of the protein structure stabilizes the active site[184]. A non-protein component, the cofactor, is often required for the activity of many enzymes, which can be an organic or inorganic molecule such as metal ions, as iron, manganese, cobalt, copper, or zinc[184]. Organic cofactors are called coenzymes. When the coenzyme is bound permanently to the protein, it is called a prosthetic group. According to the International Commission on Enzymes, there are seven classes of enzymes, namely, oxidoreductases, transferases, hydrolases, lyases, isomerases, ligases, and translocases[184, 190, 191]. Oxidoreductases catalyze oxidation and reduction reactions, transferases perform an atom or group transfer, hydrolases can perform hydrolysis, lyases can exert group removal, isomerases catalyze isomerization, ligases can conjugate two molecules[184, 190], and translocases catalyze the movement of ions or molecules across membranes[191].

The enzymatic reaction occurs by the formation of a complex of the enzyme and its substrate which lowers the activation energy of the reaction and afterwards the product dissociates from the enzyme or the substrates dissociate from the enzyme without the formation of a product (see equation(4))[184]. Each step of the reaction has a specific rate constant (k_1, k_{-1} and k_2). The Michaelis Menten equation describes the correlation of the substrate concentration and the reaction rate of the enzymatic reaction (see equation (5)). This equation was named after Michaelis and Menten[192, 193], but has been first developed by Henri in 1903[194, 195]. An important kinetic parameter is the Michaelis constant (K_m), which describes the substrate concentration at which the half maximal reaction velocity is reached (see equation (6)). Additionally, the reaction rate is highly dependent on the pH value and temperature.

$$E + S \underset{k_{-1}}{\overset{k_1}{\rightleftharpoons}} ES \xrightarrow{k_2} E + P \tag{4}$$

$$v_0 = \frac{V_{max}\,[S]}{[S] + K_m} \tag{5}$$

with

v_0: initial velocity of the reaction

V_{max}: maximal velocity

[S]: substrate concentration

K_m: Michaelis constant

$$K_m = \frac{k_{-1} + k_2}{k_1} \quad (6)$$

For biosensors, oxidoreductases, such as glucose oxidase, flavine adenine dinucleotide-dependent glucose dehydrogenase (FAD-GDH), lactate oxidase or alcohol oxidase are frequently applied[196]. One of the most prominent enzymes for biosensors is the flavoprotein glucose oxidase (GOx). It catalyzes the oxidation of β-D-glucose to D-glucono-δ-lactone, while the flavine adenine dinucleotide (FAD) cofactor is reduced to $FADH_2$ and subsequently the enzyme is reoxidized by O_2 producing H_2O_2 (see also Figure 9)[189, 197, 198].

Enzymes reacting with mycotoxins have been primarily studied for their detoxifying properties. Many different enzymes have been proposed for the detoxification of various mycotoxins, such as aflatoxins[199], zearalenone[200], ochratoxins[201], patulin[202], fumonisins[203, 204] or deoxynivalenol[205, 206].

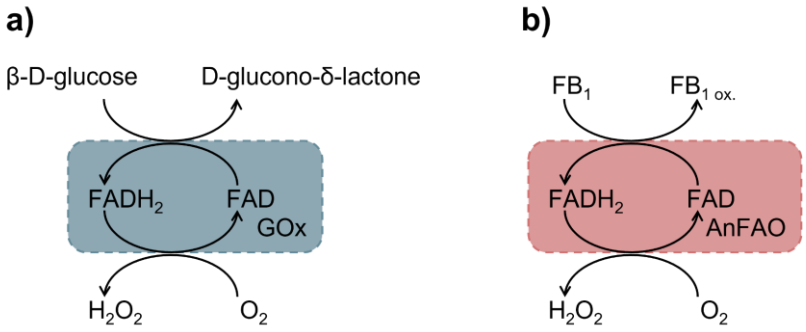

Figure 9 a) Reaction catalyzed by GOx (according to [189, 197, 198]). **b)** Reaction catalyzed by AnFAO (according to Telmer et al.[204]).

In 2020 a new enzyme, termed *Aspergillus niger* fumonisin amine oxidase (AnFAO) has been first reported for its detoxifying properties of fumonisins by Garnham et al.[203]. AnFAO has a tightly bound FAD cofactor and deaminates fumonisins and additional long-chain amino poly alcohols, while H_2O_2 is produced under a broad range of conditions (see also Figure 9)[203]. The recombinant expression of the enzyme could be demonstrated in *E. coli* and in the methylotrophic yeast *Pichia pastoris* at high yields in soluble form[203, 204]. Moreover, it was discovered that AnFAO is ~29%

identical and ~49% similar at the amino acid level to human monoamine oxidase A (MAO A) and monoamine oxidase B (MAO B)[203], which are two enzymes that have been extensively studied for neurotransmitter metabolism. Further monoamine oxidases could be used for the development of electrochemical biosensors[207, 208]. AnFAO is thus a quite promising enzyme for its application in mycotoxin biosensors.

3.2.6 Enzymatic biosensors

Enzymatic biosensors can be constructed by the combination of enzymes with electrodes. Three fundamental types of biosensors, biosensors of the first, second and third generation, can be distinguished (see Figure 10)[16]. First-generation biosensors enable the detection of enzyme-catalyzed reactions by the electrochemical detection of enzyme substrates or reaction products at the electrode[16]. Often natural co-substrates or products are detected, such as H_2O_2 or O_2 for oxidases, such as glucose oxidase. For second generation biosensors a mediated electron transfer between the electrode and enzyme takes place[16]. Frequently used mediators are for example: ferrocene carboxylic acid, ferricyanide, quinones, organic dyes (like viologen, Prussian blue, methylene blue), or osmium and ruthenium complexes[209]. Third generation biosensors are based on direct heterogenous electron transfer between the electrode and the active site of the enzyme[16]. However, for this type of biosensors a very small distance between the active site of the enzyme and the electrode surface is an essential prerequisite, which applies to only a few redox enzymes.

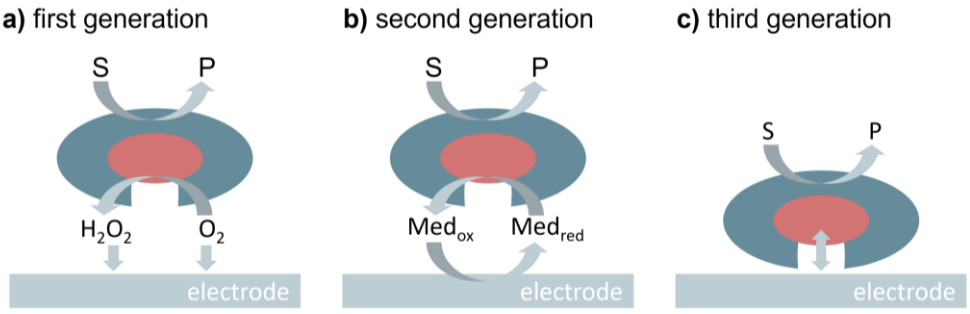

Figure 10 Three generations of enzymatic electrochemical biosensors. **a)** First generation biosensors on the example of an oxidase. A substrate is enzymatically converted to a product, in which O_2 is reduced to H_2O_2. One of the natural co-substrates or products is detected (H_2O_2 or O_2). **b)** In the second generation, artificial redox mediators are used for electrochemical detection. **c)** Third generation biosensors are based on direct heterogenous electron transfer between the enzyme and the electrode.

For food analysis, electrochemical enzymatic biosensors have been rarely reported. On one hand, this might be attributed to the lack of specific enzymes for mycotoxins and, on the other hand, to the fact that the low legal limit values require extremely sensitive methods. Enzymes typically

allow the quantification of analytes down to low micromolar to high nanomolar concentrations and some mycotoxins such as OTA and aflatoxins with legal limits of a few µg per kg, require a higher sensitivity in the nanomolar range. Nevertheless, for some mycotoxins the legal limits are significantly higher. For example, for deoxynivalenol and fumonisins, the European legal limits in unprocessed maize are as high as 1,750 µg kg^{-1} and 2,000 µg kg^{-1}, respectively[8], which equals a few µmol per kg, and therefore would allow their quantification via enzymatic reactions.

An example of an enzymatic mycotoxin sensor was reported by Soldatkin et al.[49]. In this study a pair of gold interdigitated electrodes was used as a conductometric transducer and urease with BSA was co-immobilized to the electrode[49]. The enzymatic reaction with urea generates charged ions (NH_4^+ and HCO_3^-) leading to a change of the solutions conductivity[49]. Patulin works as inhibitor of urease and thus the signal could be correlated to the patulin concentration, allowing the quantification of low micromolar concentrations[49]. However, a higher sensitivity would be required to detect patulin in food samples such as juice, below the European legal limit of 50 µg kg^{-1} (324 nmol kg^{-1})[8].

4 Materials and methods

4.1 Materials

4.1.1 Chemicals

The following chemicals were obtained from Merck (Darmstadt, Germany): Ochratoxin A from Petromyces albertensis, ≥98%; ergocristine, reference substance; sodium citrate monobasic, BioXtra, anhydrous, ≥99.5%; tris(hydroxymethyl)aminomethane (TRIS), sodium chloride BioUltra, ≥99.5%; potassium sorbate, ≥99.0%; potassium phosphate dibasic anhydrous, BioUltra, ≥99.0%; potassium phosphate monobasic, ≥99.0%; sodium phosphate dibasic dihydrate, ≥99.0%; sodium dihydrogen phosphate dihydrate, ≥99%; sodium bicarbonate, ≥99.7%; hydrogen peroxide solution, ≥30%, for trace analysis; sulfuric acid, 95.0–98.0%; N,N-dimethylacetamide (DMA), 99.8%; tetrabutylammonium borohydride (TBABH), 98%; N,N-disuccinimidyl carbonate (DSC) ≥95%; N,N-dicyclohexylcarbodiimide (DCC) for synthesis; N,N-dimethylformamide anhydrous (DMF); 99.8%, N-hydroxysuccinimide (NHS), 98%; Trifluoroacetic acid ReagentPlus, 99%; 2',4'-dihydroxyacetophenone (DHAP) 99%; acetonitrile anhydrous, 99.8%; glycerol for molecular biology, ≥99.0%; 2-mercaptoethanol, ≥99%; phenylmethanesulfonyl fluoride ≥99%; bromophenol blue; ethylenediaminetetraacetic acid disodium salt dihydrate; flavin adenine dinucleotide disodium salt hydrate, ≥95%.

3,3',5,5'-Tetramethylbenzidine (TMB); Tween® 20 and kanamycin sulfate, molecular biology grade, were obtained from Serva Electrophoresis (Heidelberg, Germany). Potassium chloride, 99% and potassium hexacyanoferrate(III), 98+% ($K_3[Fe(CN)_6]$), 99.0-100.5% was bought form Alfa Aesar (Heysham, Lancashire, UK). Ergometrine; ergotamine; fumonisin B_1 and fumonisin B_2 were obtained from LGC Standards (Teddington, Middlesex, UK). Lysergic acid–poly(ethylene glycol)(8)–biotin (lysergic acid–PEG(8)–biotin) was synthesized for this work and provided by ASCA (Berlin, Germany). Agarose standard, for electrophoresis routine applications; magnesium sulfate anhydrous, min. 98.0%; tryptone from casein (trypsin-digested casein); yeast extract; LB broth acc. to Miller powder for liquid medium, LB-agar acc. to Miller, powder, acetic acid, min. 99.5%, 2-propanol, min. 99,8%, methanol for LC-MS, min. 99.95% and ethanol absolute anhydrous, min. 99.5% were obtained from Chemsolute, Th. Geyer (Renningen, Germany). Magnesium chloride hexahydrate, 98.0-101.0% and glycine, min. 99.5% were obtained from PanReacAppliChem (Darmstadt, Germany). D(+)-glucose monohydrate for microbiology was

purchased from Merck Millipore (Darmstadt, Germany). cOmplete™, Mini, EDTA-free protease inhibitor cocktail tablets were obtained from Roche (Basel, Switzerland). MES monohydrat, ≥99%; N,N,N',N'-tetramethylethylendiamin (TEMED); ≥99%; ammonium persulfate and ROTIPHORESE®Gel 30% were obtained from Carl Roth (Karlsruhe, Germany). Imidazole, min. 99.5% and sodium dodecyl sulfate (SDS), min. 99.5% were bought from J.T. Baker, Avantor (Radnor, PA, USA). Coomassie Brilliant Blue G-250, Fisher BioReagents was obtained from Thermo Fisher Scientific (Waltham, MA, USA).

4.1.2 Biological materials

Monoclonal mouse IgG anti-OTA antibodies from three different cell clones (BC10 0.5 mg mL^{-1}, CH2 0.42 mg mL^{-1} and BG4 1 mg mL^{-1}) were provided by Hybrotec (Potsdam, Germany). Mouse monoclonal IgG1 anti-ergot alkaloid antibodies (1 mg mL^{-1}) were obtained from BioTeZ Berlin-Buch (Berlin, Germany). Polyclonal sheep anti-mouse IgG antibodies (R1256P), used as secondary antibodies, were obtained from Acris Antibody (Herford, Germany). Immunoaffinity columns (IAC) for the quantification of fumonisins were purchased from aokin (Berlin, Germany).

Horseradish peroxidase, EIA grade, was obtained from Roche (Basel, Switzerland). Albumin fraction V, biotin-free (NZ-Origin), was obtained from Carl Roth (Karlsruhe, Germany). Poly-HRP streptavidin was purchased from Thermo Fisher Scientific (Waltham, MA, USA). The marker for SDS-PAGE, Precision Plus Protein™ All Blue Standards was obtained from Bio-Rad Laboratories (Hercules, CA, USA). Lysozyme from chicken egg white was purchased from Merck (Darmstadt, Germany). Amplex® Red Hydrogen Peroxide/Peroxidase Assay Kit was obtained from Thermo Fisher Scientific (Waltham, MA, USA).

The pUC-GW-Kan-AnFAO vector was synthesized by Genewiz from Azenta (South Plainfield, NJ, USA). The pET-MBP-mSA2 plasmid was purchased from addgene (Watertown, MA, USA). NiCo21(DE3) Competent *E. coli*, NEB® 10-beta Competent *E. coli* (High Efficiency), NEB 10-beta/stable outgrowth medium, rCutSmart buffer, T4 DNA ligase and the T4 DNA ligase reaction buffer were obtained from NEB (Ipswich, MA, USA). The restriction endonucleases XhoI and NheI-HF were also bought from NEB (Ipswich, MA, USA). The E.Z.N.A.® Plasmid DNA Mini Kit I and the E.Z.N.A.® Micro-Elute Gel Extraction Kit were purchased from Omega Bio-tek (Norcross, GA, USA).

4.1.3 Food samples

Pilsner type beer, organic rye flour (type 997) and organic maize grits (polenta) were obtained from a local supermarket in Berlin.

4.1.4 Further materials

Magnetic Dynabeads™ Protein G for immunoprecipitation and Dynabeads™ M-280 tosyl-activated, both with a diameter of 2.8 µm, were purchased from Thermo Fisher Scientific (Waltham, MA, USA). Screen-printed gold electrodes, 250AT; screen-printed carbon electrodes, 110 and screen-printed Prussian blue/carbon electrodes, 710 were purchased from Metrohm DropSens (Oviedo, Asturias, Spain). A desalting Sephadex™-G25 PD10 column was obtained from GE Healthcare Life Sciences (Chicago, IL, USA). Whatman® qualitative filter paper, grade 1 was obtained from Merck (Darmstadt, Germany). Zeba™ spin micro desalting columns were bought from Thermo Fisher Scientific (Waltham, MA, USA). 30 mL luer lock syringes, Omnifix® Solo and 1 mL syringes, Injekt®-F Luer Solo were purchased from B. Braun (Melsungen, Germany). Ni-NTA Agarose was obtained from Jena Biosciences (Jena, Germany). Ultrapure water from a Milli-Q water purification system (Merck Millipore, Darmstadt, Germany) was used for all experiments.

For all ELISAs, transparent high-binding 96-well polystyrene microplates from Greiner Bio-One (Solingen, Germany) were applied. For all magnetic bead-based immunoassays transparent non-binding 96-well polystyrene microplates from Corning (Corning, NY, USA) were used. For fluorescence assays, black high-binding microplates with 96 wells and a flat bottom plate from Greiner Bio-One (Solingen, Germany) were used.

4.2 Studies on the electrochemistry of TMB[a]

4.2.1 Cyclic voltammetry

A custom-made wall-jet flow cell has been designed using FreeCAD and fabricated from poly(methyl methacrylate), see Figure 15 and Figure 16. All CV measurements were performed in this cell (with interrupted flow), with an Autolab PGSTAT101 potentiostat from Metrohm (Herisau, Switzerland). Measurements were performed at room temperature (RT) and the potential was applied against the on-chip Ag/AgCl reference electrode. The electrochemistry of screen-printed gold and carbon electrodes in buffer (220 mM sodium citrate buffer with 100 mM KCl, pH 4) was studied at pH 4. For each electrode, five CV cycles were measured. Afterwards, the electrochemistry of TMB has been studied on the same electrodes. For this purpose, 30 cycles were performed in 500 µM TMB (in 220 mM sodium citrate buffer with 100 mM KCl, pH 4). Subsequently, the electrodes were rinsed with 3 mL of the buffer, flushed through the flow cell. Finally, with those electrodes, 5 cycles were performed in buffer to compare the response with the initial measurement.

The above-described measurements were repeated at pH 1 in 150 mM sodium citrate buffer with 300 mM H_2SO_4 and 100 mM KCl, on both, screen-printed gold and carbon electrodes.

4.2.2 Amperometric measurements

For the amperometric measurements, a potentiostat (Autolab PGSTAT101, Metrohm, Herisau, Switzerland), screen-printed gold electrodes and the wall-jet flow cell, described above, were used. A flow rate of 600 µL min^{-1} was applied using a syringe pump (Bee Syringe Pump, BASi, West Lafayette, IN, USA). To test the flow cell, amperometric measurements with potassium ferricyanide were conducted at 0 V vs. Ag/AgCl to reduce ferricyanide. Buffer (100 mM potassium phosphate, 100 mM KCl pH 7) was flushed over the screen-printed gold electrode, until the basic current reached a steady state. Afterwards, potassium ferricyanide samples with different concentrations, ranging from 0.2 µM to 10 µM (in 100 mM potassium phosphate buffer with

[a] The content of this section was previously published in the following article: Höfs, S.; Hülagü, D.; Bennet, F.; Carl, P.; Flemig, S.; Schmid, T.; Schenk, J. A.; Hodoroaba, V. D.; Schneider, R. J., Electrochemical immunomagnetic ochratoxin A sensing: Steps forward in the application of 3,3',5,5'-tetramethylbenzidine in amperometric assays. ChemElectroChem 2021, 8 (13), 2597-2606.

100 mM KCl, pH 7), were flushed over the electrode until the redox current reached a steady state. After each sample, buffer was passed through the flow system until the basic current was stable again. To evaluate the repeatability, each concentration was measured three times (see Figure A 1).

To quantify the fully oxidized TMB, a potential of 300 mV vs. Ag/AgCl was applied. The influence of TMB (reduced) and H_2O_2 on the amperometric signal was tested. For this, amperometric measurements with 5 mM H_2O_2 and 0.5 mM TMB in 150 mM sodium citrate buffer with 300 mM H_2SO_4 and 100 mM KCl were performed (see Figure A 2). Furthermore, the repeatability of the current signal in amperometric measurements with oxidized TMB (6.5 µM) in 150 mM sodium citrate buffer with 300 mM H_2SO_4, 100 mM KCl at pH 1 and screen-printed gold electrodes has been tested at 300 mV vs. Ag/AgCl and a flow rate of 600 µL min^{-1} (see Figure A 3).

4.2.3 Raman microspectroscopy[b]

Raman spectra were obtained as reported by Schmid and Dariz[210]. A LabRam HR 800 instrument from Horiba (Kyoto, Japan) was coupled to a BX41 microscope from Olympus (Tokio, Japan). For excitation and collection of scattered light, a 50x/NA = 0.55 long working distance objective lens was applied. The system uses a diode-pumped solid-state (DPSS) laser (532 nm wavelength, 300 mm^{-1} grating). It offers a resolution of the spectra that were acquired with a Peltier cooled (-60°C operating temperature) charge-coupled device (CCD) camera (Syncerity CCD, Horiba Jobin Yvon) of about 3.4 cm^{-1} per CCD pixel at 1000 cm^{-1} Raman shift, 3.2 cm^{-1} at 1500 cm^{-1} and 2.6 cm^{-1} at 3000 cm^{-1}. For all measurements, the entrance slit of the spectrometer was 100 µm wide and the confocal pinhole was fully open (1000 µm). Previously to the measurements with the electrodes, the laser was allowed to stabilize for 1 h and the spectrometer was calibrated against a Raman band of silicon at 520.7 cm^{-1}.

The electrodes were investigated after the cyclic voltammetry with TMB at carbon and gold screen-printed electrodes has been conducted at different pH values (pH 1 and pH 4) as described above (see 4.2.1). Thereafter, the electrodes were rinsed with Milli-Q water and analyzed with Raman microspectroscopy to identify potential TMB precipitates on the electrode surfaces. A reference

[b] Raman microspectroscopy was conducted by Dr. Thomas Schmid, BAM.

spectrum was produced by using an electrode of each type (carbon and gold) containing visible precipitates (which was not rinsed with Milli-Q water). Raman spectra were recorded at the marked crosses in the microcopy images (see Figure A 5 and Figure A 6) using a laser power of 4 mW (full power attenuated to 10% while using a neutral density filter). Under the chosen conditions the diameter of the laser spot is approximately 1 µm and the depth resolution in transparent samples with open confocal pinhole is estimated to 40 µm[210]. Here the strongly absorbing and scattering carbon and the highly reflective gold surface limits the depth resolution since the optical penetration depth is limited.

4.2.4 Scanning electron microscopy[c]

Scanning electron microscopy was performed with a Scanning Electron Microscope (SEM, Zeiss Supra 40, Oberkochen, Germany) equipped with a high-resolution cathode (Schottky field emitter), an Everhart-Thornley secondary electron (SE) detector and an InLens SE detector.

4.3 ELISA and magnetic bead-based immunoassay for OTA[d]

4.3.1 Tracer Synthesis – OTA-HRP

An OTA-HRP tracer was synthesized by the activation of the carboxylic group of OTA with DCC/NHS and subsequent binding to amino groups of HRP. A 0.5 M stock solution was prepared freshly for both DCC and NHS. 6 µmol OTA were dissolved in 15 µl DMF. 7.2 µmol NHS, 3.9 µmol DSC and 7.2 µmol DCC were added in this order. The mixture was incubated overnight at RT under shaking at 800 rpm with a ThermoMixer from Eppendorf (Hamburg, Germany). Subsequently, the reaction mixture was centrifuged at 10,000 x g. The supernatant was further used for the reaction with HRP. 2.2 mg HRP were dissolved in 250 µL 0.13 M $NaHCO_3$ and tempered to 2 °C. 9 µL of NHS-OTA ester were added, stepwise under constant shaking (3 µl every 5 min). Afterwards, the reaction mixture was shaken for 3 h at 2 °C. To separate the obtained tracer from other components of the reaction mixture, gel permeation chromatography with a Sephadex™-G25

[c] SEM was conducted by Sigrid Benemann and Deniz Hülagü, BAM.

[d] The content of this section was previously published in the following article: Höfs, S.; Hülagü, D.; Bennet, F.; Carl, P.; Flemig, S.; Schmid, T.; Schenk, J. A.; Hodoroaba, V. D.; Schneider, R. J., Electrochemical immunomagnetic ochratoxin A sensing: Steps forward in the application of 3,3',5,5'-tetramethylbenzidine in amperometric assays. ChemElectroChem 2021, 8 (13), 2597-2606.

PD10 column was applied. To equilibrate the column, it was filled with 25 mL 1:10 diluted PBS (pH 7.6). Afterwards, the column was filled with the reaction mixture, and the sample was eluted with 7.5 mL of 1:10 diluted PBS (pH 7.6). The eluate was collected with three drops per fraction in a transparent microplate. The fractions were analyzed with UV/Vis measurements at a wavelength of 405 nm, referenced to 280 nm. The three fractions with the highest optical density (OD) were pooled, and the tracer was stored at 4 °C. The HRP concentration could be determined with a calibration function using HRP standards and UV/Vis measurements at a wavelength of 405 nm, referenced to 280 nm with a microplate reader (SpectraMaxi3, Molecular Devices, San José, CA, USA). The coupling density of OTA per HRP was determined with MALDI-ToF-MS as described in 4.3.2.

4.3.2 MALDI-ToF-MS

A MALDI-ToF-mass spectrometer (Autoflex III, Bruker Daltonics, Bremen, Germany) was used to determine the degree of labeling of the HRP tracer with OTA. The experiments were conducted with a nitrogen laser at an acceleration voltage of 20 kV. 10 µL of HRP and 10 µL of the OTA-HRP tracer (1.8 mg mL^{-1}) were desalted with a Zeba™ Micro Desalt Spin Column. The column was centrifuged at 10,000 rpm for 90 s. Afterwards, the samples were eluted with 10 µL Milli-Q water (20 mg mL^{-1} in ethanol). 125 µL of diammonium citrate solution (18 mg mL^{-1} in H_2O) were mixed with 375 µL of DHAP solution (20 mg mL^{-1} in ethanol) to prepare the matrix. A mixture of 2 µL sample, 2 µL of matrix, and 2 µL of 2% trifluoroacetic acid was applied to the target and dried. Afterwards, the MALDI-ToF-MS measurement was performed.

4.3.3 ELISA

For the direct competitive OTA ELISA with an OTA-HRP tracer and TMB/H_2O_2 as enzymatic substrate, transparent high-binding 96-well microplates were used. All incubation steps were performed at RT under shaking at 750 rpm on a 101 plate shaker (Heidolph, Schwabach, Germany). The plates were washed with a plate washer (ELx405 Select™, BioTek Instruments, Bad Friedrichshall, Germany) with three cycles per washing step using a wash buffer (0.75 mM potassium dihydrogen phosphate, 6.25 mM dipotassium hydrogen phosphate, 0.025 mM potassium sorbate, 0.05% (v/v) Tween® 20, pH 7.6). A TMB stock solution (40 mM) was prepared under argon in DMA containing 8 mM TBABH and was stored in the dark at 4 °C.

At first, 200 µL of secondary sheep anti-mouse antibody (1 mg L^{-1} in PBS, pH 7.6) were added to each well of the microplate. After 16 h of incubation, the plate was washed and coated with primary mouse anti-OTA IgG antibodies (from cell clone CH2, BG4 or BC10) with 200 µl per well (with optimized antibody concentrations for CH2: 42 ng mL^{-1}, BG4: 25 ng mL^{-1} and BC10: 25 ng mL^{-1}). After 1 h of incubation, the plate was washed again. Then, 150 µL of OTA standard solutions, prepared in Tris buffer (10 mM Tris, 150 mM NaCl) with concentrations ranging from 1 ng L^{-1} to 1 mg L^{-1}, and 50 µL of OTA-HRP tracer were added. The tracer concentrations were optimized for each antibody (80 ng mL^{-1} for CH2, 45 ng mL^{-1} for BG4 and 90 ng mL^{-1} for BC10). The plate was incubated for 30 min and washed afterwards. Finally, TMB/H_2O_2 substrate solution was added with 200 µl per well (360 µM TMB, 3.7 mM H_2O_2 in 220 mM sodium citrate buffer, pH 4) and incubated for 20 min until 100 µl of 1 M H_2SO_4 were added per well to stop the reaction. The OD was measured at a wavelength of 450 nm referenced to 620 nm. The arithmetic means of the measured OD values were plotted against concentration and a four-parameter logistic function was fitted to the data.

4.3.4 Magnetic bead-based immunoassay

The magnetic bead-based immunoassay for OTA was performed in transparent non-binding 96-well microplates. Protein G decorated magnetic beads were used to capture the anti-OTA antibodies. All incubation steps were performed at RT under shaking at 1,000 rpm on a 101 plate shaker (Heidolph, Schwabach, Germany). The beads were washed with the same wash buffer as used for the ELISA described above (see section 4.3.3). For this, wash buffer was added to each well containing the beads and manually removed with a multi-channel pipette and while the beads were magnetically captured with a plate separator (BioMag® 96-well plate separator, Polysciences, Warrington, PA, USA). This procedure was repeated two times for each washing step. The TMB stock solution was prepared as described in section 4.3.3.

For a single assay with 96 samples, 40 µL of the magnetic bead dispersion (30 mg mL^{-1}) were used. The beads were captured with a magnet in a 1.5 mL reaction tube, and the supernatant was removed. 200 µL PBS (pH 7.6) and 1 µL anti-OTA antibody solution (BG4, 1 mg mL^{-1}) were added to the beads and incubated for 30 min under shaking with a ThermoMixer at 1,000 rpm and RT. Afterwards, the beads were washed three times with 500 µL wash buffer and subsequently dispersed in 12 mL Tris buffer (10 mM Tris, 150 mM NaCl) by vortexing. 100 µL of the bead

dispersion was added to each well of a microplate and the supernatant was removed, while the beads were magnetically captured. 150 µL of the OTA standard solutions (as described in section 4.3.3) or 150 µl of the diluted beer samples and 50 µL of the OTA-HRP tracer (44 ng mL^{-1}) were added to beads and incubated under shaking for 30 min. The beads were washed and 200 µl of TMB/H_2O_2 substrate solution (360 µM TMB, 3.7 mM H_2O_2 in 220 mM sodium citrate buffer, pH 4) was added to each well and incubated for 20 min. The reaction was stopped by the addition of 100 µL of 0.9 M H_2SO_4 with 0.3 M KCl. The stop solution contained 300 mM KCl to adjust the Cl^- concentration of the samples to 100 mM for amperometric measurements. As described above, the OD was measured at a wavelength of 450 nm, referenced to 620 nm. Finally, the amperometric read-out was performed as described below (see section 4.3.6).

4.3.5 Preparation of beer samples

The beer samples (Pilsner type) were degassed by filtration through a Whatman® 1 filter. Subsequently the samples were diluted 1:1, 1:5 or 1:10 with Tris buffer (10 mM Tris, 150 mM NaCl). The samples were spiked with OTA resulting in concentrations in a range from 1 ng L^{-1} to 1 mg L^{-1}.

4.3.6 Amperometric measurements

Amperometric measurements were performed as described in section 4.2.2 at a potential of 300 mV vs. Ag/AgCl and a flow rate of 600 µL min^{-1}. 3.7 mM H_2O_2 and 360 µM TMB, as used for the magnetic bead-based immunoassay, were added to the running buffer (150 mM sodium citrate buffer, 300 mM H_2SO_4, 100 mM KCl, pH 1). The amperometric read-out of the magnetic bead-based OTA immunoassay in beer samples was performed with a handheld potentiostat EmStat3 Blue (PalmSens, Netherlands) connected via Bluetooth to an android smartphone (Samsung).

4.4 ELISA and magnetic bead-based immunoassay for ergometrine[e]

4.4.1 ELISA

For the competitive ELISA for ergometrine, transparent high-binding 96-well microplates were applied. The incubation steps, washing cycles and the preparation of the TMB stock solution were performed as described above (see section 4.3.3). The calibration standards for ergometrine, ergotamine and ergocristine were prepared from a 0.5 mg mL^{-1} stock solution. The stock solutions were produced under argon. The ergometrine stock solution was prepared in acetonitrile:water, 90:10 (v/v) and the ergotamine and ergocristine stock solutions were prepared in acetonitrile. Aliquots of the stock solutions were stored at -20 °C and used only for a single time after thawing.

The microplate was coated with secondary anti-mouse antibody from sheep, with 200 µl (1 mg L^{-1}) per well and incubated for 16 h. The plate was washed and filled with 300 µL of biotin-free BSA solution (10 mg mL^{-1} in PBS, pH 7.6). After 1 h of incubation, another washing step was performed before 200 µL of the of primary mouse anti-ergot alkaloid antibody (1.33 ng mL^{-1}, in PBS, pH 7.6) were added to each well. The plate was incubated for 1 h and washed afterwards. Subsequently, the plate was incubated for 30 min with ergometrine, ergotamine or ergocristine standards (in 10 mM Tris buffer with 150 mM NaCl, pH 8.5) and the lysergic acid PEG(8)-biotin tracer. For this, 150 µL of the standards and 50 µL of the lysergic acid PEG(8)-biotin tracer (7.5 ng mL^{-1} in 10 mM Tris buffer with 150 mM NaCl, pH 8.5) were added per well. To test the influence of preincubation of the antibody with the analyte on the sensitivity of the assay, the tracer was added directly or after 5 min, 10 min or 15 min of substrate incubation. After this incubation step, the plate was washed and incubated for 30 min with 200 µl of poly-HRP-streptavidin (20 ng mL^{-1}, in PBS, pH 7.6) per each well. The plate was washed again. Finally, the plate was incubated for 20 min with TMB/H_2O_2, stopped with H_2SO_4 and read-out optically as described in section 4.3.3.

[e] The content of this section was previously published in the following article: Höfs, S.; Jaut, V.; Schneider, R. J., Ergometrine sensing in rye flour by a magnetic bead-based immunoassay followed by flow injection analysis with amperometric detection. Talanta 2023, 254, 124172.

Both, the tracer, and the antibody concentrations were diluted as far as possible while still achieving a sufficient OD value around 1, to obtain the optimized concentrations used for this immunoassay (see Figure A 10).

4.4.2 Magnetic bead-based immunoassay

The magnetic bead-based immunoassay for ergometrine was performed in transparent non-binding 96-well microplates. Protein G decorated magnetic beads were used to capture the anti-ergometrine antibodies. The incubation and the washing steps were performed under the same conditions as described in section 4.3.4.

For one assay with 96 samples, 240 µL of the magnetic bead dispersion (30 mg mL^{-1}) were used. The beads were captured with a magnet in a 2 mL reaction tube, and the supernatant was removed. 1.2 mL PBS (pH 7.6) and 6 µL of anti-ergot alkaloid antibody solution (1 mg mL^{-1}) were added to the beads and incubated for 30 min under shaking with a ThermoMixer at 1,000 rpm and RT. Afterwards, the beads were washed three times with 500 µL wash buffer and subsequently dispersed in 33 mL PBS (pH 7.6) by vortexing. 300 µL of the bead dispersion was added to each well of a microplate and the supernatant was removed, while the beads were magnetically captured. 150 µl of the ergometrine standard solutions (in 10 mM Tris, 150 mM NaCl, pH 8.5) were added to each well containing the antibody-decorated beads. The beads were incubated with the standards for 15 min before 50 µL of the lysergic acid PEG (8)-biotin tracer (7.5 ng mL^{-1} in Tris buffer, 10 mM Tris, 150 mM NaCl, pH 8.5) were added to each well. The beads were incubated for another 15 min. After a washing step the beads were incubated for 30 min with poly-HRP streptavidin (20 ng mL^{-1}, in PBS, pH 7.6) and washed again. Finally, the plate was incubated for 20 min with TMB/H_2O_2, stopped with 0.9 M H_2SO_4 containing 0.3 M KCl. Optical read-out was carried out as described in section 4.3.4.

4.4.3 Amperometric measurements in a flow injection system

A flow injection system was constructed by using a manual six-port injection valve (RH 7725i IDEX, Oak Harbor, WA, USA), teflon tubing, 30 mL luer/lock syringes and a syringe pump (model Fusion 720, Chemyx, Stafford, TX, USA). Flow rates between 0.5 and 4 mL min^{-1} have been used. A bubble trap (Darwin Microfluidics, Paris, France) was connected upstream to the wall-jet flow cell (as described in section 4.2.1), to remove air bubbles from the flowing solution (see also Figure

21 a). A sample loop of 300 µL was constructed from Teflon tubing. For each injection, the sample loop was overfilled with at least 600 µL, ensuring complete filling. Samples were injected into the running flow for amperometric measurements by flipping the switch of the injection valve. Amperometric measurements were performed with an EmStat3 Blue handheld potentiostat (PalmSens, Houten, The Netherlands), connected either to the laptop or via Bluetooth to an android smartphone. A Faraday cage (Metrohm, Herisau, Switzerland) was applied to shield the flow cell.

Screen-printed gold electrodes were used for all amperometric measurements. KCl was added at a molarity of 100 mM to each sample and to the running buffer, to obtain a 100 mM Cl^- concentration, stabilizing the reference electrode potential. To analyze the influence of the flow rate, potassium ferricyanide samples were analyzed amperometrically. 10 µM ferricyanide samples were injected to the running flow of the buffer (100 mM potassium phosphate buffer, 100 mM KCl, pH 7). The ferricyanide samples were prepared in the same buffer. For the injection, the samples were filled into a 1 mL syringe and subsequently filled into the ample loop for injection.

For the read-out of the magnetic bead-based immunoassay for ergometrine, amperometric measurements were performed directly after optical detection has been conducted. To ensure complete filling of the sample loop, three replicate samples from the magnetic bead-based immunoassay were pooled to obtain a total volume of 900 µL. The TMB/H_2O_2 substrate solution (360 µM TMB, 3.7 mM H_2O_2 in 220 mM sodium citrate buffer, pH 4) mixed with the stop solution (0.9 M H_2SO_4, 0.3 M KCl) in a 2:1 ratio was used as running buffer for amperometric measurements. A flow rate of 4 mL min^{-1} and a potential of 300 mV vs. Ag/AgCl was applied. The first injection was performed after the basic current reached a steady level. Further injections were performed after the baseline current returned to the steady state.

4.4.4 Detection of ergometrine in spiked rye flour samples

2 g rye flour samples were spiked with 200 µL PBS (pH 7.6) containing 50 ng, 125 ng, 250 ng and 500 ng of ergometrine. The samples were stored for one hour in an open vessel at RT. Afterwards, 10 mL of PBST (phosphate-buffered saline with 0.05% Tween®, pH 7.6) were added to the spiked flour. The samples were vortexed carefully for 2 min. For a matrix-matched calibration the extraction procedure was also applied to unspiked flour. The samples were centrifuged at 10,000 rpm for 10 min, and the supernatant was analyzed by the magnetic bead-based immunoassay. The extracts were diluted 1:5 in PBS (pH 7.6). To analyze the samples, the magnetic bead-based

immunoassay for ergometrine was performed as described in section 4.4.2. With the exception that the 1:5 diluted extracts of unspiked flour were used for the preparation of the ergometrine standards and that PBS was used as diluent for the lysergic acid PEG(8)-biotin tracer (7.5 ng mL^{-1}, pH 7.6).

4.5 Enzymatic fumonisin assays using AnFAO

4.5.1 Recombinant protein expression and purification of AnFAO[f]

All buffers and media used for the recombinant protein expression were autoclaved at 121 °C for 20 min with a LABOKLAV 160-MSV (SHP Steriltechnik AG, Detzel, Germany).

A vector containing the codon-optimized DNA sequence encoding for AnFAO and a kanamycin resistance gene (pUC-GW-Kan-AnFAO) was synthesized by Genewiz from Azenta (South Plainfield, NJ, USA). To insert the DNA sequence of AnFAO into the expression vector pET-MBP-mSA2, the pUC-GW-Kan-AnFAO vector and the expression vector were cleaved enzymatically, using the restriction endonucleases XhoI and NheI-HF in rCutSmart buffer at 37 °C for 15 min. The cleaved products were analyzed in 1% agarose gel in 1xTAE-buffer (40 mM Tris-acetate, 1 mM EDTA, pH 8.3) performed for 40 min at 90 V. The bands for the codon-optimized sequence for AnFAO and the vector backbone, pET-MBP, were cut out from the gel and the DNA fragments were extracted with the E.Z.N.A.® Micro-Elute Gel Extraction Kit (Omega Bio-tek, GA, USA) according to the manufacturer's protocol. Ligation was performed using a T4 ligase using a 1:3 ratio of vector (pET-MBP) and insert (AnFAO) in T4 DNA ligase reaction buffer at 16 °C overnight. Afterwards, the vector containing the codon-optimized sequence (pET-MBP-AnFAO), was transformed into NEB-10 beta competent *E. coli* cells. For this, plasmid DNA and competent cells were incubated for 30 min on ice. Subsequently, transformation was performed via a heat shock for 30 s at 42 °C on a ThermoMixer. The cells were stored for 5 min on ice and afterwards incubated in NEB10-beta Outgrowth Medium for 1 h at 37 °C and 300 rpm on a ThermoMixer. To select transformed cell clones the cell suspension was plated onto an LB agar plate (40 g L^{-1} of LB-Agar powder, acc. to Miller), supplemented with 30 µg mL^{-1} kanamycin and 2% glucose. The plate was wrapped with parafilm and incubated over night at 37 °C in an incubation shaker. Inoculated liquid cultures were grown in 10 mL LB medium (10 g L^{-1} tryptone,

[f] The protocol for the recombinant protein expression of MBP-AnFAO was established by Rabia Bayram, BAM.

5 g L^{-1} yeast extract, 10 g L^{-1} NaCl) containing 30 µg mL^{-1} kanamycin and 2% glucose under shaking at 200 rpm and 37 °C in an incubation shaker (ZWYR-293, Labwit Scientific, Burwood East, Victoria, Australia). The plasmids were isolated with an E.Z.N.A.® Plasmid DNA Mini Kit I, according to the manufacturer's protocol and the plasmid was sequenced by LGC Genomics (Teddington, UK).

The plasmid DNA (pET-MBP-AnFAO) and the *E. coli* NiCo21(DE3) cells were incubated for 30 min on ice. Subsequently, transformation was performed via a heat shock for 30 s at 42 °C on a ThermoMixer. The cells were stored for 5 min on ice and afterwards incubated in SOC medium (20 mM glucose, 10 mM $MgCl_2$, 10 mM $MgSO_4$, 10 mM NaCl, 2.5 mM KCl, 2% tryptone, 0.5% yeast extract) for 1 h at 37 °C and 300 rpm on a ThermoMixer. Finally, the transformed cell suspension was plated onto an LB agar plate containing 40 g L^{-1} of LB-Agar powder (acc. to Miller) and 30 µg mL^{-1} kanamycin. The plate was wrapped with parafilm and incubated over night at 37 °C in an incubation shaker.

With a sterile toothpick, clones were picked and incubated over night at 37 °C in 5 mL LB medium (10 g L^{-1} tryptone, 5 g L^{-1} yeast extract, 10 g L^{-1} NaCl) containing 30 µg mL^{-1} kanamycin and 2% glucose using the incubation shaker at 200 rpm. Prewarmed TB medium (17 mM KH_2PO_4, 72 mM K_2HPO_4, 12 g L^{-1} tryptone, 24 g L^{-1} yeast extract, 4% (v/v) glycerol) containing 30 µg mL^{-1} kanamycin was inoculated 1:100 with overnight culture and grown under shaking at 200 rpm and 37 °C in an incubation shaker until the OD at 600 nm of 0.5 was reached. Protein expression was induced with 0.5 mM isopropyl β-D-1-thiogalactopyranoside (IPTG) and the culture was incubated overnight at 16 °C under shaking at 200 rpm. *E. coli* cells were harvested by centrifugation at 10,000 x g and 4 °C for 20 min. The cell pellets were stored at -20 °C.

For cell lysis, the pellet was thawed and resuspended in lysis buffer (50 mM MES, 500 mM NaCl, 14.3 mM 2-mercaptoethanol, 0.1 mM phenylmethanesulfonyl fluoride, 5 mM imidazole, 40 µM of the flavine adenine dinucleotide (FAD) cofactor and one protease inhibitor cocktail tablet per 25 mL buffer). Thereafter, 1.5 mg lysozyme per mL^{-1} resuspended cells was added. The cells were treated with 10 s ultrasonic pulses with 10 s cooling, repeated three times using a sonicator (QSonica Q125, Newtown, CT, USA). The lysate was centrifuged at 10,000 x g and 4 °C for 20 min. Purification of the enzyme, produced as maltose-binding protein (MBP) fusion protein, was performed via its polyhistidine-tag (His-tag), using Ni-NTA agarose from Jena Biosciences

(Jena, Germany) for immobilized metal affinity chromatography (IMAC) according to the manufacturer's protocol. The protein concentration of the eluate fractions was determined by measuring the absorption at 280 nm. Fractions of the highest enzyme concentration were pooled and dialyzed (molecular weight cut-off: 12.4 kDa) over night at 4 °C against MES buffer (50 mM MES, 150 mM NaCl, 5 µM FAD, pH 6) in stirred solution. The purified solution was aliquoted and stored at -20 °C.

4.5.2 SDS-PAGE

SDS-PAGE has been performed according to Laemmli[211]. 1 mm thick polyacrylamide gels with 12% separating gel and 4% stacking gel were prepared. The separating gel was prepared by mixing the following components in the listed order: 4.12 mL Milli-Q water, 0.13 mL 10% SDS, 3.13 mL 1.5 M Tris-HCl pH 8.8, 5 mL 30% acrylamide, 125 µL 10% APS, 5 µL TEMED. The solution was filled into a gel chamber (Hoefer™ Gel Casters for Mini Vertical Electrophoresis Systems, Hoefer, Holliston, MA, USA) and covered with isopropanol. After polymerization, the isopropanol was removed, and the separating gel was prepared. For this, the following components were mixed in the listed order: 3 mL Milli-Q water, 50 µL 10% SDS, 1.3 mL 0.5 M Tris-HCl pH 6.8, 0.7 mL 30% acrylamide, 50 µL 10% APS, 5 µL TEMED. After polymerization, the SDS-gel could be applied for SDS-PAGE.

5 µL of each sample was mixed with 2.5 µL Milli-Q water and 2.5 µL SDS running buffer (200 mM Tris-base pH 6.8, 40% (v/v) glycerol, 8% SDS, 0.004% bromophenol blue). The samples were heated to 95 °C for 5 min in a ProFlex PCR System from Thermo Fisher Scientific (Waltham, MA, USA). The electrophoresis chamber (miniVE Vertical Electrophoresis System, Hoefer, Holliston, MA, USA) was filled with running buffer (25 mM Tris-base, 250 mM glycine, 0.1% SDS) and the pockets of the gel were filled with 8 µL of the samples. One lane was filled with 5 µL of the marker (Precision Plus Protein™ All Blue Standards). Separation was performed for 55 min at 150 V using an Electrophoresis Power Supply system from Amersham Biosciences (Amersham, UK). Subsequently, the gel was stained under shaking for 30 min in Coomassie (2.9 mM Coomassie in water with 45% ethanol and 10% acetic acid). Afterwards, the gel was destained under shaking overnight in Milli-Q water.

4.5.3 Optical activity measurements of AnFAO

To test the activity of the recombinantly expressed MBP-AnFAO by the detection of enzymatically produced H_2O_2 under different conditions, an Amplex Red hydrogen peroxide/peroxidase assay kit was used. The assay was performed according to the manufacturer's protocol. H_2O_2, MBP-AnFAO, FB_1 and FB_2 standards were prepared in the reaction buffer of the kit (50 mM sodium phosphate buffer, pH 7.4). The reaction was performed in black microplates. Fluorescence detection was performed at 560 nm excitation and 590 nm emission with a microplate reader (SpectraMax i3, Molecular Devices, San José, CA, USA).

4.5.4 Coupling of AnFAO to magnetic beads

Tosyl-activated Dynabeads were washed three times in PBS buffer (pH 7.6) using 1 mL per 30 mg beads. Subsequently, MBP-AnFAO was mixed with the washed beads at 18.5 µg MBP-AnFAO and 70 µL PBS buffer (pH 7.6) per 1 mg beads. Coupling was performed under shaking in a ThermoMixer at 1,000 rpm and 37 °C for 19 h. Afterwards, the beads were separated from the supernatant under magnetic capturing and washed three times in phosphate buffer (100 mM potassium phosphate, 100 mM KCl, pH 7). Beads with coupled MBP-AnFAO were suspended in phosphate buffer and aliquots of 500 µL bead-dispersion each containing 5.8 mg beads were prepared and used immediately for the FB_1 assay.

4.5.5 Magnetic bead-based FB_1 assay

The supernatant of the MBP-AnFAO beads aliquots, was removed under magnetic capturing of the beads. (The preparation of aliquots is described in 4.5.4.). For calibration, the beads with coupled MBP-AnFAO were incubated with different FB_1 substrate concentrations (0 µM, 1.5 µM, 2.5 µM, 5 µM, 10 µM, 20 µM). To start the enzymatic reaction, 1.55 mL of FB_1 substrate solution prepared in phosphate buffer (100 mM potassium phosphate, 100 mM KCl, pH 7) was added to each aliquot of the beads with coupled MBP-AnFAO. Incubation was performed for 40 min under shaking at 1,000 rpm and 45 °C in a ThermoMixer. Thereafter, the supernatant was collected under magnetic capturing of the beads and analyzed amperometrically as described in 4.5.6.

4.5.6 Amperometric detection of H_2O_2

Amperometric measurements were performed in the custom-made wall-jet flow cell and flow injection system described in 4.2.1 and 4.4.3, respectively. Prussian blue-modified screen-printed carbon electrodes were pretreated amperometrically at -0.1 V vs. Ag/AgCl under continuous flow of 100 µM H_2O_2 in phosphate buffer (100 mM potassium phosphate, 100 mM KCl, pH 7) for 5 min at 600 µL min^{-1}. Thereafter, the electrode was rinsed with phosphate buffer until the basic current reached again the steady state. For each day, a new and freshly pretreated electrode was calibrated with H_2O_2 and subsequently applied for the detection of enzymatically produced H_2O_2. The electrode was calibrated with H_2O_2 concentrations of 0.2 µM, 0.5 µM, 1 µM, 2.5 µM, 5 µM, 10 µM and 20 µM prepared in phosphate buffer at -0.1 V vs. Ag/AgCl. Samples were injected at 4 mL min^{-1} using 300 µL injections (as determined by the sample loop described in 4.4.3) alternating with phosphate buffer.

For the detection of enzymatically produced H_2O_2 in the magnetic bead-based FB_1 assay, the solution containing the FB_1 substrate and the enzymatically produced H_2O_2 was injected into the flow system under the same conditions as used for the H_2O_2 calibration described above.

4.5.7 Detection of fumonisin B_1 in spiked maize grits samples

Extraction and immunoaffinity column clean-up of FB_1 in maize was performed according to Visconti et al.[212]. 10 g of maize grits were spiked with 6 µg of FB_1 (600 µg kg^{-1}) and left to dry for 1.5 h and afterwards stored overnight at 4 °C. Thereafter, 25 mL extraction solution (25% acetonitrile, 25% methanol, 50% water) were added to each sample (spiked and unspiked) and incubated for 20 min under rotation on an overhead shaker RS-RR 5 from Phoenix Instruments (Naperville, IL, USA). Subsequently, the samples were centrifuged for 10 min at 2,500 g and the supernatant was filtered through a Whatman® 1 filter. The pellet was extracted again with 25 mL of the extraction solution, again for 20 min under rotation. Afterwards, the sample was centrifuged under the same conditions as mentioned above. The supernatant was filtered through the same filter paper previously used. The filtrate was diluted 1:5 in PBS (pH 7.6).

For clean-up and pre-concentration, immunoaffinity columns (IACs) for fumonisins were used. The columns were equilibrated with 2 mL PBS (pH 7.6). 12.5 mL of the diluted extract were passed through the columns and afterwards the columns were rinsed with 10 mL (pH 7.6). Elution was

performed by adding 1 mL of methanol to each column under stopped flow and another 2 mL of methanol while the eluate was collected. To increase the FB_1 concentration, eluates of five columns were pooled. The eluate was centrifuged at 15,000 g to remove precipitates. The supernatant was collected, and the solvent was evaporated. The dried residue was stored at 4 °C until it was analyzed.

Before analysis, the dried residues were dissolved in 1.1 mL 100 mM potassium phosphate buffer with 100 mM KCl (pH 7), and 1.01 mL were mixed with 3.9 mg beads with coupled MBP-AnFAO and incubated at 45 °C for 40 min, as described for the FB_1 calibration (see 4.5.5). Amperometric detection was performed as described in 4.5.6.

5 Results and discussion

5.1 Magnetic bead-based electrochemical ochratoxin A Sensing: Steps forward in the application of 3,3',5,5'-tetramethylbenzidine in amperometric assays[g]

5.1.1 Concept of the magnetic bead-based OTA assay with amperometric TMB detection

It was the aim to demonstrate suitable reaction conditions for the electrochemical detection of TMB in an HRP-based magnetic bead-based immunoassay for OTA. Therefore, the stability of the electrode response to TMB and the electrochemical behavior before and after the redox reaction with TMB was investigated. A competitive assay format has been applied to develop the magnetic bead-based OTA assay, in which OTA competes with the tracer (OTA-HRP) for the binding sites at the anti-OTA antibody (see Figure 11).

The enzymatic reaction of the HRP tracer is detected amperometrically. To capture the antibodies, protein G decorated magnetic beads with a size of 2.8 µm were used (see Figure A 7). The protein G has a specific affinity to the Fc region of human, rabbit, mouse or goat IgG antibodies[213], allowing an oriented immobilization of the antibodies. Thus, only a single incubation step of 30 min was required to bind the antibodies to the surface of the beads. Under magnetic capturing of the beads, any unbound species could be removed with a washing step. In comparison to microplate-based ELISA formats, no time-consuming overnight incubation step of the antibody is required here. The particles coated with anti-OTA antibodies were subsequently incubated with different OTA concentrations and the OTA-HRP tracer. After another washing step, the enzymatic substrates TMB/H_2O_2 were added, and TMB was enzymatically oxidized. The reaction was stopped by the addition of H_2SO_4, and the fully oxidized product could be either detected by amperometry or photometry. Screen-printed gold electrodes were applied in a custom-made flow system to detect the oxidized TMB amperometrically. For miniaturization of the detection system, a handheld potentiostat connected via Bluetooth to a smartphone was used.

[g] The results and the content of this section were previously published in the following article: Höfs, S.; Hülagü, D.; Bennet, F.; Carl, P.; Flemig, S.; Schmid, T.; Schenk, J. A.; Hodoroaba, V. D.; Schneider, R. J., Electrochemical immunomagnetic ochratoxin A sensing: Steps forward in the application of 3,3',5,5'-tetramethylbenzidine in amperometric assays. ChemElectroChem 2021, 8 (13), 2597-2606.

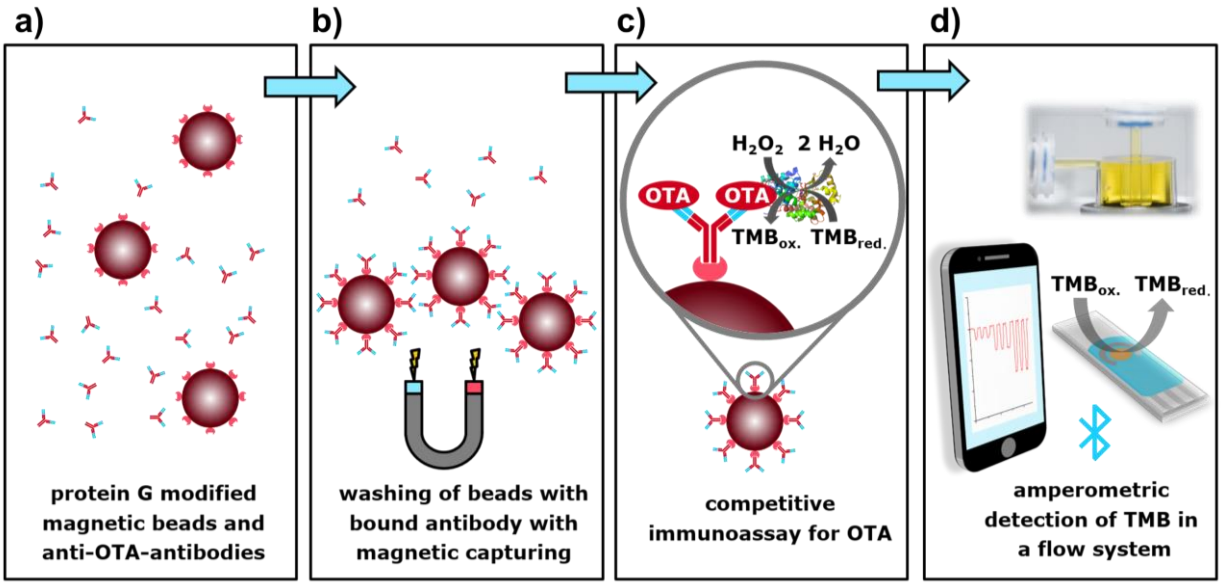

Figure 11 "Schematic illustration of the immunomagnetic assay for OTA with amperometric TMB detection. **a)** Protein G modified magnetic beads are incubated with anti-OTA-antibodies and **b)** subsequently captured by a magnet and washed to remove unbound antibodies. **c)** Afterwards, antibody-functionalized beads are applied to perform a competitive immunoassay for OTA in which OTA competes with an OTA-HRP tracer for the binding sites of the antibody. **d)** The amount of bound OTA is quantified by the enzymatic reaction of the OTA-HRP tracer with H_2O_2 and TMB. Enzymatically oxidized TMB is detected in the presence of H_2SO_4 by amperometry in a custom-made wall-jet flow cell. The signal read-out is performed with a smartphone which is connected via Bluetooth to a miniaturized potentiostat." (Figure and caption reproduced from Höfs et al.[51]).

5.1.2 Cyclic voltammetry of TMB on different electrode materials

A pH value between 5 and 6 is well-suited for the enzymatic reaction of HRP with TMB/H_2O_2, obtaining high turnover rates[147]. However, in sodium citrate buffer at pH 4 TMB is less likely to precipitate than in several other buffer systems with a pH between 5 and 6[214]. Thus, for all immunoassays described in this work, the HRP reaction was performed at pH 4 in sodium citrate buffer. Nevertheless, it is noteworthy, that the ability of TMB to form electroactive precipitates after its enzymatic oxidation with HRP, can also be exploited in biosensors by detecting the precipitates on electrode surfaces[166]. Nevertheless, precipitates on the electrode surface will change the response of the electrode which is disadvantageously for consecutive measurements required for the intended application in immunoassays.

To identify suitable reaction conditions for the detection of TMB in successive measurements, the electrochemistry of TMB has been studied by CV at pH 4 and pH 1 on carbon and gold screen-printed electrodes. For this purpose, 30 CV cycles at pH 4 were performed at both electrode materials, allowing to evaluate the stability of the reaction (see Figure 12 a and d). It could be

observed that the redox reaction of TMB occurs in two steps, since two oxidation and reduction peaks could be detected on both materials, which is in good agreement with other literature reporting a similar behavior on gold electrodes at pH values ranging from 5 to 7.4[167, 215]. The peak potentials obtained with the carbon electrode were 0.21 V and 0.47 V vs. Ag/AgCl and 0.4 V and 0.16 V vs. Ag/AgCl for the oxidation and reduction reaction, respectively. Oxidation peak potentials of 0.23 V and 0.43 V vs. Ag/AgCl and reduction peak potentials of 0.36 V and 0.18 V vs. Ag/AgCl were detected on gold electrodes. Thus, it can be concluded that the electrochemistry of TMB is quite similar on both electrode materials. For both electrode materials it could be observed that the redox currents decreased with the number of cycles and dark blue precipitates were visibly deposited on the electrode surfaces. The electrodes were rinsed with sodium citrate buffer (pH 4) to remove the precipitates and afterwards the same electrode was analyzed again by CV in sodium citrate buffer without TMB. The results were compared to the measurement performed with the fresh electrode. On both, carbon and gold, an electrochemical response of TMB could still be detected, indicating that TMB remains partially at the electrode surface (see Figure 12 b and e).

Raman microspectroscopy of the electrode surfaces (carbon and gold) was conducted according to Schmid and Dariz, to verify the findings (see Figure A 5 and Figure A 6)[210]. For the visible TMB precipitates deposited on the electrode surface after 30 cycles, characteristic Raman spectra corresponding to oxidized TMB could be observed on both materials, which are in good agreement with spectra described in literature[152]. On the gold surface, also after carefully rinsing of the electrodes with Milli-Q water, local residues of TMB precipitates could be identified by their Raman spectra (see Figure A 5 d), which confirms the CV results. On the carbon screen-printed electrode, no residues of TMB precipitates could be identified after rinsing the electrode. This might be attributed to the small penetration depth of Raman measurements caused by optical scattering or by the absorption of TMB inside the porous material. In contrast to the carbon electrodes, the gold electrode provides a rather reflective surface to this technique.

The surface morphology of the screen-printed electrodes, after electrochemical experiments with TMB were characterized by SEM depicted in Figure 12 c and f[h]. The carbon electrode provides a

[h] SEM was conducted by Sigrid Benemann and Deniz Hülagü, BAM.

porous structure with some cracks of a few hundred nanometers, while the gold electrode has a non-porous structure.

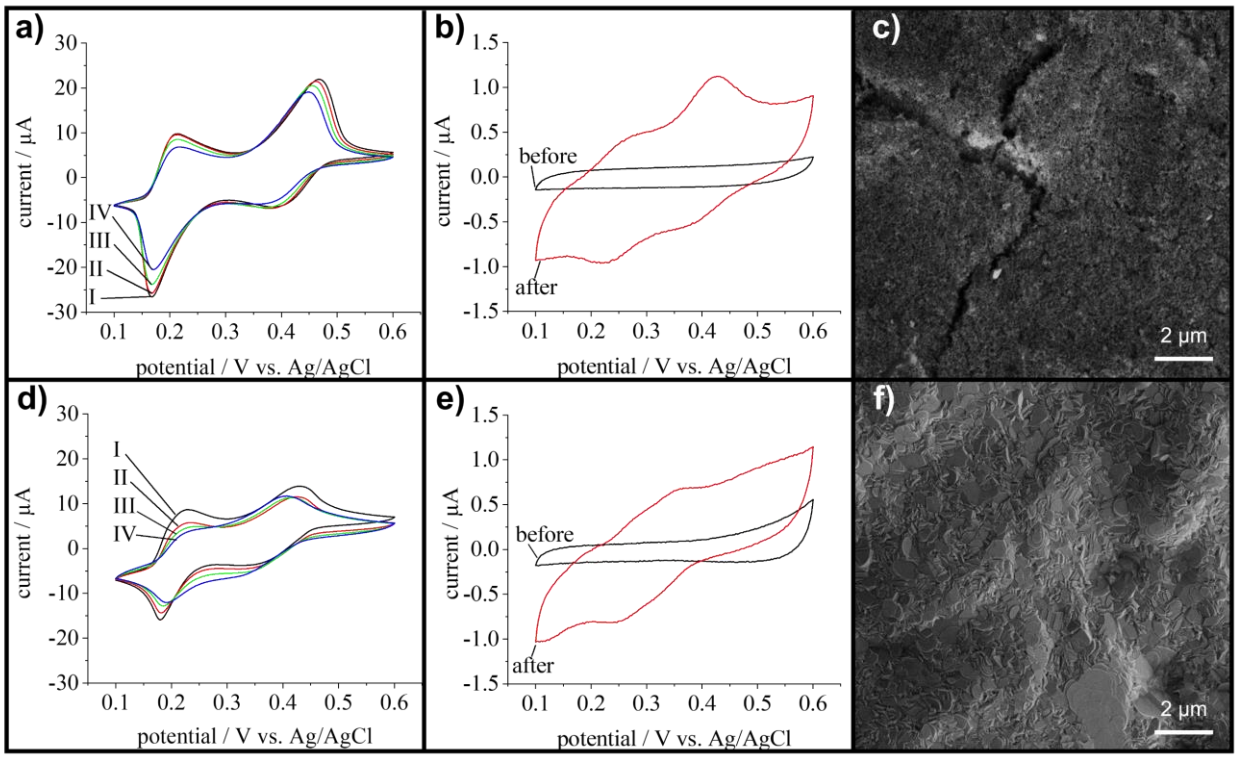

Figure 12 "Cyclic voltammetry of TMB at pH 4 at a scan rate of 100 mV s^{-1} on carbon and gold screen-printed electrodes and corresponding SEM images. **a)** Cycle 2 (I), 10 (II), 20 (III) and 30 (IV) performed in 500 µM TMB at pH 4 in 220 mM sodium citrate buffer with 100 mM KCl at a screen-printed carbon electrode**. b)** Results obtained with the same electrode (carbon) at pH 4 in 220 mM sodium citrate buffer with 100 mM KCl without TMB in solution before and after 30 cycles in TMB were performed. **c)** SEM image of the surface of the carbon screen-printed electrode after the electrochemical measurements presented in a) and b) at an acceleration voltage of 5 kV. **d)** Cycle 2 (I), 10 (II), 20 (III) and 30 (IV) performed in 500 µM TMB at pH 4 in 220 mM sodium citrate buffer with 100 mM KCl at a screen-printed gold electrode. **e)** Results obtained with the same electrode (gold) at pH 4 in 220 mM sodium citrate buffer with 100 mM KCl without TMB in solution before and after 30 cycles in TMB. **f)** SEM image of the surface of the gold screen-printed electrode after the electrochemical measurements presented in d) and e) at an acceleration voltage of 5 kV." (Figure and caption reproduced from Höfs et al.[51]).

Further detailed studies, on the surface morphology and the elemental composition have been conducted by SEM, energy dispersive X-ray spectroscopy (EDS) and Time-of-Flight–Secondary Ion Mass Spectrometry (ToF-SIMS), comparing fresh electrodes with those used for CV with TMB and were reported by Höfs et al.[51]. In short, it can be stated that, no significant morphological differences between fresh electrodes and those used for CV with TMB could be observed for both materials, indicating that no larger precipitates of TMB remain on the electrode surface after rinsing. Furthermore, no significant differences in the elemental composition, analyzed by EDS, could be observed, between fresh carbon electrodes and those applied for TMB electrochemistry.

Also, with the extremely sensitive Tof-SIMS analyzing the upper atomic layers of the carbon electrode surfaces, no residues of TMB could be identified on the upper surface of the carbon electrode, used for CV experiments with TMB. Thus, the results suggest, that TMB precipitates may not remain on the upper surface of the carbon electrode, but rather at a deeper level in pores or cracks of the electrode, causing the remaining redox reaction after the removal of visible precipitates from the electrodes with buffer. In conclusion, at pH 4 neither on carbon nor on gold a stable electrode response could be achieved with TMB. Thus, the CV experiments were repeated on both materials at pH 1 (after the addition of H_2SO_4).

At pH 1, for both, the carbon, and the gold electrode, only one oxidation and reduction peak for TMB could be observed at 0.48 V and 0.43 V vs. Ag/AgCl, respectively (see Figure 13 a and d). Consequently, oxidation and reduction occur in a single step. The electrode response to TMB is stable over 30 cycles with no decrease of the peak currents. In contrast to the experiments at pH 4, no precipitation was visible. Nevertheless, for the carbon electrode, still small redox currents could be detected after rinsing the TMB-treated electrode with buffer, whereas the charging current of the gold electrode shows almost no difference compared to the results obtained with the fresh electrode. Also, for those electrodes, Raman spectroscopy was performed (see Figure A 5 and Figure A 6). At several investigated spots of the TMB exposed electrodes the spectra showed no significant difference to the spectra obtained for the bare electrode. Also, at pH 1 no significant difference of the morphology could be observed by SEM between a fresh and a TMB-exposed electrode. Overall, the results suggest, that the remaining redox current of TMB at the carbon electrode at pH 1 might be related with the porous structure, causing TMB to persist in the structure, while the closed structure of the gold surface facilitates its removal.

For further characterization of the TMB electrochemistry at pH 1, CV was performed at different scan rates (see Figure 14). Both the anodic and the cathodic peak potentials (*E*pa and *E*pc) were not a function of the scan rate, indicating a reversible character of the redox reaction. Furthermore, the peak current ratio was near unity over the whole investigated scan rate range (0.1 -1.2 V). The results suggest that the reaction is diffusion controlled, since the peak currents are a linear function of the square root of the scan rate (see Figure A 8). To the best of knowledge, scan rate dependent CV measurements of TMB at highly acidic pH values were first reported by Höfs et al.[51]. The formal potential of the reaction was 0.437 ± 0.001 V vs. Ag/AgCl, which is in good agreement

with another study, reporting a formal potential of 0.452 V vs. Ag/AgCl for TMB at highly acidic conditions[158].

It can be concluded that the quite reversible character of the reaction allows a stable electrode response, which is highly favorable for the analytic detection of TMB in sequential measurements. Thus, the amperometric detection of TMB for all immunoassay experiments was performed at pH 1.

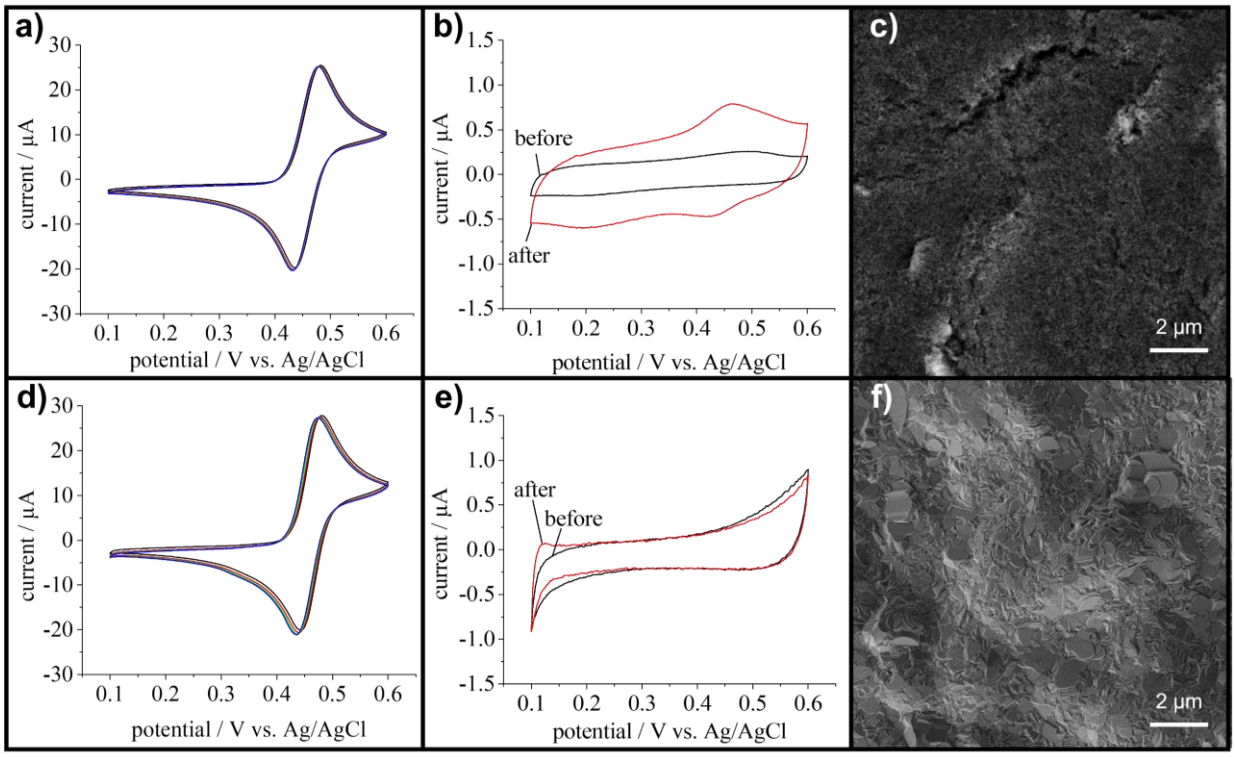

Figure 13 "Cyclic voltammetry of TMB at pH 1 at a scan rate of 100 mV s^{-1} on carbon and gold screen-printed electrodes and corresponding SEM images. **a)** Cycle 2, 10, 20 and 30 performed in 500 µM TMB at pH 1 in 150 mM sodium citrate buffer with 300 mM H_2SO_4 and 100 mM KCl at a screen-printed carbon electrode. **b)** Results obtained with the same electrode (carbon) at pH 1 in 150 mM sodium citrate buffer with 300 mM H_2SO_4 and 100 mM KCl without TMB in solution before and after 30 cycles in TMB were performed. **c)** SEM image of the surface of the carbon screen-printed electrode after the electrochemical measurements presented in a) and b) at an acceleration voltage of 5 kV. **d)** Cycle 2, 10, 20 and 30 performed in 500 µM TMB at pH 1 in 150 mM sodium citrate buffer with 300 mM H_2SO_4 and 100 mM KCl at a screen-printed gold electrode. **e)** Results obtained with the same electrode (gold) at pH 1 in 150 mM sodium citrate buffer with 300 mM H_2SO_4 and 100 mM KCl without TMB in solution before and after 30 cycles in TMB. **f)** SEM image of the gold screen-printed electrode after the electrochemical measurements presented in d) and e) at an acceleration voltage of 5 kV." (Figure and caption reproduced from Höfs et al.[51]).

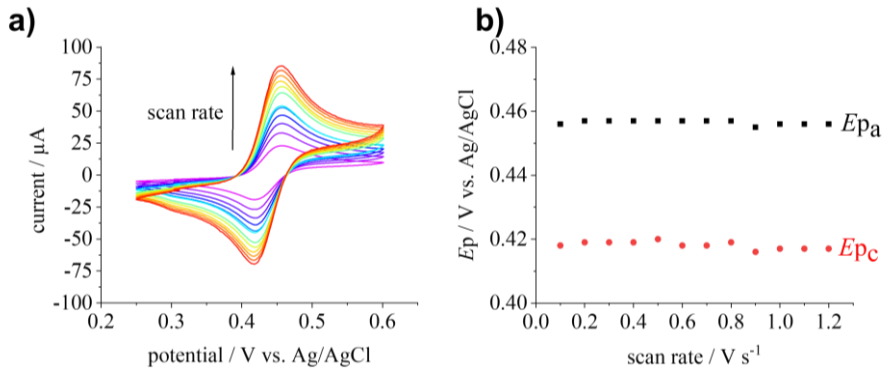

Figure 14 "**a)** Cyclic voltammetry with scan rates ranging from 0.1 – 1.2 V s^{-1} performed in 500 µM TMB at pH 1 in 150 mM sodium citrate buffer with 300 mM H_2SO_4 at a screen-printed gold electrode. **b)** Peak potentials (*E*p) obtained for the anodic (Ep_a) and cathodic peak (Ep_c) vs. the scan rate." (Figure and caption reproduced from Höfs et al.[51]).

5.1.3 Development of a wall-jet flow cell for screen-printed electrodes

On the market, there are quite a few flow cells available for screen-printed electrodes. However, they often suffer from air bubble build-up on the electrode surface or leakage. Narrow flow chambers can cause the adherence of air bubbles on the surface of the reaction chamber and the electrode and can therefore lead to interferences in the electrochemical reaction. Another problem is an uneven force distribution on sealing elements (O-rings) which can cause leakage.

Therefore, a custom-made wall-jet flow cell for screen-printed electrodes was designed by CAD and fabricated from poly(methyl methacrylate) in an in-house workshop, solving these problems. The detailed construction is depicted in Figure 15 and Figure 16. The flow cell consists of two parts, the lower part holding the electrode in place, and the upper part with the reaction chamber, inlet, outlet, and an O-ring. Both parts are pressed together by four screws that are evenly spaced from the O-ring.

With a reaction chamber height of 5 mm, potential air bubbles can rise to the top of the chamber, preventing the electrochemical reaction from being interrupted. Due to the spacious reaction chamber and the diameter of the inlets and outlets of 1 mm, relatively high flow rates of at least 4 mL min^{-1} can be achieved since the back pressure is not as high as in microfluidic systems using channel sizes of ten to hundreds of nm.

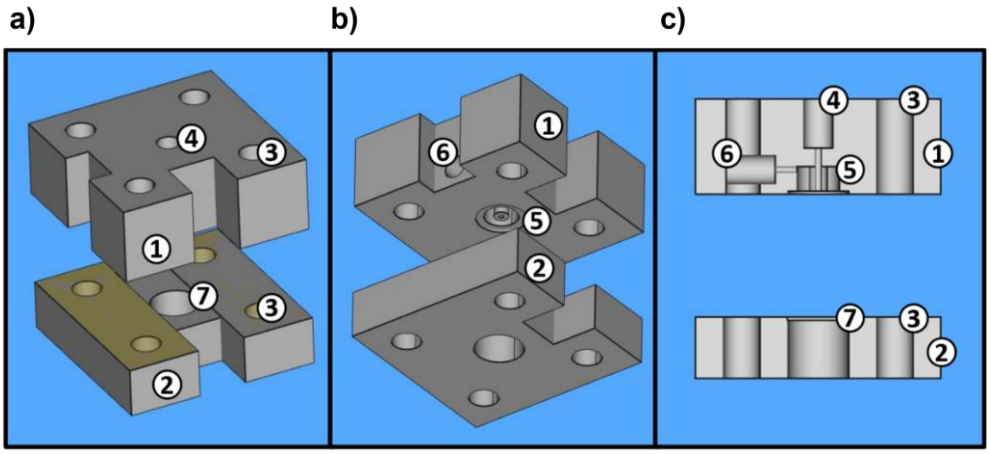

Figure 15 "CAD of the custom-made flow cell for screen-printed electrodes (created with FreeCAD). **a)** Shows a top-view, **b)** a bottom-view and **c)** shows a cross-sectional view of the flow cell and the reaction chamber. The individual parts serve the following purposes: 1 – upper part of the flow cell, 2 – bottom part of the flow cell, 3 – two of eight holes for screws to press the upper and bottom part together, 4 – hole for the inlet which can be connected to a tubing system via fittings, 5 – cylindrical reaction chamber with an O-ring cavity and a smaller cylindrical nozzle connected to the inlet, 6 – hole for the outlet which can be connected to a tubing system via fittings, 7 – electrode cavity (with round hole for the optional use of a magnet)." (Figure and caption reproduced from Höfs et al.[51]).

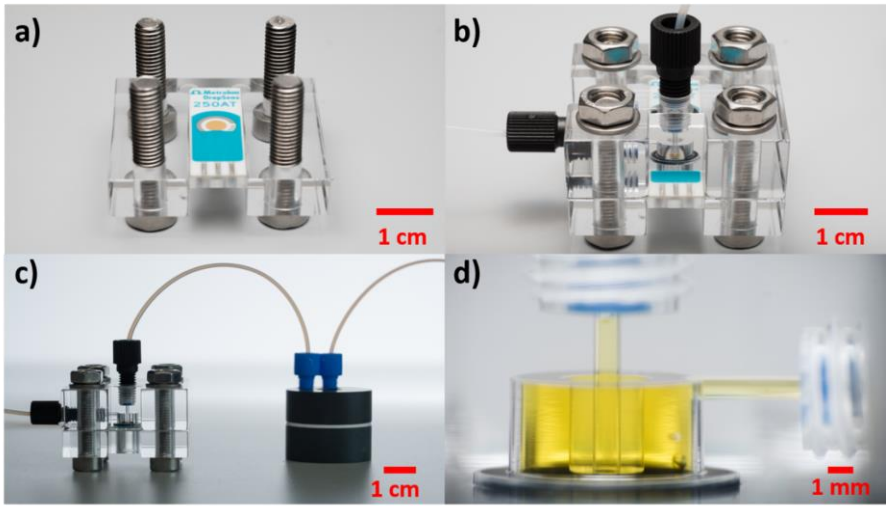

Figure 16 "Photos of the custom-made flow cell for screen-printed electrodes. **a)** Bottom part of the flow cell with a screen-printed gold electrode and the screws assembled for the connection with the upper part. **b)** The assembled flow cell connected via fittings to a tubing system. **c)** Flow cell with an upstream connected bubble trap. **d)** The reaction chamber with the perpendicularly arranged inlet nozzle and the horizontally arranged outlet channel (filled with solution containing fully oxidized TMB)." (Figure and caption reproduced from Höfs et al.[51]).

For the intended application of the flow cell for the read-out of immunoassays, amperometric measurements should be performed in a flowing solution. Therefore, samples need to be injected sequentially into a flow of buffer. To test the flow cell, the redox probe potassium ferricyanide was detected at screen-printed gold electrodes. It was found that the measured current is a linear function of the ferricyanide concentration, and that the reproducibility is high (see Figure A 1).

Thus, the flow cell is well-suited for the sequential analysis of samples by amperometric measurements but can also be used for static measurements with interrupted flow. The developed cell has therefore already been used for various measurement techniques such as CV, differential pulse voltammetry, amperometry or impedance spectroscopy[51, 56, 216].

5.1.4 Comparison of different antibodies by ELISA

Three different anti-OTA mouse IgG antibodies (BG4, BC10 and CH2) were tested by a competitive ELISA for its applicability in the magnetic bead-based OTA assay (see Figure 17). For this purpose, a tracer, consisting of OTA and HRP was synthesized by coupling OTA via the carboxylic group to the amino groups of HRP using DCC NHS chemistry. The coupling density of OTA per HRP could be determined by MALDI-ToF-MS. It was determined that approximately one OTA molecule binds per one HRP molecule (see Figure A 4).

To test the antibodies, the microplates were first coated with a secondary rabbit anti-mouse IgG antibody and afterwards with the primary anti-OTA antibodies, which were captured by the secondary antibody. The OTA-HRP tracer and the analyte then compete for the binding sites of the antibody. To generate a signal TMB/H_2O_2 were used as enzymatic substrates. To compare the sensitivity of the ELISA obtained with the three different antibodies, the C-value, which is the inflection point of the sigmoidal curve was used. With the BG4 antibody a quite low C-value of 1.26 ± 0.03 nM was obtained, which is about one order of magnitude lower than those obtained for the two other antibodies (C_{BC10} = 10.7 ± 0.4 nM; C_{CH2} = 16.5 ± 0.7 nM). Consequently, all further experiments were carried out, using the BG4 antibody.

The non-chlorinated and less-toxic OTB, which is not regulated in food often occurs simultaneously with OTA[217]. Hence, the antibody should be able to discriminate between OTA and OTB. The cross-reactivity of the antibody was therefore tested by ELISA and a value of only 1.8% could be determined (see Figure 17 b). Consequently, the antibody fulfills the criteria for the analytical detection of OTA, with a good sensitivity and specificity for OTA.

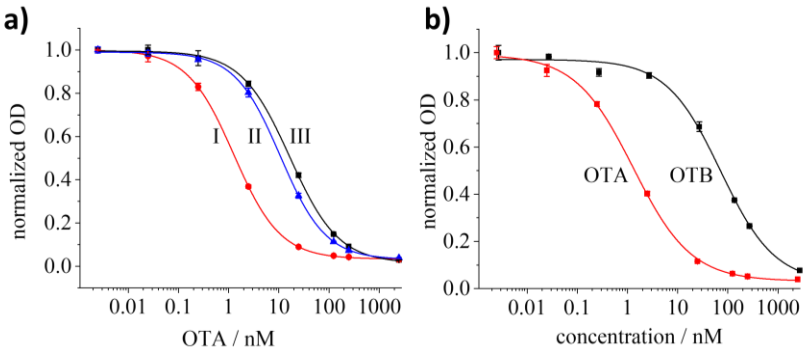

Figure 17 "**a)** ELISA for ochratoxin A for the comparison of different mouse IgG anti-OTA antibodies obtained from different cell clones (I) BG4 (II) BC10 (III) CH2. The obtained C-values were: C_{BG4} = 1.26 ± 0.03 nM; C_{BC10} = 10.7 ± 0.4 nM; C_{CH2} = 16.5 ± 0.7 nM. **b)** ELISA for Ochratoxin A and Ochratoxin B with the BG4 antibody. A cross-reactivity of 1.8% was calculated. C-Values were C_{OTA} = 1.3 ± 0.1 nM, C_{OTB} = 72 ± 13 nM. Error bars were obtained from four independent measurements." (Figure and caption reproduced from Höfs et al.[51]).

5.1.5 Magnetic bead-based OTA assay with amperometric detection

As described in 5.1.1 the protein G decorated magnetic beads were used for the development of the magnetic bead-based OTA assay, allowing to shorten the assay time since no overnight incubation steps are required as for the ELISA. For the miniaturization of the detection step, the developed flow cell was used to detect the enzymatically oxidized TMB after addition of H_2SO_4. Amperometric measurements were performed at a fixed potential of 0.3 V vs. Ag/AgCl, which is sufficiently lower than the formal potential of TMB of 0.437 V vs. Ag/AgCl, allowing the reduction of oxidized TMB under diffusion-controlled reaction conditions. To stabilize the potential of the Ag/AgCl reference electrode, 0.1 M KCl was added to the running buffer and each sample. Since the detection of TMB must be performed in the presence of all other substrates and reaction products, the influence of H_2O_2 and reduced TMB on the amperometric signal was tested at 0.3 V vs. Ag/AgCl. Both TMB and H_2O_2 gave a small signal of a few nA (see Figure A 2). To avoid any interference, TMB and H_2O_2 were added to the running buffer.

Figure 18 b shows the amperometric curve obtained for the read-out of the magnetic bead-based assay with eight calibrants, each measured in triplicate. With the magnetic bead-based assay a C-value of 2.1 ± 0.3 nM could be achieved, which is similar as for the classical ELISA (see Figure 17 a). To verify the results, obtained by electrochemical detection, the same samples were read-out optically. It was found, that both methods are in good agreement (see Figure 18 d).

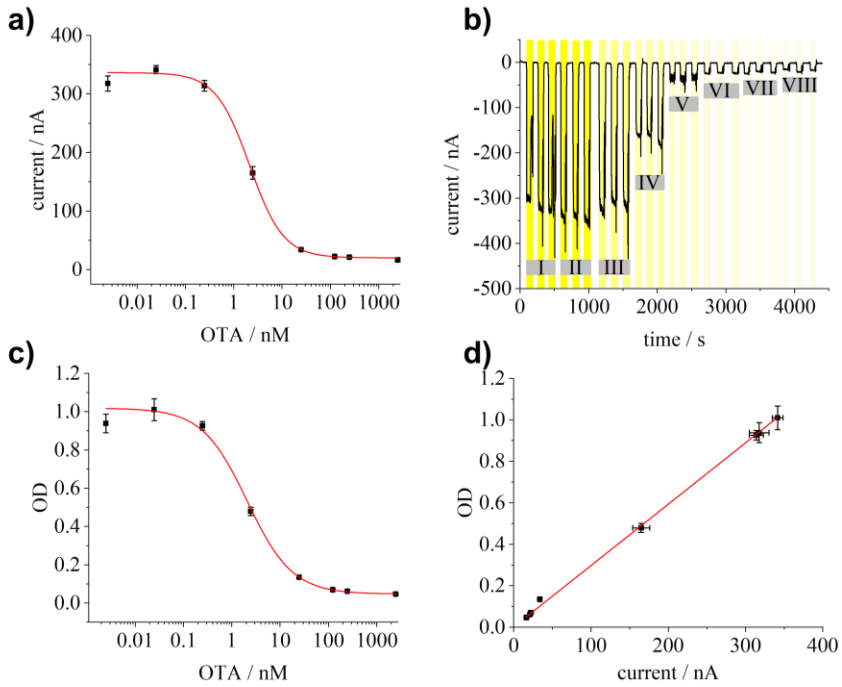

Figure 18 "**a)** Results of the immunomagnetic OTA assay with amperometric detection of TMB (C = 2.1 ± 0.3 nM) **b)** Amperometric curve measured at 300 mV vs. Ag/AgCl with a flow rate of 600 µL min^{-1} in 150 mM sodium citrate buffer with 0.33 M H_2SO_4 (pH 1). For each OTA concentration three independent samples were measured (I 2.5 pM, II 25 pM, III 250 pM, IV 2.5 nM, V 25 nM, VI 124 nM, VII 250 nM, VIII 2.5 µM). **c)** Results of the same immunomagnetic assay measured by photometry (C = 2.1 ± 0.3 nM) and **d)** shows the correlation of both detection techniques (R^2 = 0.99715). Error bars were obtained from three independent measurements." (Figure and caption reproduced from Höfs et al.[51]).

To demonstrate the applicability of the electrochemical OTA detection system, measurements were performed in OTA-spiked beer. So far, no legal limits have applied for OTA in beer, but the European Commission has announced that maximum levels for OTA in beer are under consideration[8].

The effect of the beer matrix on the magnetic bead-based assay was tested, by performing the assay in different dilutions of beer (1:1; 1:5 and 1:10) in buffer (see Figure 19 a). With a higher beer content, the total signal intensity significantly decreases and the C-value shifts to higher concentrations, which might be associated to the ethanol content or other matrix components of the beer.

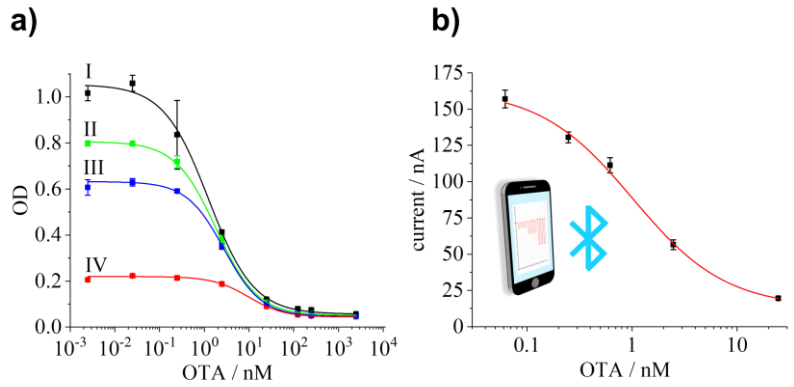

Figure 19 "**a)** Immunomagnetic OTA assay with four different dilutions of OTA-spiked beer (with Tris buffer) and photometric TMB detection (I – without beer; II – 1:10 diluted; III - 1:5 diluted; IV – 1:1 diluted; C-values: C_I = 1.25 ± 0.14 nM; C_{II} = 1.83 ± 0.20 nM; C_{III} = 2.75 ± 0.22 nM; C_{IV} = 9.7 ± 0.9 nM). **b)** Results of the amperometric detection for 1:5 diluted OTA-spiked beer which was performed with a smartphone connected via Bluetooth to a miniaturized potentiostat. Error bars were obtained from three independent measurements." (Figure and caption reproduced from Höfs et al.[51]).

Under optimized assay conditions in buffer without beer a C-value of 1.25 ± 0.14 nM, a limit of detection of 150 pM (60 ng L^{-1}) and a maximum OD signal of approximately 1 could be achieved. In 1:1 diluted OTA-spiked beer samples, the OD value was about five times smaller than under optimized conditions and the C-value increased to 9.7 ± 0.9 nM. With higher dilutions of the beer, only a small decrease of sensitivity was determined, and C-values of 2.75 ± 0.22 nM and 1.83 ± 0.20 nM were obtained for 1:5 and 1:10 diluted beer, respectively. The recovery rate obtained in 1:5 diluted beer was 138%, whereas in 1:10 diluted beer a recovery rate of 117% was obtained. However, the dilution factor should be kept as low as possible, to allow the detection of small OTA concentrations in a real beer sample. To further prove the applicability of the developed magnetic bead-based assay and electrochemical detection system, the read-out of the assay with spiked beer samples was performed with a handheld potentiostat connected via Bluetooth to a smartphone. In 1:5 diluted spiked beer OTA concentration ranging from 1.25 nM to 12.5 nM (= 0.5 µg L^{-1} to 5 µg L^{-1}, see Figure 19 b) could be determined. In other alcoholic beverages and non-alcoholic beverages, such as wine and grape juice, the legal limit value is as low as 2 µg L^{-1} and in other foodstuffs only a few µg per kg are allowed[8]. Thus, the interesting measuring range would be covered by the developed detection system.

With the obtained results a miniaturized detection system for the quantification of OTA in beer could be demonstrated. Moreover, the developed electrochemical detection method for oxidized TMB can be applied for many other TMB/HRP-based ELISAs or enzymatic assays.

5.2 Ergometrine sensing in rye flour by a magnetic bead-based immunoassay followed by flow injection analysis with amperometric detection[i]

5.2.1 Concept of the magnetic bead-based immunoassay for ergometrine

In this chapter, the applicability of the developed amperometric detection system for TMB to another important mycotoxin is demonstrated. Ergometrine was chosen as a marker compound for the rapid screening of ergot alkaloids, which are newly regulated in foodstuffs by the European Commission since 2021[10]. Furthermore, the chapter is dedicated to further optimization of the electrochemical detection system by adjustments in sample injection and flow rate.

A similar magnetic bead-based immunoassay as described for OTA (see 5.1.1) was developed for ergometrine (see Figure 20 a). Here a competitive assay format was chosen, in which monoclonal mouse anti-ergot alkaloid antibodies were bound to protein G modified beads. For the anti-ergometrine antibody a novel tracer, consisting of a lysergic acid mimic, a polyethylene glycol (PEG) spacer with 8 units, and a terminating biotin (PEG(8)-biotin) was obtained. The antibody-decorated beads were incubated with the analyte (ergometrine) and the tracer, which were competing for the binding sites at the antibodies. Thereafter, unbound species were removed by washing and the beads were incubated with poly-HRP labeled streptavidin, which is binding to the captured tracer via biotin-streptavidin interactions. Subsequently, TMB/H_2O_2 were added as enzymatic substrates and the reaction was stopped by the addition of H_2SO_4. Finally, the read-out could be performed either by measuring the OD statically in a microtiter plate or amperometrically in a flow injection system. For the amperometric detection optimized conditions were used to quantify the fully oxidized TMB, which have been previously identified (see 5.1.2).

Ergometrine was detected in spiked rye flour samples, which is schematically depicted in Figure 20 b. Ergometrine was extracted by vortexing a spiked flour sample in PBST. After centrifugation the diluted extract could be analyzed by the magnetic bead-based immunoassay as described above, and amperometric detection of the fully oxidized TMB was performed using a handheld potentiostat connected via Bluetooth to a smartphone.

[i] The results and the content of this section was previously published in the following article: Höfs, S.; Jaut, V.; Schneider, R. J., Ergometrine sensing in rye flour by a magnetic bead-based immunoassay followed by flow injection analysis with amperometric detection. Talanta 2023, 254, 124172.

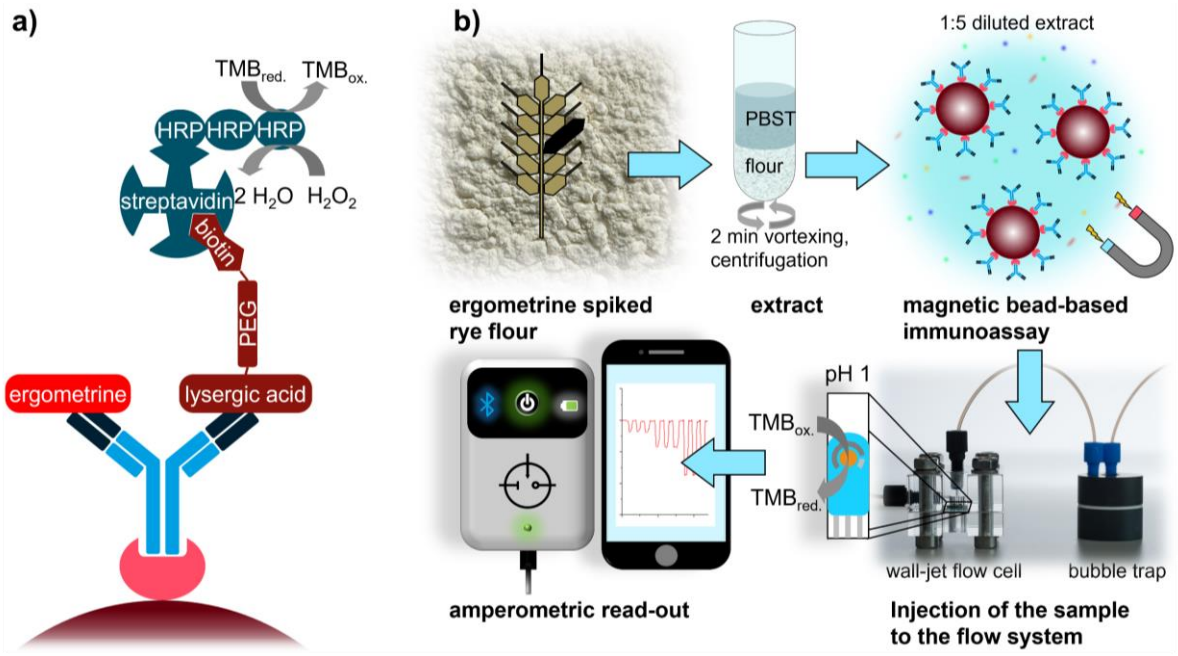

Figure 20 "**a)** Principle of the magnetic bead-based immunoassay for ergometrine. Protein G decorated beads were used to capture the anti-ergot alkaloid antibodies. Lysergic acid PEG(8)-biotin was used as a tracer, competing with ergometrine for the binding sites at the antibody. For signal generation, poly-HRP-streptavidin was bound to the biotin moiety of the tracer and TMB/H_2O_2 were used as enzymatic substrates. TMB was enzymatically oxidized (blue charge-transfer complex), and the reaction was stopped by the addition of sulfuric acid generating the fully oxidized TMB (yellow diimine); **b)** Procedure to determine ergometrine in spiked rye flour samples. A short extraction with PBST and 2 min vortexing was performed. The samples were centrifuged for 10 min and the 1:5 diluted extract was analyzed by the magnetic bead-based assay as shown in a). The samples containing the fully oxidized TMB are injected into the flow system with a wall-jet flow cell and a screen-printed gold electrode. TMB is reduced at pH 1 and 300 mV vs. Ag/AgCl and the current is measured with a handheld potentiostat connected via Bluetooth to a smartphone." (Figure and caption reproduced from Höfs et al. [56]).

5.2.2 Amperometric detection in a flow injection system

As described in section 5.1.2 and 5.1.5, screen-printed gold electrodes are well suited to amperometrically detect the fully oxidized TMB at pH 1 and 300 mV vs. Ag/AgCl. In the above described amperometric measurements, as depicted in Figure 18 b, the samples containing the fully oxidized TMB were pumped through the flow system until a steady current level was reached. When manually controlling the injected volume, this method has the advantage of a high precision and furthermore the maximum peak current can be reached by this method. However, measuring the steady state current is quite time-consuming and requires a relatively high sample volume. Consequently, a flow injection system and a sample loop were introduced to the flow system with the wall-jet flow cell. This allows to control the injected volume precisely, and thus transient currents can be used as a signal for quantification, which has the advantages that the sample volume and time of analysis can be reduced.

Short analysis times are crucial in the food industry. Therefore, the focus of the following investigations was to reduce the duration of the amperometric detection. Consequently, the custom-made wall-jet flow cell was installed into a flow injection system with a six-port manual injection valve with a 300 µL sample loop (see Figure 21 a). To remove air bubbles from the running solution, a bubble trap was installed upstream to the flow cell. A syringe pump was used to adjust the flow rate.

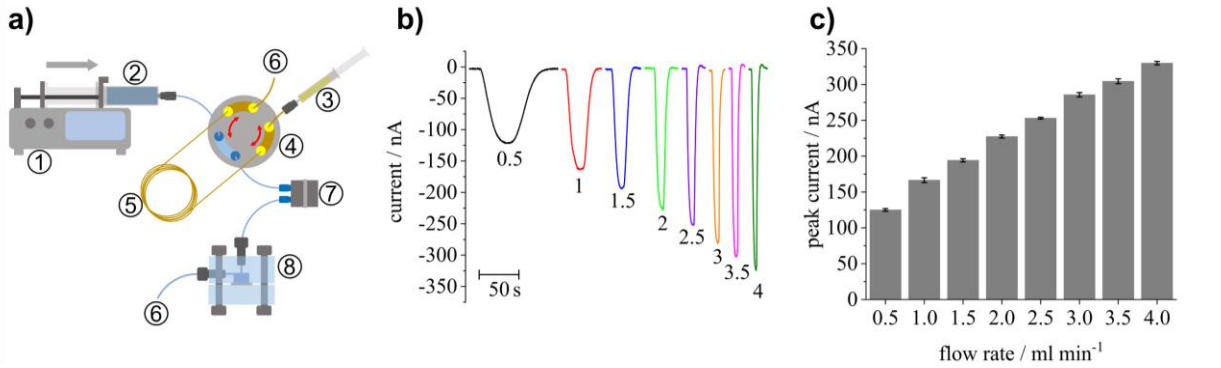

Figure 21 "**a)** Flow injection system consisting of: (1) syringe pump; (2) syringe filled with buffer; (3) syringe with sample for injection; (4) six-port manual injection valve; (5) sample loop; (6) waste; (7) bubble trap, (8) wall-jet flow cell with screen-printed electrode **b)** Amperometric current signals obtained with the flow injection system and screen-printed gold electrodes at 0 V vs. Ag/AgCl. Samples of 300 µL 10 µM potassium ferricyanide in 100 mM potassium phosphate buffer with 100 mM KCl (pH 7) were injected at different flow rates ranging from 0.5 to 4 mL min^{-1} **c)** Peak currents obtained for different flow rates in amperometric measurements as depicted in b) (n = 3)." (Figure and caption reproduced from Höfs et al. [56]).

In amperometric measurements, the current should be limited by mass transport and therefore, typically a sufficient overpotential is applied to the electrode. Since forced convection can improve mass transport to the electrode, the flow rate influences the current densities in amperometric measurements. It was first reported by Yamada and Matsuda that the limiting current value is among other parameters, proportional to the power of 0.75 of the volume flow rate[218]. Thus, it is possible to increase the current densities in amperometric measurements to some extend by increasing the flow rates. The influence of the flow rate on the current intensity was investigated in the custom-made flow cell by injecting potassium ferricyanide, as a redox probe. Ferricyanide was reduced at the electrode at a potential of 0 V vs. Ag/AgCl after injection of 300 µl of the redox probe at flow rates ranging from 0.5 to 4 ml min^{-1}. It could be shown that the current peak height increases with the flow rate, while the peak width decreases (see Figure 21 b and Figure A 9). The peak height is highly reproducible (see Figure 21 c). From this it can be concluded that higher flow rates enable improved mass transport and thus higher currents. Another advantage is the shorter measuring time, which is achieved at higher flow rates. Hence, for all further experiments a flow

rate of 4 mL min^{-1} was applied, allowing that one sample can be analyzed in around 45 s (including the time for the manual injection).

5.2.3 Magnetic bead-based immunoassay for ergometrine with amperometric detection

To test a commercially available monoclonal mouse anti-ergot alkaloid antibody with the lysergic acid PEG(8)-biotin as tracer, poly-HRP streptavidin and TMB/H_2O_2 as substrates, a competitive ELISA was developed. With this assay a C-value of 25.5 ± 0.8 nM (8.3 ± 0.3 µg L^{-1}) was obtained (see Figure A 11 a).

To produce the mouse anti-ergot alkaloid antibodies a lysergic acid-BSA conjugate was used as immunogen. Accordingly, a high affinity of the antibody to lysergic acid derivatives such as ergometrine was expected. The cross-reactivity of the antibody with different structurally different ergopeptines was tested by the ELISA with ergotamine and ergocristine (see Figure A 11 a). For both relatively low cross-reactivities were determined, with 7% for ergotamine and <0.1% for ergocristine. Hence, the antibody is well-suited for its application in specific ergometrine immunoassays. Also for other antibodies which were produced against the ergoline moiety (using lysergol[219] or lysergic acid protein conjugates as immunogens[133]) low cross-reactivities with ergopeptines could be observed.

To improve the sensitivity of the assay, the primary antibody-coated microplate was preincubated with ergometrine standards before adding the tracer. This favors the binding of the analyte instead of the tracer and may therefore shift the C-value to lower concentrations. For this purpose, the antibody-coated plate was preincubated with ergometrine standards for 5, 10 or 15 min before adding the tracer, which was then incubated for another 25, 20 or 15 min, respectively.

With immediate addition of the tracer a C-value of 26 ± 9 nM (9 ± 3 µg L^{-1}) was achieved, whereas upon addition after 15 min a much lower C-value of 12 ± 3 nM (3.8 ± 0.8 µg L^{-1}) was obtained. Longer preincubation times were not tested here since this would lead to a further decrease of the maximum signal intensity. For all further experiments, including the magnetic bead-based immunoassay, 15 min preincubation time with ergometrine standards was used.

For the magnetic bead-based ergometrine assay, the monoclonal mouse anti-ergot alkaloid antibody tested by ELISA was applied and the flow injection system with the wall-jet flow cell was used to detect TMB amperometrically. As described for the OTA assay, a potential of 300 mV

vs. Ag/AgCl was applied to the screen-printed gold electrode and detection was performed at pH 1. For the ergometrine magnetic bead-based immunoassay a higher flow rate of 4 mL min^{-1} was used, to shorten the detection step. A calibration curve was determined by using 12 ergometrine standards ranging from 0.1 nM to 1.23 µM. Figure 22 shows the amperometric curve obtained for the 12 calibrants, proving that the read-out can be completed in less than 10 min (~45 s per sample).

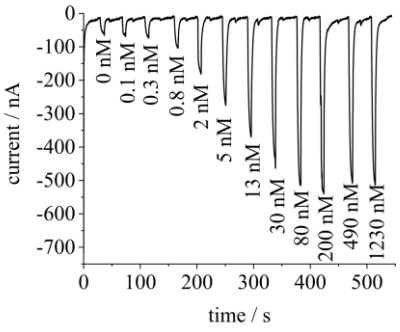

Figure 22 "Amperometric curve for the read-out of the magnetic bead-based immunoassay for different ergometrine concentrations (0 – 1230 nM) obtained with the flow injection system. The samples containing the fully oxidized TMB are injected sequentially. Redox peaks result from the reduction of TMB at 300 mV vs. Ag/AgCl at screen-printed gold electrodes. All samples and the running buffer contain 150 mM sodium citrate, 300 mM H_2SO_4, 100 mM KCl, 240 µM TMB and 2.5 mM H_2O_2." (Figure and caption reproduced from Höfs et al. [56]).

For verification and comparison, optical read-out of the same samples was conducted for all calibrants. Figure 23 a and b show the calibration curves obtained with optical and amperometric detection, respectively. For the amperometric read-out the calibration curve was determined from three replicates and for the optical read-out it was determined from eight replicates. Similar C-values of 13.8 ± 0.5 nM (4.50 ± 0.17 µg L^{-1}) for amperometric and 13.8 ± 0.7 nM (4.5 ± 0.2 µg L^{-1}) for optical detection were obtained. Thus, the obtained sensitivity is very similar to the sensitivity obtained with the classical microplate-based ELISA described above. However, the applicability of the magnetic bead-based immunoassay is significantly improved, since no overnight incubation step and blocking of the surface is required. Furthermore, a lower background signal was obtained with the magnetic bead-based immunoassay as with the classical ELISA. This can be deduced from the comparison of both methods with optical detection (see also Figure A 11).

The developed magnetic bead-based immunoassay achieves a similar sensitivity as other immunoassays for ergometrine, since the reported C-values for competitive microplate-based ELISAs or RIAs for ergometrine range from 0.5 to 100 nM[133, 181, 220, 221].

The relative error of the concentration was calculated for both calibration curves, allowing to create a precision profile for the calibration range according to Ekins (see Figure 23 a and b)[222]. It was specified that the measuring range of the test should be defined as the range in which the relative concentration error does not exceed a limit of 30%. Thus, a working range for ergometrine quantification between 3 nM (1 µg L^{-1}) and 300 nM (100 µg L^{-1}) for amperometric read-out and between 6 nM (2 µg L^{-1}) and 1.2 µM (400 µg L^{-1}) for optical read-out could be obtained. Both detection methods achieve a similar limit of detection (LOD) and offer high precision in the central part of the calibration curve (i. e. around the inflection point). However, in terms of precision, the optical read-out achieves better results at high ergometrine concentrations than the amperometric read-out. Due to the inverse proportionality of the signal (current or OD) and the concentration, lower signals are obtained at high ergometrine concentration. Thus, in amperometric measurements relatively low currents (> 50 nA) are obtained, which may cause a higher relative error as obtained for optical read-out. However, in practice the quantification of low ergometrine levels is of greater importance. The signals obtained from the electrochemical and the optical detection are in good correlation (see Figure 23 c), demonstrating again that the amperometric detection of TMB is a reliable alternative to optical read-out in immunoassays.

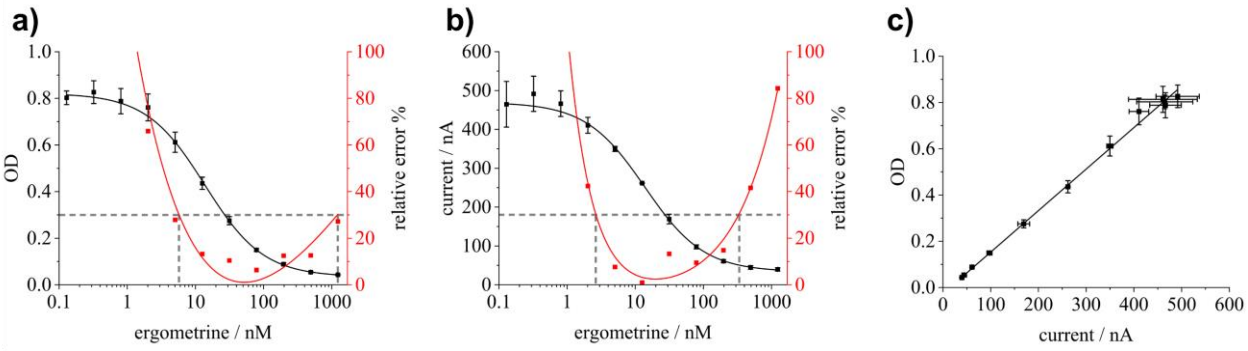

Figure 23 "Calibration curves of the magnetic bead-based immunoassay for ergometrine with **a)** optical and **b)** amperometric read-out and their corresponding precision profiles, indicating the relative error of the concentration determination. The LODs were calculated allowing an error of max. 30%, indicated by the grey dashed lines. For the optical read-out, a working range from 6 nM (2 µg L^{-1}) to 1.2 µM (400 µg L^{-1}) and a C-value of 13.8 ± 0.7 nM (4.5 ± 0.2 µg L^{-1}) were obtained. For the calibration curve with amperometric read-out, a working range from 3 nM (1 µg L^{-1}) to 300 nM (100 µg L^{-1}) and a C-value of 13.8 ± 0.5 nM (4.50 ± 0.17 µg L^{-1}) were determined. **c)** Correlation of optical and amperometric signal (y = 0.00179 x – 0.02652; R^2 = 0.99858)." (Figure and caption reproduced from Höfs et al. [56]).

The highest levels of ergot alkaloid contamination are typically found in rye and rye products[84, 86]. A useful application of the magnetic bead-based immunoassay for ergometrine would therefore be to use it to detect ergometrine as an indicator compound in rye flour. Spiked rye flour was

analyzed for this purpose, since, to the best of knowledge, no reference materials are available in this context. Rye flour samples were spiked with different concentrations of ergometrine (25, 62.5, 125 and 250 µg kg^{-1}) and were subsequently extracted with PBST. The use of PBST as extraction solution in ergot alkaloid ELISAs has been previously reported by Shelby et al.[182]. Matrix-matched calibration of the magnetic bead-based immunoassay was performed in 1:5 diluted flour extracts, to avoid potential errors caused by matrix effects. The diluted extracts of the spiked flour were analyzed by the assay, and the amperometric detection was performed with the handheld potentiostat connected via Bluetooth to a smartphone as described above. Also, here all results were verified by optical detection. The obtained recovery rates of the spiked samples range from 37% to 51% and are depicted in Figure 24. It could be proven that the results of both detection techniques are in good agreement.

The developed method offers great promise for the screening of ergot alkaloids in cereals. Since 2022 the legal limit of the sum of the 12 major ergot alkaloids has applied for different food products. For rye milling products a legal limit of 500 µg kg^{-1} applies, which will be lowered to 250 µg kg^{-1} after July 1, 2024[10]. The magnetic bead-based immunoassay could enable in the future the fast determination of the ergometrine proportion of the total ergot alkaloid content in food and thus help to remove highly contaminated batches of grain from the production facility (e.g. in mills). This has the advantage, that in the case of a highly contaminated sample, no further expensive and time-consuming analysis by chromatographic methods must be performed. This can avoid further high costs for the mills, by avoiding the storage of contaminated grain for several days. For the intended application in the food industry the developed method is very promising, as only simple, and inexpensive devices are required. At the production site, mills usually have a kind of small laboratory where the quality of the grain is checked upon arrival by several bench-top devices evaluating for instance the protein proportion or the baking properties of the grain. Establishing a bench-top flow injection analysis system at the production site would be easily feasible.

Nevertheless, the potential of the developed method could be even further increased in the future by introducing several further highly specific tests for the other major ergot alkaloids. Therefore, the focus should lay in the development of new antibodies. Another approach could be the development of a rather generic antibody, which is able to return a proxy for a sum parameter. Moreover, the recovery rates could be improved by introducing an optimized extraction procedure

which is suitable for immunoassays. In the case of ergot alkaloids, this remains challenging, since the stability and degree of epimerization of ergot alkaloids are higher in aprotic solvents, such as acetonitrile[91], which is unsuitable for immunoassays. This could also be demonstrated by the ergometrine ELISA in the presence of 5% acetonitrile, showing a significant decrease of the signal intensity and loss of sensitivity (see Figure A 12). However, with the obtained recovery rates, together with the relative abundance of ergometrine in complex samples, the developed method is a promising approach for ergot alkaloid screening.

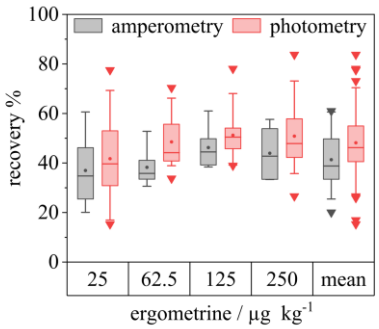

Figure 24 "Recovery rates of the magnetic bead-based assay obtained with electrochemical or optical read-out for ergometrine spiked rye flour samples containing 25 µg kg^{-1}, 62.5 µg kg^{-1}, 125 µg kg^{-1}, and 250 µg kg^{-1}. For each concentration two independent samples were spiked, and each sample was analyzed in 3 replicates by amperometric detection (n = 6) and in 12 replicates by optical detection (n = 24). Whiskers represent the interval of 5−95% of all data; dots represent the arithmetic mean and triangles represent the outliers." (Figure and caption reproduced from Höfs et al. [56]).

5.3 Fumonisin sensing by Aspergillus niger fumonisin amine oxidase (AnFAO) and amperometric hydrogen peroxide detection

5.3.1 Concept of AnFAO-based fumonisin sensing with magnetic particles and amperometric hydrogen peroxide detection

In this chapter, a different approach has been developed, which, compared to the previous approaches relying on antibodies, is based on the use of an enzyme (AnFAO) as recognition element for the detection of fumonisins. This new concept allows to directly quantify the product of the enzymatic reaction with the mycotoxins, by electrochemical detection. This has the advantage that the enzyme is not only the recognition element, but also generates a quantifiable reaction product. Thus, it gives great promise for the development of a specific enzymatic biosensor for fumonisins. A classic enzymatic biosensor has not yet been shown for fumonisins or any other mycotoxin. Therefore, the developed enzymatic sensing system with electrochemical detection represents a novel approach.

The enzyme, AnFAO, was recombinantly expressed as fusion protein with MBP in *E. coli*, similarly as it was reported by Garnham et al.[203]. To establish a FB_1 detection system, the enzymatically catalyzed reaction of AnFAO in which FB_1 is oxidatively deaminated producing H_2O_2 was exploited for electrochemical detection. Therefore, H_2O_2 was amperometrically detected by its reduction at -0.1 V vs. Ag/AgCl on a screen-printed Prussian blue/ carbon electrode. MBP-AnFAO was covalently coupled to tosyl-activated magnetic beads, allowing to perform the enzymatic reaction in the bead dispersion under shaking and to remove the enzyme from the solution under magnetic capturing of the beads. This has the advantage that the reaction product, H_2O_2, can be accumulated over the incubation time, obtaining a higher electrochemical signal and that the enzyme has no direct contact with the electrode, which could give an interfering signal. Thus, one electrode can be used for multiple measurements. The amperometric detection was performed in the custom-made wall-jet flow cell and flow injection system as described in 5.1.3 and 5.2.2. The read-out was performed with a handheld potentiostat connected via Bluetooth to a smartphone.

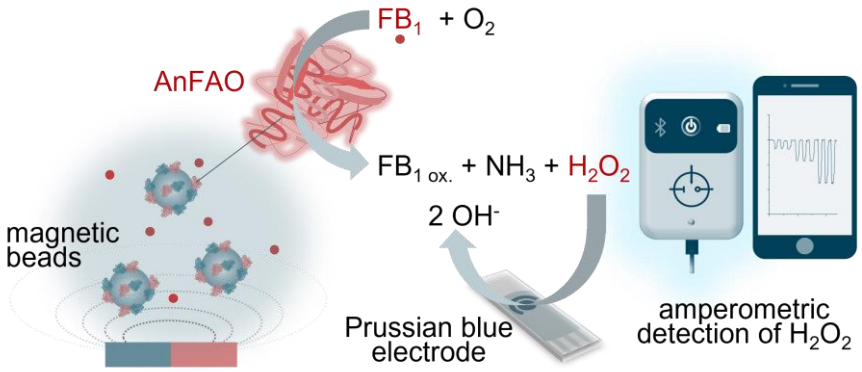

Figure 25 Schematic illustration of the enzymatic FB_1 oxidation by MBP-AnFAO coupled to magnetic beads and the amperometric detection of the enzymatically produced H_2O_2 with a Prussian blue electrode and a handheld potentiostat connected via Bluetooth to a smartphone.

5.3.2 MBP-AnFAO activity

MBP-AnFAO was purified from *E. coli* cell lysates via its polyhistidine-tag (His-tag), using Ni-NTA purification. Figure 26 shows the SDS-PAGE of the cell lysates and the purified fusion protein. For AnFAO a molecular weight of 51,320.7 Da has been reported[203]. For the MBP-AnFAO fusion protein, consisting of AnFAO, a tobacco etch virus protease cleavage site and the MBP with an N-terminal 6x His-tag, a theoretical mass of 96,970 Da can be expected (without the FAD cofactor). This is in good agreement with SDS-PAGE results showing a clear protein band

for MBP-AnFAO at around 100 kDa. The eluted MBP-AnFAO was dialyzed against 50 mM MES buffer (with 150 mM NaCl, 5 µM FAD, pH 6) to exchange the buffer and to remove potential impurities. For the protein expression an optimized engineered expression strain NiCo21(DE3) has been used, which minimizes the contamination of IMAC fractions with endogenous *E. coli* metal binding proteins. However, since some other protein fractions were still visible in SDS-PAGE, it has been verified that the enzymatic activity towards fumonisins results from AnFAO. Therefore, lysates of *E. coli* cells containing the MBP-AnFAO vector after expression was induced and lysates of *E. coli* cells without the MBP-AnFAO vector were tested for their enzymatic activity in 20 µM FB_1 solution (see Figure 26 a and b). An Amplex Red H_2O_2/HRP fluorescence assay was used, in which the enzymatically produced H_2O_2 from FB_1 turnover is quantified with the HRP/Amplex Red reaction. The obtained fluorescence signal is thus proportional to the enzyme activity of AnFAO. The results clearly show that enzymatic activity could only be observed for the lysate of *E. coli* cells containing the MBP-AnFAO vector after expression was induced. For all experiments, the MBP-tagged AnFAO version was used, since it could be already demonstrated by Garnham et al. that the MBP-tagged version has identical activity compared to the wild-type tag-free enzyme[203].

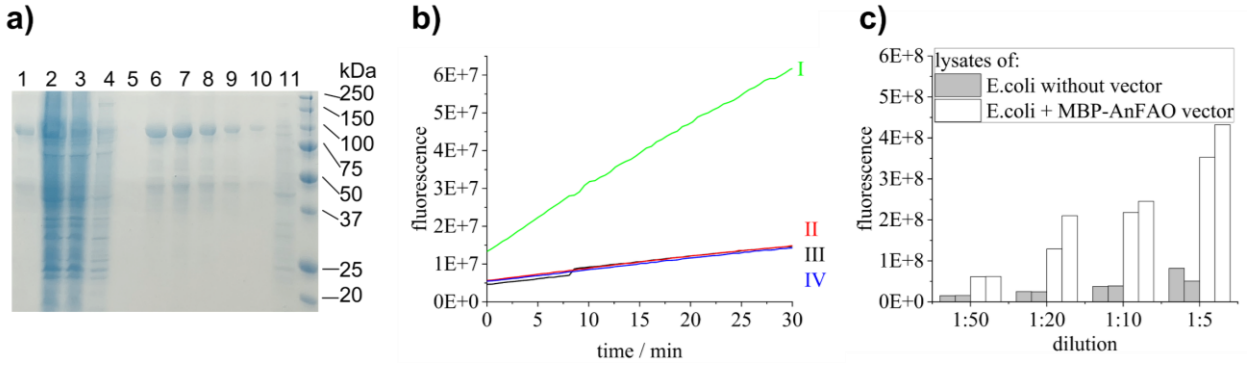

Figure 26 a) SDS-PAGE of the recombinantly expressed MBP-AnFAO. The lanes show the following samples:**1** MBP-AnFAO after Ni-NTA purification and dialysis (12.4 kDa cut off) **2** lysate of *E. coli* containing the MBP-AnFAO vector in which the expression was induced, **3** flow through of the lysate in Ni-NTA purification, **4** first wash fraction of the Ni-NTA after MBP-AnFAO has bound, **5** second wash fraction, **6** first elution step of MBP-AnFAO from Ni-NTA, **7** second elution step, **8** third elution step, **9** fourth elution step, **10** fifth elution step, **11** lysate of *E. coli* containing the MBP-AnFAO vector in which the expression was not induced. **b)** Results of the Amplex Red H_2O_2/HRP fluorescence assay comparing the activity of: **I** lysate of *E. coli* cells containing the MBP-AnFAO vector and 20 µM FB_1, **II** lysate of *E. coli* cells without the MBP-AnFAO vector and 20 µM FB_1, **III** lysate of *E. coli* cells containing the MBP-AnFAO vector without FB_1 **IV** lysate of *E. coli* cells without the MBP-AnFAO vector and without FB_1. Fluorescence detection was performed at 560 nm excitation and 590 nm emission. Lysates were diluted 1:50 and the assay was performed at 37°C. **c)** Results of the fluorescence assay conducted with the Amplex Red H_2O_2/HRP fluorescence assay comparing the activity of *E. coli* lysates with and without the MBP-AnFAO vector (negative control) at different dilutions.

In the European Union only maximum levels of the sum of FB_1 and FB_2 in certain foodstuffs are established[8, 9].However, in the most naturally contaminated maize samples FB_1 is the dominant fumonisin compared to FB_2 and FB_3 [98-101]. For example, in a study from Shephard et al., in which naturally contaminated maize samples from Iran were analyzed, it was found that FB_1 accounts on average for 74% (range: 65-79%) of the total fumonisin content in a sample[99]. Thus, analytical tests should ideally determine the concentration of the sum of FB_1 and FB_2. However, since FB_1 accounts for the biggest proportion of fumonisins contamination in food, the detection of FB_1 may be sufficient for a rapid fumonisin screening test.

For the untagged AnFAO Garnham et al. reported a stronger enzymatic affinity towards FB_2 than for FB_1[203]. Furthermore, a strong activity towards other long-chain amino poly alcohols such as sphinganine and hydrolyzed fumonisins could be observed[203]. Here the activity of MBP-AnFAO towards FB_1 and FB_2 was tested by the Amplex Red H_2O_2/HRP fluorescence assay. For FB_1 a higher specific enzyme activity could be observed as for FB_2, with 0.0037 U mg^{-1} and 0.0014 U mg^{-1} at 0.5 µM MBP-AnFAO and 25 µM FB_1 or FB_2, respectively. Moreover, it was found, that the enzymatic reaction of MBP-AnFAO with FB_2 stops much earlier than with FB_1 and in total higher H_2O_2 concentrations are reached with FB_1 than with FB_2 (see Figure 27, Figure A 13, Figure A 14 and Figure A 15). At 10 µM FB_2 and 1 µM MBP-AnFAO a signal increase due to the increasing concentration of the enzymatically produced H_2O_2 could be only observed until 10 min of incubation time, whereas for 10 µM FB_1 much higher signal intensities where observed and the H_2O_2 concentration increased until 90 min of incubation time were reached (see Figure 27 a). Furthermore, it could be observed that under the chosen conditions the concentration of enzymatically produced H_2O_2 increases linearly with FB_1 or FB_2 concentration, respectively (see Figure 27 b and c). However, with increasing MBP-AnFAO concentration (0.1 – 5 µM) an increase of the enzyme activity could be only observed when FB_1 was used as enzymatic substrate, whereas with FB_2 the enzyme activity increases only at small enzyme concentrations (0.1 - 0.5 µM) before it reaches a plateau (see Figure A 15). Consequently, MBP-tagged AnFAO is more suitable for the application in an FB_1 detection system. However, for the application of the enzyme in specific FB_1 detection, a clean-up step of a fumonisin containing food extract e.g., by an antibody column may be required to enhance the specificity of the test. In addition, the specificity of the enzyme towards FB_1 could be improved in the future through enzyme engineering and further studies on the catalytic mechanism of the enzyme.

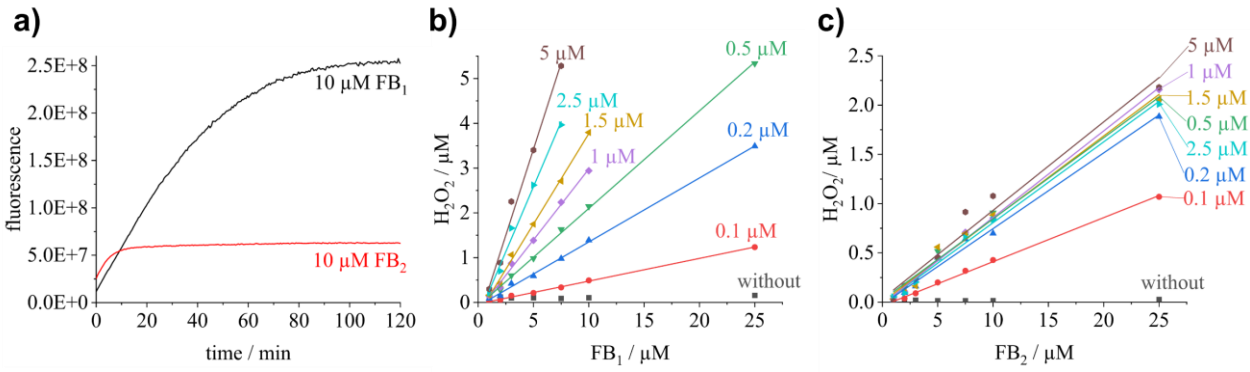

Figure 27 a) Results of the Amplex Red H_2O_2/HRP fluorescence assay comparing the activity of 1 µM MBP-AnFAO in 10 µM FB_1 and 10 µM FB_2 at 37°C. **b)** Enzymatically produced H_2O_2 vs. the FB_1 concentrations with different MBP-AnFAO concentrations ranging from 0-5 µM after 30 min incubation time at 37°C. **c)** Enzymatically produced H_2O_2 at different FB_2 concentrations with different MBP-AnFAO concentrations ranging from 0-5 µM after 30 min incubation time at 37°C.

5.3.3 Amperometric detection of H_2O_2 with Prussian blue electrodes

The electrochemical properties of Prussian blue and its application as electrode material for H_2O_2 sensing have been widely studied[223-228]. Prussian blue is also sometimes denoted as "artificial peroxidase"[224], since it allows the reduction of H_2O_2 at low applied potentials (around 0 V vs. Ag/AgCl)[226, 228]. For the present work, commercially available screen-printed Prussian blue/carbon electrodes were used. To reduce H_2O_2, a potential of -0.1 V vs. Ag/AgCl was applied to the electrode. As reported earlier, a short pretreatment of the electrode using 100 µM H_2O_2 was applied to condition the electrodes for highly reproducible measurements (see also 4.5.6)[207]. The results of the amperometric calibration are depicted in Figure 28. The H_2O_2 concentration could be quantified down to 0.5 µM. However, some variation in the signal intensity from electrode to electrode could be observed, as typical for screen-printed electrodes. Therefore, each electrode should be calibrated before analytical measurements are performed. The results demonstrate that the Prussian blue electrodes are well-suited for the detection of low micromolar concentrations of H_2O_2, which is an important prerequisite for its application in the enzymatic FB_1 detection.

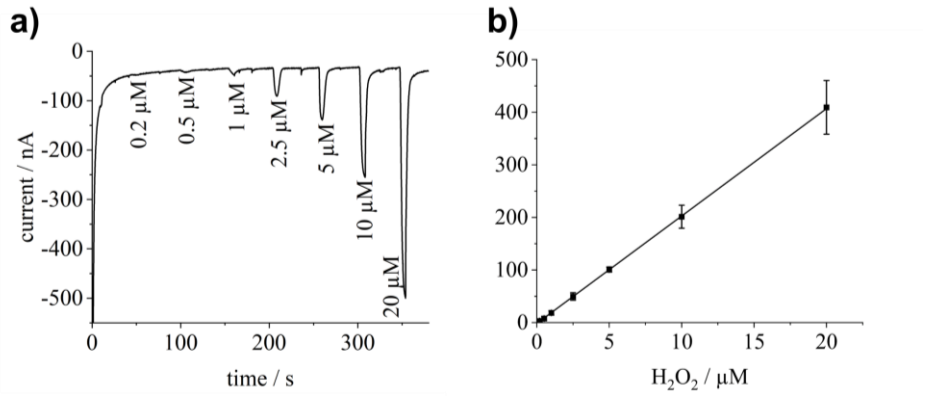

Figure 28 a) Amperometric curve obtained for the H_2O_2 calibration using a Prussian blue/carbon electrode. The measurement was performed at -0.1 V vs. Ag/AgCl in 100 mM potassium phosphate buffer with 100 mM KCl, pH 7 in a flow injection system at a flow rate of 4 mL min^{-1}. **b)** H_2O_2 calibration graph obtained from three different electrodes (R^2 = 0.99986).

5.3.4 AnFAO-based fumonisin sensing with magnetic particles and amperometric hydrogen peroxide detection

MBP-AnFAO was covalently coupled to tosyl-activated magnetic beads, allowing to bind the enzyme via amino or sulfhydryl groups to the beads. The coupling was performed over night for 19 h at 37°C. When 18.5 µg MBP-AnFAO and 70 µL PBS buffer (pH 7.6) per 1 mg beads were used for the coupling, it was found that 70% of the enzyme has bound to the beads (12.9 ± 1.8 ng mg^{-1} beads).

For the development of an enzymatic amperometric detection system for FB_1 quantifying the enzymatically produced H_2O_2, the concentration of H_2O_2 should be at least in the high nanomolar to low micromolar range. Therefore, the enzymatic reaction of AnFAO with FB_1 should be performed under favorable conditions, to obtain high H_2O_2 concentrations. For AnFAO the highest deamination activities of fumonisins could be observed at an incubation temperature of about 50°C and at around pH 6[203]. Thus, for the enzymatic reaction with MBP-AnFAO coupled to the magnetic beads the substrate incubation was performed under similar conditions at 45°C and pH 7. The incubation of the beads with FB_1 as substrate was performed under shaking for 40 min, allowing to accumulate the enzymatically produced H_2O_2 in the bead-dispersion. After substrate incubation the reaction is stopped by separation of the solution and the MBP-AnFAO-modified magnetic beads. To perform the read-out, the samples are injected to the flow injection system, and the detection is performed as described above (see 5.3.3). With this approach FB_1 concentrations down to 1.5 µM could be quantified and a linear current increase could be observed with the FB_1

concentration in the range between 1.5 to 20 µM FB_1. The results could be verified by the optical Amplex Red H_2O_2/HRP fluorescence assay. Therefore, the read-out of the FB_1 assay with MBP-AnFAO-modified magnetic beads was performed optically and amperometrically to determine the enzymatically produced H_2O_2. The results demonstrate, that both methods are in good agreement (see Figure A 16).

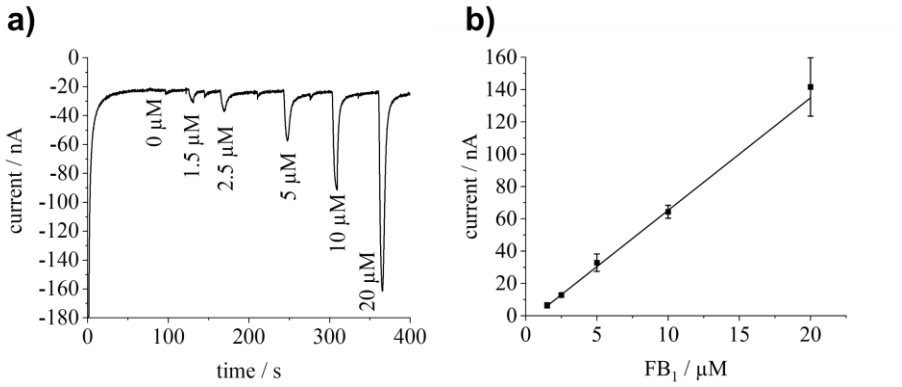

Figure 29 a) Amperometric curve obtained for different FB_1 concentrations used in the assay with MBP-AnFAO-modified magnetic beads. The amperometric measurement was performed at -0.1 V vs. Ag/AgCl in 100 mM potassium phosphate buffer with 100 mM KCl, pH 7 in a flow injection system at a flow rate of 4 mL min^{-1}. **b)** Calibration curve for the FB_1 assay with MBP-AnFAO-modified magnetic beads. The results were obtained from five separately performed assays (R^2 = 0.99901).

Garnham et al. have already reported, that AnFAO has a high thermostability and does not lose activity in the presence of various divalent cations[203]. To further test the applicability of MBP-AnFAO for its use in a fumonisin sensing system the storage and thermostability of the enzyme was further characterized. Aliquots of MBP-AnFAO were stored at -20°C in 50 mM MES buffer (containing 150 mM NaCl, 5 µM FAD and pH 6) until use. To test the storage stability, thawed aliquots were stored at 4°C for up to 77 days. Activity tests of the enzyme performed with the optical Amplex Red H_2O_2/HRP fluorescence assay showed that no loss of activity was observed over the entire storage period (see Figure 30 a). For the magnetic bead-based assay, the enzyme is coupled covalently by incubation of the tosyl-activated beads with MBP-AnFAO for 19 h at 37°C. Thus, it was tested if the incubation of the enzyme under these conditions has an influence on the enzyme activity (see Figure 30 b). It could be demonstrated that only a small loss of activity of 14 ± 17 % was obtained after 19 h at 37°C. Furthermore, the stability of the enzyme coupled to magnetic beads was investigated. MBP-AnFAO modified magnetic beads were stored for two weeks at 4°C and their activity was compared to freshly prepared beads. For this purpose, three aliquots of bead dispersion were incubated in 10 µM FB_1 and the read-out was performed amperometrically as described above (see Figure 30 c). No loss of activity was obtained with the

stored MBP-AnFAO modified magnetic beads. Therefore, the enzyme is quite promising for its application in fumonisin sensing.

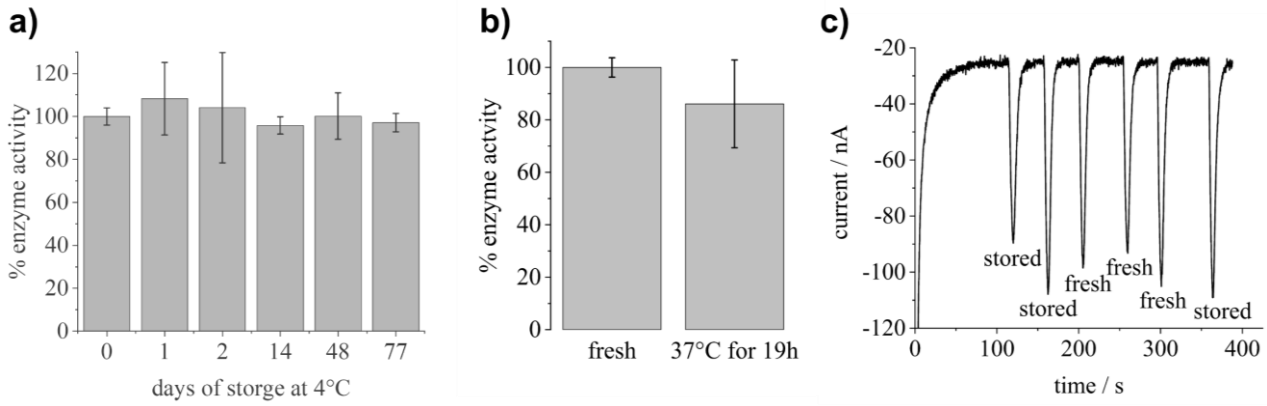

Figure 30 a) Enzyme activity of MBP-AnFAO at different storage times at 4°C in 50 mM MES buffer with 150 mM NaCl, 5 µM FAD, pH 6. Results were obtained with the Amplex Red H_2O_2/HRP fluorescence assay using 1.5 µM MBP-AnFAO and 20 µM FB_1. **b)** Enzyme activity of freshly thawed MBP-AnFAO and after incubation for 19 h at 37°C. Results were obtained with the Amplex Red H_2O_2/HRP fluorescence assay using 1.5 µM MBP-AnFAO and 5 µM FB_1. **c)** Amperometric curve obtained for the assay comparing freshly prepared MBP-AnFAO beads (fresh) with MBP-AnFAO beads stored for two weeks at 4°C (stored). For the assay 10 µM FB_1 was used. The amperometric measurement was performed at -0.1 V vs. Ag/AgCl in 100 mM potassium phosphate buffer with 100 mM KCl, pH 7 in a flow injection system at a flow rate of 4 mL min^{-1}.

To test the applicability of the developed enzymatic FB_1 detection system, FB_1 spiked maize grits samples have been analyzed. Samples were spiked with 600 µg kg^{-1} FB_1, which is below the legal limit of the European Commission of 1000 µg kg^{-1} for the sum of FB_1 and FB_2[8]. The maize grits samples were extracted using an acetonitrile-methanol-water mixture (25% acetonitrile, 25% methanol, 50% water) and cleaned up by immunoaffinity columns according to a slightly modified protocol of the Association of Official Agricultural Chemists (AOAC) which has been used for the analysis of FB_1 and FB_2 in maize and corn flakes by liquid chromatography[212]. The cleaned-up samples were incubated with MBP-AnFAO modified magnetic beads and the detection of enzymatically produced H_2O_2 was performed as described above. The obtained results for the spiked samples were compared to unspiked samples (see Figure 31). It could be observed that both the spiked and unspiked sample give a redox current, which could be either associated to the fact that the maize grits samples obtained from a local supermarket were already contaminated with FB_1 to a certain extend or to interferences of the matrix with the electrochemical measurement. However, higher signals were obtained for the spiked samples. Thus, the delta of both signals (for the spiked and unspiked samples) was used to calculate the FB_1 concentration. For the 600 µg kg^{-1} spiked sample a concentration of 761.5 µg kg^{-1} was calculated and thus a recovery of 127 % could

be obtained. Consequently, the developed system allows to identify FB_1 contaminated maize grits samples.

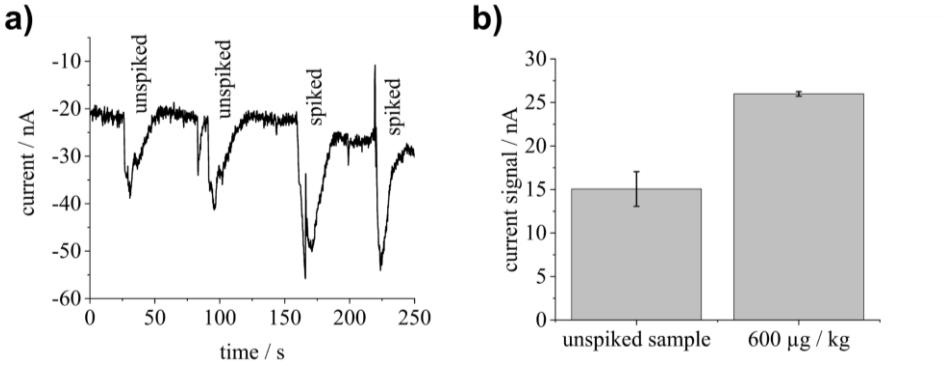

Figure 31 a) Amperometric curve obtained for the assay with MBP-AnFAO-modified magnetic beads, comparing the current signals obtained for unspiked maize grits samples and maize grits samples spiked with 600 µg kg^{-1} FB_1. The amperometric measurement was performed at -0.1 V vs. Ag/AgCl in 100 mM potassium phosphate buffer with 100 mM KCl, pH 7 in a flow injection system at a flow rate of 4 mL min^{-1}. **b)** Current signals obtained for the unspiked and spiked samples.

For the application of AnFAO as detoxifying agent in food and feed Telmer et al. could already demonstrate that AnFAO deaminates fumonisins in milled maize flour in Milli-Q water, effectively[204]. However, for the development of an FB_1 detection system, further development should primarily deal with the applicability of the electrochemical test system in real food matrices. Overall, a proof of concept was demonstrated, enabling for the first time that the sensorial detection of FB_1 becomes feasible by combining the enzymatic recognition of FB_1 using the robust enzyme AnFAO as MBP fusion protein with amperometric H_2O_2 detection with Prussian blue electrodes.

6 Summary

For the application of analytical detection methods for mycotoxins in the food industry, the simplification and miniaturization of the test methods is of great importance. In the present work different strategies for mycotoxins sensing, based on immunoassays and an enzymatic assay, both with electrochemical detection, have been developed.

The most frequently applied enzymatic label for immunoassays based on optical detection is HRP which is often used in combination with the substrates TMB/H_2O_2. In this study, the electrochemistry of TMB was characterized by cyclic voltammetry on different electrode materials (carbon and gold) and at different pH values (pH 1 and pH 4), to identify conditions well suited for the amperometric read-out of immunoassays. Both, the electrode material, and the pH value, have a significant effect on the electrochemistry of TMB. At pH 1 the oxidation and reduction reaction occurred in a single step, whereas it occurs in two steps at pH 4. While at pH 4 neither for carbon nor gold electrodes a reproducible redox reaction of TMB could be achieved, it was demonstrated that screen-printed gold electrodes are well suited for the detection of TMB at pH 1, due to the reversible character of the redox reaction under these conditions. Furthermore, the electrode response is highly stable under these conditions allowing to use one electrode for multiple measurements. In contrast, for carbon electrodes the signal response changes after electrochemical reaction with TMB at pH 1. Thus, by using gold electrodes and a pH value of 1, good conditions have been found for the reproducible detection of TMB, providing a solid basis for the further construction of electrochemical mycotoxin assays. The electrochemical measurements have been conducted in a newly developed wall-jet flow cell for screen-printed electrodes.

For OTA, which is one of the most toxic mycotoxins regulated by the European Commission, a magnetic bead-based competitive immunoassay was developed using an OTA-HRP tracer and TMB/H_2O_2 as substrates. The magnetic bead-based immunoassay requires no further blocking of the bead-surface or overnight incubation and is, therefore, a quicker alternative to the classical microplate-based ELISA. The read-out of the assay was performed by amperometric detection of the fully oxidized TMB at pH 1 and the results were in good agreement with those obtained with optical detection. A limit of detection of 150 pM (60 ng L^{-1}) was obtained under optimized assay conditions. The applicability of the magnetic bead-based immunoassay was demonstrated in OTA-spiked beer using a handheld potentiostat connected via Bluetooth to a smartphone, enabling

amperometric detection. OTA concentrations down to 1.2 nM (0.5 µg L^{-1}) could be quantified in spiked beer.

Another group of mycotoxins, the ergot alkaloids, has caused tens of thousands of deaths throughout human history. Nevertheless, maximum levels on the sum of the six major ergot alkaloids and their corresponding epimers were not introduced until 2021 by the European Commission. Therefore, a magnetic bead-based immunoassay for ergometrine, which is one of the six major ergot alkaloids was developed. A competitive assay format was chosen and a newly conceived tracer consisting of a lysergic acid mimic, a polyethylene glycol (PEG) spacer with 8 units, and a terminating biotin was applied together with poly-HRP-streptavidin.

Again, the amperometric detection system with the handheld potentiostat and custom-made wall-jet flow cell was used for the TMB-based detection. Here the amperometric detection could be further optimized using a flow injection system. It could be demonstrated that the current signal increases with the flow rate, which also leads to a shorter measuring time. Under optimized assay conditions ergometrine could be quantified down to 3 nM (1 µg L^{-1}) in buffer and from 25 to 250 µg kg^{-1} in spiked rye flour. All results were verified by optical detection. To the best of knowledge, this is the first magnetic bead-based immunoassay and electrochemical detection method for ergometrine.

The developed amperometric detection method for TMB gives great promise for the detection of TMB in many other HRP-based assays. For the food industry it offers great promise in meeting the demand for inexpensive devices for mycotoxin analysis.

Another group of highly abundant mycotoxins, regulated by the European Commission are the fumonisins. In the present study an enzymatic electrochemical FB_1 sensing system could be demonstrated for the first time. For this purpose, an *Aspergillus niger* fumonisin amine oxidase (AnFAO) catalyzing the oxidative deamination of fumonisins, producing hydrogen peroxide, was recombinantly produced in *E. coli* as MBP fusion protein. A specific enzyme activity of 0.0037 U mg^{-1} and 0.0014 U mg^{-1} at 0.5 µM MBP-AnFAO was determined for 25 µM FB_1 and 25 µM FB_2 respectively. For FB_1 detection, the enzyme was coupled covalently to magnetic particles, and the enzymatically produced H_2O_2 was detected amperometrically in a flow injection system using Prussian blue/carbon electrodes and the custom-made wall-jet flow cell for screen-printed electrodes. With the developed method FB_1 could be quantified down to

1.5 µM (≈ 1 mg L^{-1}) and it could be demonstrated that MBP-AnFAO can deaminate different concentrations of FB_1 even in immobilized form. Furthermore, the enzyme provides a high storage and temperature stability and is therefore well suited for its application in the food industry. The applicability of the sensing system was also tested in FB_1 spiked maize grits samples which were cleaned up by immunoaffinity columns.

7 References

[1] E. Azziz-Baumgartner, K. Lindblade, K. Gieseker, H. S. Rogers, S. Kieszak, H. Njapau, R. Schleicher, L. F. McCoy, A. Misore, K. DeCock, C. Rubin, L. Slutsker, A. I. Grp, *Environmental Health Perspectives* **2005**, *113*, 1779-1783.

[2] A. Kamala, C. Shirima, B. Jani, M. Bakari, H. Sillo, N. Rusibamayila, S. De Saeger, M. Kimanya, Y. Y. Gong, A. Simba, I. Team, *World Mycotoxin Journal* **2018**, *11*, 311-320.

[3] L. Claeys, C. Romano, K. De Ruyck, H. Wilson, B. Fervers, M. Korenjak, J. Zavadil, M. J. Gunter, S. De Saeger, M. De Boevre, I. Huybrechts, *Comprehensive Reviews in Food Science and Food Safety* **2020**, *19*, 1449-1464.

[4] F. Fung, R. F. Clark, *Journal of Toxicology: Clinical Toxicology* **2004**, *42*, 217-234.

[5] M. Eskola, G. Kos, C. T. Elliott, J. Hajšlová, S. Mayar, R. Krska, *Critical Reviews in Food Science and Nutrition* **2020**, *60*, 2773-2789.

[6] P. M. Scott, *Journal of Food Protection* **1984**, *47*, 489-499.

[7] W. Mücke, C. Lemmen, in *Schimmelpilze - Vorkommen, Gesundheitsgefahren, Schutzmaßnahmen*, ecomed, Landsberg am Lech, pp. 84-135.

[8] *COMMISSION REGULATION (EC) No 1881/2006*, **2006**, *L 364/5*, 1-20.

[9] *COMMISSION REGULATION (EC) No 1126/2007*, **2007**, *L 255/14*, 1-4.

[10] *COMMISSION REGULATION (EU) 2021/1399*, **2021**, *L 301/1*, 1-5.

[11] *COMMISSION REGULATION (EU) 2019/1901*, **2019**, *L 293/2*, 1-3.

[12] Abbott, https://www.freestylelibre.de/produkte/freestyle-libre-3-sensor.html, **12.12.2022**.

[13] A. P. F. Turner, B. N. Chen, S. A. Piletsky, *Clinical Chemistry* **1999**, *45*, 1596-1601.

[14] J. D. Newman, A. P. F. Turner, *Biosensors & Bioelectronics* **2005**, *20*, 2435-2453.

[15] L. A. Zhang, C. C. Gu, H. Ma, L. L. Zhu, J. J. Wen, H. X. Xu, H. Y. Liu, L. H. Li, *Analytical and Bioanalytical Chemistry* **2019**, *411*, 21-36.

[16] J. Wang, *Chemical Reviews* **2008**, *108*, 814-825.

[17] W. Mücke, C. Lemmen, in *Schimmelpilze - Vorkommen, Gesundheitsgefahren, Schutzmaßnahmen*, ecomed, Landsberg am Lech, pp. 14-32.

[18] M. I. Hutchings, A. W. Truman, B. Wilkinson, *Current Opinion in Microbiology* **2019**, *51*, 72-80.

[19] A. Fleming, *British Journal of Experimental Pathology* **1929**, *10*, 226-236.

[20] R. Gaynes, *Emerging Infectious Diseases* **2017**, *23*, 849-853.

[21] D. E. Aylor, *Agricultural and Forest Meteorology* **1986**, *38*, 263-288.

[22] S. Bräse, A. Encinas, J. Keck, C. F. Nising, *Chemical Reviews* **2009**, *109*, 3903-3990.

[23] N. Venkatesh, N. P. Keller, *Frontiers in Microbiology* **2019**, *10*.

[24] M. Diamond, T. J. Reape, O. Rocha, S. M. Doyle, J. Kacprzyk, F. M. Doohan, P. F. McCabe, *Plos One* **2013**, *8*.

[25] M. J. Sweeney, A. D. W. Dobson, *International Journal of Food Microbiology* **1998**, *43*, 141-158.

[26] R. Krska, C. Crews, *Food Additives and Contaminants - Part A Chemistry, Analysis, Control, Exposure and Risk Assessment* **2007**, *25*, 722-731.

[27] H. S. Hussein, J. M. Brasel, *Toxicology* **2001**, *167*, 101-134.

[28] A. Alshannaq, J. H. Yu, *International Journal of Environmental Research and Public Health* **2017**, *14*, 632.

[29] F. Galvano, V. Galofaro, G. Galvano, *Journal of Food Protection* **1996**, *59*, 1079-1090.

[30] M. De Boevre, J. D. Di Mavungu, S. Landschoot, K. Audenaert, M. Eeckhout, P. Maene, G. Haesaert, S. De Saeger, *World Mycotoxin Journal* **2012**, *5*, 207-219.

[31] A. W. Hayes, R. D. Hood, H. L. Lee, *Teratology* **1974**, *9*, 93-97.
[32] W. C. A. Gelderblom, K. Jaskiewicz, W. F. O. Marasas, P. G. Thiel, R. M. Horak, R. Vleggaar, N. P. J. Kriek, *Applied and Environmental Microbiology* **1988**, *54*, 1806-1811.
[33] J. P. Rheeder, W. F. O. Marasas, P. G. Thiel, E. W. Sydenham, G. S. Shephard, D. J. Vanschalkwyk, *Phytopathology* **1992**, *82*, 353-357.
[34] A. Mally, W. Dekant, *Molecular Nutrition & Food Research* **2009**, *53*, 467-478.
[35] J. J. Wong, D. P. Hsieh, *Proceedings of the National Academy of Sciences* **1976**, *73*, 2241-2244.
[36] V. Sava, O. Reunova, A. Velasquez, R. Harbison, J. Sanchez-Ramos, *Neurotoxicology* **2006**, *27*, 82-92.
[37] P. Dwivedi, R. B. Burns, *Avian Pathology* **1985**, *14*, 213-225.
[38] R. Krska, A. Molinelli, *Analytical and Bioanalytical Chemistry* **2007**, *387*, 145-148.
[39] G. S. Shephard, *Journal of AOAC International* **2016**, *99*, 842-848.
[40] V. L. Pereira, J. O. Fernandes, S. C. Cunha, *Trends in Food Science & Technology* **2014**, *36*, 96-136.
[41] T. B. Whitaker, A. S. Johansson, *Journal of Food Protection* **2005**, *68*, 1306-1313.
[42] M. Miraglia, B. De Santis, V. Minardi, F. Debegnach, C. Brera, *Food Additives & Contaminants* **2005**, *22*, 31-36.
[43] R. Krska, P. Schubert-Ullrich, A. Molinelli, M. Sulyok, S. MacDonald, C. Crews, *Food Additives & Contaminants: Part A* **2008**, *25*, 152-163.
[44] *COMMISSION REGULATION (EC) No 401/2006*, **2006**, *L 70/12*, 1-23.
[45] P. Zöllner, B. Mayer-Helm, *Journal of Chromatography A* **2006**, *1136*, 123-169.
[46] D. Z. Kong, L. Q. Liu, S. S. Song, S. Suryoprabowo, A. K. Li, H. Kuang, L. B. Wang, C. L. Xu, *Nanoscale* **2016**, *8*, 5245-5253.
[47] Y. Uludag, E. Esen, G. Kokturk, H. Ozer, T. Muhammad, Z. Olcer, H. I. O. Basegmez, S. Simsek, S. Barut, M. Y. Gok, M. Akgun, Z. Altintas, *Talanta* **2016**, *160*, 381-388.
[48] L. Rivas, C. C. Mayorga-Martinez, D. Quesada-Gonzalez, A. Zamora-Galvez, A. de la Escosura-Muniz, A. Merkoci, *Analytical Chemistry* **2015**, *87*, 5167-5172.
[49] O. O. Soldatkin, K. V. Stepurska, V. M. Arkhypova, A. P. Soldatkin, A. V. El'skaya, F. Lagarde, S. V. Dzyadevych, *Sensors and Actuators B: Chemical* **2017**, *239*, 1010-1015.
[50] Y. R. Wang, C. Zhang, J. L. Wang, D. Knopp, *Toxins* **2022**, *14*.
[51] S. Höfs, D. Hülagü, F. Bennet, P. Carl, S. Flemig, T. Schmid, J. A. Schenk, V. D. Hodoroaba, R. J. Schneider, *ChemElectroChem* **2021**, *8*, 2597-2606.
[52] E. Valera, R. Garcia-Febrero, C. T. Elliott, F. Sanchez-Baeza, M. P. Marco, *Analytical and Bioanalytical Chemistry* **2019**, *411*, 1915-1926.
[53] M. Hervas, M. A. Lopez, A. Escarpa, *Analyst* **2011**, *136*, 2131-2138.
[54] A. Jodra, M. A. Lopez, A. Escarpa, *Biosensors & Bioelectronics* **2015**, *64*, 633-638.
[55] J. Kudr, L. Zhao, E. P. Nguyen, H. Arola, T. K. Nevanen, V. Adam, O. Zitka, A. Merkoci, *Biosensors & Bioelectronics* **2020**, *156*.
[56] S. Höfs, V. Jaut, R. J. Schneider, *Talanta* **2023**, *254*, 124172.
[57] S. Jafari, J. Guercetti, A. Geballa-Koukoula, A. S. Tsagkaris, J. L. D. Nelis, M. P. Marco, J. P. Salvador, A. Gerssen, J. Hajslova, C. Elliott, K. Campbell, D. Migliorelli, L. Burr, S. Generelli, M. W. F. Nielen, S. J. Sturla, *Foods* **2021**, *10*, 1399.
[58] *FDA-2013-S-0610- Guidance for Industry: Action Levels for Poisonous or Deleterious Substances in Human Food and Animal Feed* **2000**, 1-20.
[59] H. P. van Egmond, M. A. Jonker, *JSM Mycotoxins* **2003**, *2003*, 1-15.
[60] G. Schatzmayr, E. Streit, *World Mycotoxin Journal* **2013**, *6*, 213-222.

[61] *COMMISSION RECOMMENDATION (2013/165/EU)*, **2013**, *L 91/12*, 1-4.
[62] T. B. Whitaker, *Food Additives and Contaminants* **2006**, *23*, 50-61.
[63] T. F. Schatzki, *Journal of Agricultural and Food Chemistry* **1995**, *43*, 1561-1565.
[64] *REGULATION (EC) No 882/2004* **2004**, *L 165/1*, 1-141.
[65] E. Anklam, J. Stroka, A. Boenke, *Food Control* **2002**, *13*, 173-183.
[66] K. J. van der Merve, P. S. Steyn, L. Fourie, D. B. Scott, J. J. Theron, *Nature* **1965**, *205*, 1112-1113.
[67] A. el Khoury, A. Atoui, *Toxins* **2010**, *2*, 461-493.
[68] F. Malir, V. Ostry, A. Pfohl-Leszkowicz, J. Malir, J. Toman, *Toxins* **2016**, *8*, 191.
[69] J. C. Frisvad, J. M. Frank, J. A. M. P. Houbraken, A. F. A. Kuijpers, R. A. Samson, *Studies in Mycology* **2004**, *50*, 23-43.
[70] H. D. T. Nguyen, D. R. McMullin, E. Ponomareva, R. Riley, K. R. Pomraning, S. E. Baker, K. A. Seifert, *Fungal Biology* **2016**, *120*, 1041-1049.
[71] R. A. Samson, J. A. M. P. Houbraken, A. F. A. Kuijpers, J. M. Frank, J. C. Frisvad, *Studies in Mycology* **2004**, *69*, 45-61.
[72] I. Studer-Rohr, D. R. Dietrich, J. Schlatter, C. Schlatter, *Food and Chemical Toxicology* **1995**, *33*, 341-355.
[73] C. Juan, A. Pena, C. Lino, J. C. Moltó, J. Mañes, *International Journal of Food Microbiology* **2008**, *127*, 284-289.
[74] M. Vlachou, A. Pexara, N. Solomakos, A. Govaris, *Toxins* **2022**, *14*, 67.
[75] J. Bellver Soto, M. Fernández-Franzón, M.-J. Ruiz, A. Juan-García, *Journal of Agricultural and Food Chemistry* **2014**, *62*, 7643-7651.
[76] IARC, in *IARC Monographs on the Evaluation of Carcinogenic Risks to Humans Volume 56 Some Naturally Occurring Substances: Food Items and Constituents, Heterocyclic Aromatic Amines and Mycotoxins Vol. 56*, **1993**, pp. 489-521.
[77] A. E. Pohland, P. L. Schuller, P. S. Steyn, H. P. V. Egmond, *Pure and Applied Chemistry* **1982**, *54*, 2219-2284.
[78] A. Pfohl-Leszkowicz, R. A. Manderville, *Chemical Research in Toxicology* **2012**, *25*, 252-262.
[79] Y. D. Hsuuw, W. H. Chan, J. S. Yu, *International Journal of Molecular Sciences* **2013**, *14*, 935-953.
[80] L. Al-Anati, E. Petzinger, *Journal of Veterinary Pharmacology and Therapeutics* **2006**, *29*, 79-90.
[81] T. Kőszegi, M. Poór, *Toxins* **2016**, *8*, 111.
[82] A. Hofmann, *Pharmacology* **1978**, *16*, 1-11.
[83] M. Flieger, M. Wurst, R. Shelby, *Folia Microbiologica* **1997**, *42*, 3-29.
[84] J. Alexander, D. Benford, A. Boobis, S. Ceccatelli, B. Cottrill, J. P. Cravedi, A. Di Domenico, D. Doerge, E. Dogliotti, L. Edler, P. Farmer, M. Filipic, J. Fink-Gremmels, P. Furst, T. Guerin, H. K. Knutsen, M. Machala, A. Muni, M. Rose, J. Schlatter, R. van Leeuwen, E. P. C. F. Chain, *EFSA Journal* **2012**, *10*.
[85] A. Stoll, *Chemical Reviews* **1950**, *47*, 197-218.
[86] D. Arcella, J. A. G. Ruiz, M. L. Innocenti, R. Roldan, E. F. S. Authority, *EFSA Journal* **2017**, *15*.
[87] K. Lorenz, *Critical Reviews in Food Science and Nutrition* **1979**, *11*, 311-354.
[88] M. Appelt, F. M. Ellner, *Mycotoxin Research* **2009**, *25*, 95-101.
[89] J. C. Young, *Journal of Environmental Science and Health - Part B Pesticides, Food Contaminants, and Agricultural Wastes* **1981**, *16*, 381-393.

[90] J. C. Young, Z. J. Chen, *Journal of Environmental Science and Health Part B-Pesticides Food Contaminants and Agricultural Wastes* **1982**, *17*, 93-107.
[91] P. M. Scott, *Mycotoxin Research* **2007**, *23*, 113-121.
[92] Gabbai, Lisbonne, Pourquier, *British Medical Journal* **1951**, *2*, 650-651.
[93] J. P. Rheeder, W. F. O. Marasas, H. F. Vismer, *Applied and Environmental Microbiology* **2002**, *68*, 2101-2105.
[94] J. C. Frisvad, J. Smedsgaard, R. A. Samson, T. O. Larsen, U. Thrane, *Journal of Agricultural and Food Chemistry* **2007**, *55*, 9727-9732.
[95] J. M. Mogensen, J. C. Frisvad, U. Thrane, K. F. Nielsen, *Journal of Agricultural and Food Chemistry* **2010**, *58*, 954-958.
[96] J. P. Chen, C. J. Mirocha, W. P. Xie, L. Hogge, D. Olson, *Applied and Environmental Microbiology* **1992**, *58*, 3928-3931.
[97] M. S. Braun, M. Wink, *Comprehensive Reviews in Food Science and Food Safety* **2018**, *17*, 769-791.
[98] S. N. Chulze, M. L. Ramirez, M. C. Farnochi, M. Pascale, A. Visconti, G. March, *Journal of Agricultural and Food Chemistry* **1996**, *44*, 2797-2801.
[99] G. S. Shephard, W. F. O. Marasas, N. L. Leggott, H. Yazdanpanah, H. Rahimian, N. Safavi, *Journal of Agricultural and Food Chemistry* **2000**, *48*, 1860-1864.
[100] P. M. Scott, *Food Additives and Contaminants Part a-Chemistry Analysis Control Exposure & Risk Assessment* **2012**, *29*, 242-248.
[101] T.-C. Tseng, C.-Y. Liu, *Journal of Agricultural and Food Chemistry* **1999**, *47*, 4799-4801.
[102] T. S. Kellerman, W. F. Marasas, P. G. Thiel, W. C. Gelderblom, M. Cawood, J. A. Coetzer, *Onderstepoort Journal of Veterinary Research* **1990**, *57*, 269-275.
[103] W. F. O. Marasas, T. S. Kellerman, W. C. A. Gelderblom, J. A. W. Coetzer, P. G. Thiel, J. J. Vanderlugt, *Onderstepoort Journal of Veterinary Research* **1988**, *55*, 197-203.
[104] L. R. Harrison, B. M. Colvin, J. T. Greene, L. E. Newman, J. R. Cole, *Journal of Veterinary Diagnostic Investigation* **1990**, *2*, 217-221.
[105] K. A. Voss, R. T. Riley, *Food Safety* **2013**, *1*, 2013006-2013006.
[106] F. S. Chu, G. Y. Li, *Appl Environ Microbiol* **1994**, *60*, 847-852.
[107] S. A. Missmer, L. Suarez, M. Felkner, E. Wang, A. H. Merrill, K. J. Rothman, K. A. Hendricks, *Environmental Health Perspectives* **2006**, *114*, 237-241.
[108] IARC, in *IARC Monographs on the Evaluation of Carcinogenic Risks to Humans Volume 56 Some Naturally Occurring Substances: Food Items and Constituents, Heterocyclic Aromatic Amines and Mycotoxins Vol. 56*, **1993**, pp. 445-466.
[109] A. Farhadi, Y. Fakhri, R. Kachuei, Y. Vasseghian, E. Huseyn, A. M. Khaneghah, *Environmental Science and Pollution Research* **2021**, *28*, 20998-21008.
[110] K. Aoyama, M. Nakajima, S. Tabata, E. Ishikuro, T. Tanaka, H. Norizuki, Y. Itoh, K. Fujita, S. Kai, T. Tsutsumi, M. Takahashi, H. Tanaka, S. Iizuka, M. Ogiso, M. Maeda, S. Yamaguchi, K. Sugiyama, Y. Sugita-Konishi, S. Kumagai, *Journal of Food Protection* **2010**, *73*, 344-352.
[111] C. Sacchi, H. H. L. Gonzalez, L. E. Broggi, A. Pacin, S. L. Resnik, G. Cano, D. Taglieri, *Animal Feed Science and Technology* **2009**, *152*, 330-335.
[112] M. Kushiro, Y. Z. Zheng, R. Nagara, H. Nakagawa, H. Nagashima, *Journal of Food Protection* **2009**, *72*, 1327-1331.
[113] H. K. Abbas, R. D. Cartwright, W. T. Shier, M. M. Abouzied, C. B. Bird, L. G. Rice, P. F. Ross, G. L. Sciumbato, F. I. Meredith, *Plant Disease* **1998**, *82*, 22-25.
[114] L. M. Amzel, R. J. Poljak, *Annual Review of Biochemistry* **1979**, *48*, 961-997.

[115] G. M. Edelman, W. E. Gall, *Annual Review of Biochemistry* **1969**, *38*, 415-466.
[116] D. S. Smyth, S. Utsumi, *Nature* **1967**, *216*, 332-335.
[117] M. L. Chiu, D. R. Goulet, A. Teplyakov, G. L. Gilliland, *Antibodies* **2019**, *8*, 55.
[118] R. J. Poljak, *Nature-New Biology* **1972**, *235*, 137-140.
[119] R. J. Poljak, L. M. Amzel, H. P. Avey, B. L. Chen, R. P. Phizackerley, F. Saul, *Proceedings of the National Academy of Sciences of the United States of America* **1973**, *70*, 3305-3310.
[120] M. L. Petermann, *Journal of Physical Chemistry* **1942**, *46*, 183-191.
[121] R. R. Porter, *Nature* **1958**, *182*, 670-671.
[122] G. Köhler, C. Milstein, *Nature* **1975**, *256*, 495-497.
[123] G. Köhler, in *Immunological Methods* (Eds.: I. Lefkovits, B. Pernis), Academic Press, **1979**, pp. 391-395.
[124] M. E. Clementi, S. Marini, S. G. Condò, B. Giardina, *Annali dell'Istituto superiore di sanita* **1991**, *27*, 139-143.
[125] T. Gefen, J. Vaya, S. Khatib, I. Rapoport, M. Lupo, E. Barnea, A. Admon, E. D. Heller, E. Aizenshtein, J. Pitcovski, *Immunology* **2015**, *144*, 116-126.
[126] J. Hanes, C. Schaffitzel, A. Knappik, A. Pluckthun, *Nature Biotechnology* **2000**, *18*, 1287-1292.
[127] J. M. Fowler, D. K. Y. Wong, H. B. Halsall, W. R. Heineman, in *Electrochemical Sensors, Biosensors and their Biomedical Applications* (Eds.: X. Zhang, H. Ju, J. Wang), Academic Press, San Diego, **2008**, pp. 115-143.
[128] R. J. Schneider, in *Angewandte instrumentelle Lebensmittelanalytik* (Eds.: L. W. Kroh, S. Drusch, R. Matissek), BEHR'S Verlag, **2020**, pp. 477-499.
[129] A. Raysyan, R. Moerer, B. Coesfeld, S. A. Eremin, R. J. Schneider, *Analytical and Bioanalytical Chemistry* **2021**, *413*, 999-1007.
[130] D. S. Smith, S. A. Eremin, *Analytical and Bioanalytical Chemistry* **2008**, *391*, 1499-1507.
[131] C. Maragos, *Toxins* **2009**, *1*, 196-207.
[132] Y. Gao, Y. Z. Zhou, R. Chandrawati, *ACS Applied Nano Materials* **2020**, *3*, 1-21.
[133] H. Arens, M. H. Zenk, *planta medica* **1980**, *39*, 336-347.
[134] R. S. Yalow, S. A. Berson, *Journal of Clinical Investigation* **1960**, *39*, 1157-1175.
[135] B. K. Van Weemen, A. H. Schuurs, *FEBS Letters* **1971**, *15*, 232-236.
[136] E. Engvall, P. Perlmann, *Immunochemistry* **1971**, *8*, 871-874.
[137] F. G. R. Taylor, D. Patel, F. J. Bourne, *Journal of Immunological Methods* **1983**, *65*, 65-73.
[138] K. Shah, P. Maghsoudlou, *British Journal of Hospital Medicine* **2016**, *77*, C98-C101.
[139] E. Shannon Lm Fau - Kay, J. Y. Kay E Fau - Lew, J. Y. Lew, **1965**.
[140] N. C. Veitch, *Phytochemistry* **2004**, *65*, 249-259.
[141] K. G. Welinder, *FEBS Letters* **1976**, *72*, 19-23.
[142] K. G. Welinder, *European Journal of Biochemistry* **1979**, *96*, 483-502.
[143] R. H. Haschke, J. M. Friedhoff, *Biochemical and Biophysical Research Communications* **1978**, *80*, 1039-1042.
[144] G. I. Berglund, G. H. Carlsson, A. T. Smith, H. Szöke, A. Henriksen, J. Hajdu, *Nature* **2002**, *417*, 463-468.
[145] B. Chance, *Journal of Biological Chemistry* **1943**, *151*, 553-577.
[146] A. M. Azevedo, V. C. Martins, D. M. F. Prazeres, V. Vojinović, J. M. S. Cabral, L. P. Fonseca, in *Biotechnology Annual Review, Vol. 9*, Elsevier, **2003**, pp. 199-247.
[147] E.S. Bos, A.A. van der Doelen, N. van Rooy, A. H. W. M. Schuurs, *Journal of Immunoassay* **1981**, *2*, 187-204.

[148] V. R. Holland, B. C. Saunders, F. L. Rose, A. L. Walpole, *Tetrahedron* **1974**, *30*, 3299-3302.
[149] T. Porstmann, S. T. Kiessig, *Journal of Immunological Methods* **1992**, *150*, 5-21.
[150] C. E. Voogd, J. J. Van der Stel, J. J. J. A. A. Jacobs, *Journal of Immunological Methods* **1980**, *36*, 55-61.
[151] P. D. Josephy, T. Eling, R. P. Mason, *Journal of Biological Chemistry* **1982**, *257*, 3669-3675.
[152] Y. Misono, Y. Ohkata, T. Morikawa, K. Itoh, *Journal of Electroanalytical Chemistry* **1997**, *436*, 203-212.
[153] L. F. Oldfield, J. O. M. Bockris, *The Journal of Physical Chemistry* **1951**, *55*, 1255-1274.
[154] H. H. Liem, F. Cardenas, M. Tavassoli, M. B. Poh-Fitzpatrick, U. Muller-Eberhard, *Analytical Biochemistry* **1979**, *98*, 388-393.
[155] G. Y. Lee, J. H. Park, Y. W. Chang, S. Cho, M. J. Kang, J. C. Pyun, *Analytica Chimica Acta* **2017**, *971*, 33-39.
[156] G. Volpe, D. Compagnone, R. Draisci, G. Palleschi, *Analyst* **1998**, *123*, 1303-1307.
[157] S. Amaya-Gonzalez, N. de-los-Santos-Alvarez, M. J. Lobo-Castanon, A. J. Miranda-Ordieres, P. Tunon-Blanco, *Electroanalysis* **2011**, *23*, 108-114.
[158] P. Fanjul-Bolado, M. B. Gonzalez-Garia, A. Costa-Garcia, *Analytical and Bioanalytical Chemistry* **2005**, *382*, 297-302.
[159] J. J. Ezenarro, N. Parraga-Nino, M. Sabria, F. J. Del Campo, F. X. Munoz-Pascual, J. Mas, N. Uria, *Biosensors* **2020**, *10*.
[160] J. Barallat, R. Olive-Monllau, J. Gonzalo-Ruiz, R. Ramirez-Satorras, F. X. Munoz-Pascual, A. G. Ortega, E. Baldrich, *Analytical Chemistry* **2013**, *85*, 9049-9056.
[161] A. Crew, C. Alford, D. C. C. Cowell, J. P. Hart, *Electrochimica Acta* **2007**, *52*, 5232-5237.
[162] X. Doldán, P. Fagúndez, A. Cayota, J. Laíz, J. P. Tosar, *Analytical Chemistry* **2016**, *88*, 10466-10473.
[163] U. Zupančič, P. Jolly, P. Estrela, D. Moschou, D. E. Ingber, *medRxiv* **2020**, 1-39.
[164] M. H. Shamsi, K. Choi, A. H. C. Ng, A. R. Wheeler, *Lab on a Chip* **2014**, *14*, 547-554.
[165] A. González-López, M. C. Blanco-López, M. T. Fernández-Abedul, *ACS Sensors* **2019**, *4*, 2679-2687.
[166] J. S. del Rio, O. Y. F. Henry, P. Jolly, D. E. Ingber, *Nature Nanotechnology* **2019**, *14*, 1143-1149.
[167] M. L. Liu, Y. Y. Zhang, Y. D. Chen, Q. J. Xie, S. Z. Yao, *Journal of Electroanalytical Chemistry* **2008**, *622*, 184-192.
[168] A. Warsinke, A. Benkert, F. W. Scheller, *Fresenius Journal of Analytical Chemistry* **2000**, *366*, 622-634.
[169] S. H. Alarcón, L. Micheli, G. Palleschi, D. Compagnone, *Analytical Letters* **2004**, *37*, 1545-1558.
[170] A. Jodra, M. Hervas, M. A. Lopez, A. Escarpa, *Sensors and Actuators B: Chemical* **2015**, *221*, 777-783.
[171] P. R. Perrotta, F. J. Arevalo, N. R. Vettorazzi, M. A. Non, H. Fernandez, *Sensors and Actuators B: Chemical* **2012**, *162*, 327-333.
[172] M. K. Abdul Kadir, I. E. Tothill, *Toxins* **2010**, *2*, 382-398.
[173] L. Lu, R. Seenivasan, Y.-C. Wang, J.-H. Yu, S. Gunasekaran, *Electrochimica Acta* **2016**, *213*, 89-97.
[174] G. Catanante, A. Rhouati, A. Hayat, J. L. Marty, *Electroanalysis* **2016**, *28*, 1750-1763.
[175] J. Wang, in *Analytical electrochemistry*, Wiley-VCH, Hoboken, N.J., **2006**, pp. 201-238.

[176] E. Katz, I. Willner, *Electroanalysis* **2003**, *15*, 913-947.
[177] R. Chauhan, J. Singh, T. Sachdev, T. Basu, B. D. Malhotra, *Biosensors and Bioelectronics* **2016**, *81*, 532-545.
[178] A.-E. Radi, X. Muñoz-Berbel, V. Lates, J.-L. Marty, *Biosensors and Bioelectronics* **2009**, *24*, 1888-1892.
[179] K. Kunene, M. Weber, M. Sabela, D. Voiry, S. Kanchi, K. Bisetty, M. Bechelany, *Sensors and Actuators B: Chemical* **2020**, *305*.
[180] R. A. Shelby, V. C. Kelley, *Journal of Agricultural and Food Chemistry* **1990**, *38*, 1130-1134.
[181] R. A. Shelby, V. C. Kelley, *Food and Agricultural Immunology* **1991**, *3*, 169-177.
[182] R. A. Shelby, V. C. Kelley, *Journal of Agricultural and Food Chemistry* **1992**, *40*, 1090-1092.
[183] R. A. Shelby, in *Immunoassays for Residue Analysis: Food Safety* (Eds.: R. C. Beier, L. H. Stanker), ACS, **1996**, pp. 231-242.
[184] P. K. Robinson, *Essays in Biochemistry* **2015**, *59*, 1-41.
[185] W. Kühne, *FEBS Letters* **1876**, *62*, 8-12.
[186] H. Neurath, R. Zwilling, in *Semper Apertus Sechshundert Jahre Ruprecht-Karls-Universität Heidelberg 1386–1986* (Eds.: W. Doerr, P. A. Riedl), Springer **1985**, pp. 915-928.
[187] J. B. Sumner, *Journal of Biological Chemistry* **1926**, *69*, 435-441.
[188] U. Sharma, D. Pal, R. Prasad, *Indian Journal of Clinical Biochemistry* **2014**, *29*, 269-278.
[189] S. B. Bankar, M. V. Bule, R. S. Singhal, L. Ananthanarayan, *Biotechnology Advances* **2009**, *27*, 489-501.
[190] W. Aehle, *Enzymes in Industry: Production and Applications*, Wiley, **2008**.
[191] A. G. McDonald, K. F. Tipton, *The FEBS Journal* **2021**, *n/a*.
[192] L. Michaelis, M. L. Menten, *Biochemische Zeitschrift* **1913**, 333-369.
[193] K. A. Johnson, *FEBS Letters* **2013**, *587*, 2753-2766.
[194] V. Henri, *Lois générales de l'action des diastases*, Paris, **1903**.
[195] A. Cornish-Bowden, J.-P. Mazat, S. Nicolas, *Biochimie* **2014**, *107*, 161-166.
[196] G. Rocchitta, A. Spanu, S. Babudieri, G. Latte, G. Madeddu, G. Galleri, S. Nuvoli, P. Bagella, M. I. Demartis, V. Fiore, R. Manetti, P. A. Serra, *Sensors* **2016**, *16*, 780.
[197] R. Bentley, A. Neuberger, *Biochemical Journal* **1949**, *45*, 584-590.
[198] Q. H. Gibson, B. E. P. Swoboda, V. Massey, *Journal of Biological Chemistry* **1964**, *239*, 3927-3934.
[199] D. Xiong, J. Wen, G. Lu, T. Li, M. Long, *Toxins* **2022**, *14*, 250.
[200] R. Hui, X. Hu, W. Liu, W. Liu, Y. Zheng, Y. Chen, R.-T. Guo, J. Jin, C.-C. Chen, *Acta Crystallographica Section F* **2017**, *73*, 515-519.
[201] D. Dobritzsch, H. Wang, G. Schneider, S. Yu, *Biochemical Journal* **2014**, *462*, 441-452.
[202] X. Li, X. Peng, Q. Wang, H. Zuo, X. Meng, B. Liu, *Food Control* **2017**, *78*, 48-56.
[203] C. P. Garnham, S. G. Butler, P. G. Telmer, F. E. Black, J. B. Renaud, M. W. Sumarah, *Journal of Agricultural and Food Chemistry* **2020**, *68*, 13779-13790.
[204] P. G. Telmer, M. J. Kelman, J. B. Renaud, M. W. Sumarah, C. P. Garnham, *Toxins* **2022**, *14*, 544.
[205] I. Lyagin, E. Efremenko, *Molecules* **2019**, *24*, 2362.
[206] J. Carere, Y. I. Hassan, D. Lepp, T. Zhou, *Microbial Biotechnology* **2018**, *11*, 1106-1111.
[207] S. Höfs, T. Greiner, G. Göbel, A. Talke, F. Lisdat, *Sensors and Actuators B: Chemical* **2021**, *328*, 129020.

[208] T. Minamide, K. Mitsubayashi, H. Saito, *Sensors and Actuators B: Chemical* **2005**, *108*, 639-645.
[209] P. Ugo, P. Marafini, M. Meneghello, in *From Biomolecular Recognition to Nanobiosensing*, De Gruyter, **2021**, pp. 103-162.
[210] T. Schmid, P. Dariz, *Heritage* **2019**, *2*, 1662-1683.
[211] U. K. Laemmli, *Nature* **1970**, *227*, 680-685.
[212] A. Visconti, M. Solfrizzo, A. De Girolamo, *Journal of AOAC International* **2001**, *84*, 1828-1837.
[213] L. Björck, G. Kronvall, *Journal of Immunology* **1984**, *133*, 969-974.
[214] A. Frey, B. Meckelein, D. Externest, M. A. Schmidt, *Journal of Immunological Methods* **2000**, *233*, 47-56.
[215] W. J. Yang, H. Y. Zhang, M. X. Li, Z. H. Wang, J. Zhou, S. H. Wang, G. D. Lu, F. F. Fu, *Analytica Chimica Acta* **2014**, *850*, 85-91.
[216] C. Singh, S. Höfs, Z. Konthur, V.-D. Hodoroaba, J. Radnik, J. A. Schenk, R. J. Schneider, *ACS Applied Engineering Materials* **2023**, *1*, 495-507.
[217] A. H. Heussner, L. E. Bingle, *Toxins* **2015**, *7*, 4253-4282.
[218] J. Yamada, H. Matsuda, *Journal of Electroanalytical Chemistry* **1973**, *44*, 189-198.
[219] J. M. Schnitzius, N. S. Hill, C. S. Thompson, A. M. Craig, *Journal of Veterinary Diagnostic Investigation* **2001**, *13*, 230-237.
[220] M. Gross, V. Curtui, E. Usleber, *Journal of AOAC International* **2018**, *101*, 618-626.
[221] N. S. Hill, C. S. Agee, *Crop Science* **1994**, *34*, 530-534.
[222] R. Ekins, *The Ligand quarterly* **1981**, *4*, 33-44.
[223] A. A. Karyakin, O. V. Gitelmacher, E. E. Karyakina, *Analytical Chemistry* **1995**, *67*, 2419-2423.
[224] A. A. Karyakin, E. E. Karyakina, L. Gorton, *Analytical Chemistry* **2000**, *72*, 1720-1723.
[225] A. A. Karyakin, *Electroanalysis* **2001**, *13*, 813-819.
[226] F. Ricci, G. Palleschi, *Biosensors and Bioelectronics* **2005**, *21*, 389-407.
[227] V. D. Neff, *Journal of The Electrochemical Society* **1978**, *125*, 886.
[228] A. A. Karyakin, O. V. Gitelmacher, E. E. Karyakina, *Analytical Letters* **1994**, *27*, 2861-2869.

Appendix

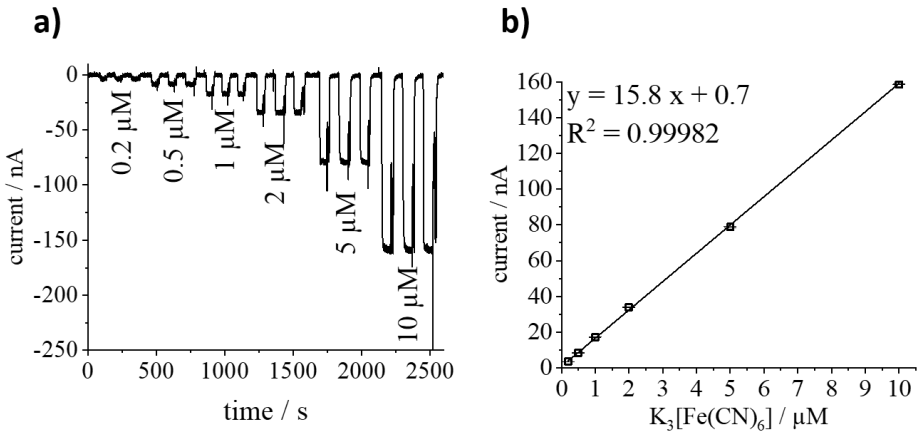

Figure A 1 "Testing of the custom-made flow cell by amperometric measurements with different concentrations of $K_3[Fe(CN)_6]$ in 100 mM potassium phosphate buffer with 100 mM KCl, pH 7 at 0 V vs. Ag/AgCl and a flow rate of 600 µL min^{-1}. **a)** Amperometric measurement with $K_3[Fe(CN)_6]$ samples with each concentration measured three times. **b)** Redox current signal obtained from a) vs. concentration of $K_3[Fe(CN)_6]$." (Figure and caption reproduced from Höfs et al.[51]).

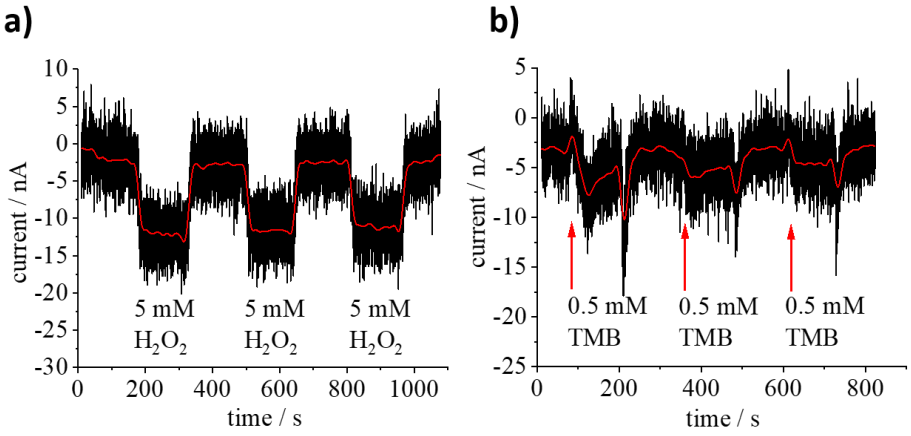

Figure A 2 "Amperometric measurements with **a)** 5 mM H_2O_2 and **b)** 0.5 mM TMB in 150 mM sodium citrate buffer with 300 mM H_2SO_4, 100 mM KCl at pH 1 with screen-printed gold electrodes at 300 mV vs. Ag/AgCl and a flow rate of 600 µL min^{-1}. Each sample was injected three times to study the influence of H_2O_2 and TMB in amperometric measurements. The black line shows the original signal, and the red line shows the smoothed signal (100 point fast Fourier transformed)." (Figure and caption reproduced from Höfs et al.[51]).

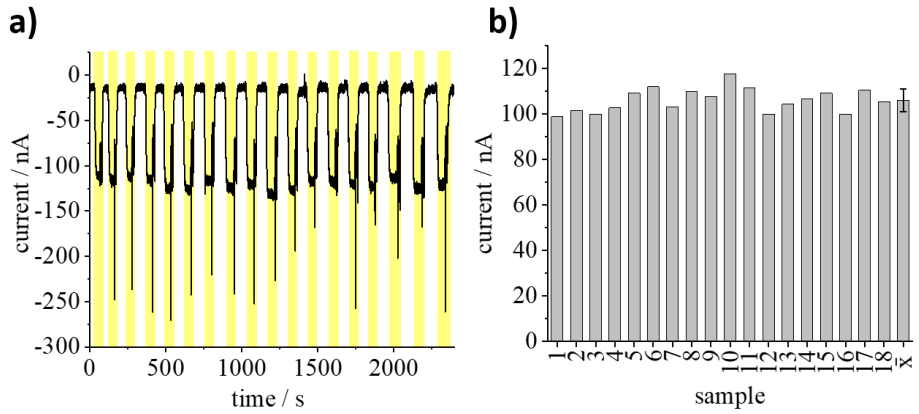

Figure A 3 "Repeatability of the current signal in amperometric measurements obtained for TMB in 150 mM sodium citrate buffer with 300 mM H_2SO_4, 100 mM KCl with pH 1 and screen-printed gold electrodes at 300 mV vs. Ag/AgCl and a flow rate of 600 µL min^{-1}. **a)** Amperometric measurements in which fully oxidized TMB with a concentration of 6.5 µM was injected 18 times alternately with buffer and **b)** depicts the signal intensity and its mean value of the 18 measurements." (Figure and caption reproduced from Höfs et al.[51]).

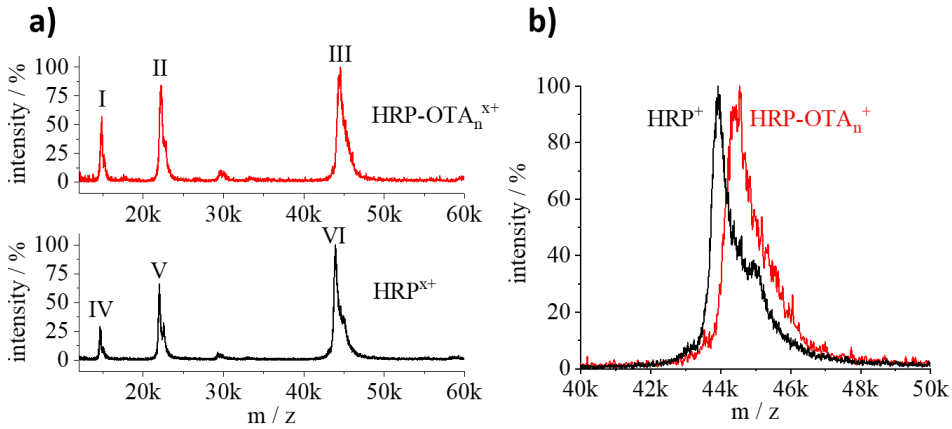

Figure A 4 "MALDI-ToF-MS data of the OTA-HRP Tracer and HRP as reference. **a)** shows both spectra in comparison and **b)** shows part of the spectra depicted in a), which was used for the determination of the mass. For HRP a mass of 44,007 ± 42 Da (n = 6) and for OTA-HRP a mass of 44,448 ± 15 Da (n = 2) was obtained." (Figure and caption reproduced from Höfs et al.[51]).[j]

[j] MALDI-ToF-MS was conducted by Sabine Flemig, BAM.

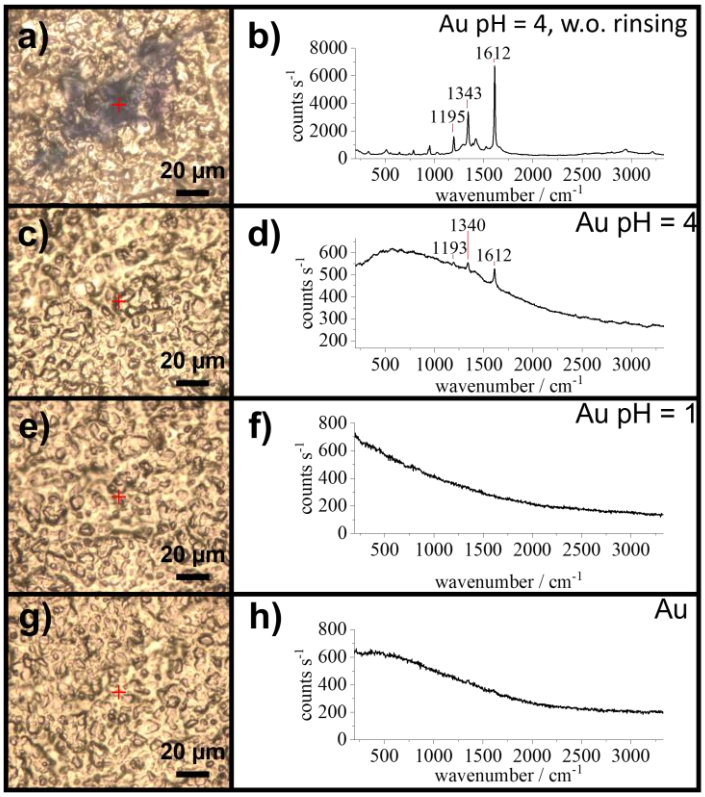

Figure A 5 "Light microscopic images and corresponding Raman spectra of screen-printed gold electrodes. **a)** and **b)** were obtained after cyclic voltammetry in 500 µM TMB at pH 4 in 220 mM sodium citrate buffer with 100 mM KCl was performed without removing visible TMB precipitates by ultrapure water. a) shows a blue TMB precipitate on the gold surface of the working electrode. **c)** and **d)** were obtained after cyclic voltammetry in 500 µM TMB at pH 4 in 220 mM sodium citrate buffer was performed and subsequent rinsing of the electrode with ultrapure water. **e)** and **f)** show the results after cyclic voltammetry in 500 µM TMB at pH 1 in 150 mM sodium citrate buffer with 300 mM H_2SO_4 and 100 mM KCl was performed and subsequent rinsing of the electrode with ultrapure water. **g)** and **h)** were obtained from the bare gold electrode surface as reference. All spectra were measured at the red marked spots in the light micrographs with 532 nm excitation wavelength, a laser power of 4 mW (full power attenuated to 10% while using a neutral density filter) and a laser spot diameter of approximately 1 µm. As different acquisition times were applied (b, f, and h: two averaged acquisitions of 5 s each; d: 4 acquisitions of 30 s each) to avoid saturation of the detector and to ensure detection of the small amounts of TMB after rinsing, the intensity axes are expressed in counts per seconds to enable best comparability." (Figure and caption reproduced from Höfs et al.[51]).[k]

[k] Raman microspectroscopy was conducted by Dr. Thomas Schmid, BAM.

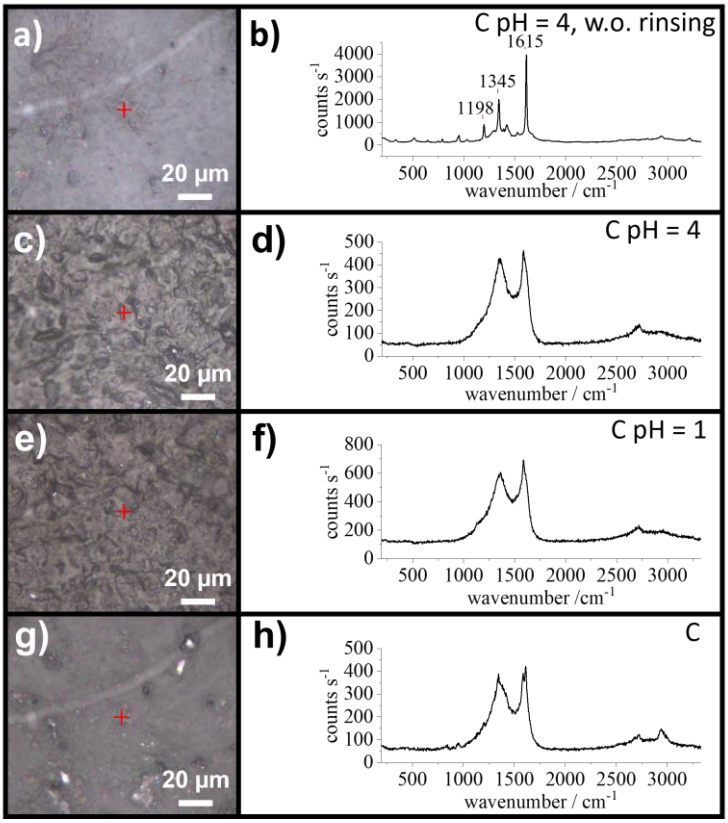

Figure A 6 "Light microscopic images and corresponding Raman spectra of screen-printed carbon electrodes. **a)** and **b)** were obtained after cyclic voltammetry in 500 µM TMB at pH 4 in 220 mM sodium citrate buffer with 100 mM KCl was performed without removing visible TMB precipitates by ultrapure water. **c)** and **d)** were obtained after cyclic voltammetry in 500 µM TMB at pH 4 in 220 mM sodium citrate buffer was performed and subsequent rinsing of the electrode with ultrapure water. **e)** and **f)** show the results after cyclic voltammetry in 500 µM TMB at pH 1 in 150 mM sodium citrate buffer with 300 mM H_2SO_4 and 100 mM KCl was performed and subsequent rinsing of the electrode with ultrapure water. **g)** and **h)** were obtained from the bare carbon electrode surface as reference. All spectra were measured at the red marked spots in the light micrographs with 532 nm excitation wavelength, a laser power of 4 mW (full power attenuated to 10% while using a neutral density filter) and a laser spot diameter of approximately 1 µm." (Figure and caption reproduced from Höfs et al.[51]).[1]

[1] Raman microspectroscopy was conducted by Dr. Thomas Schmid, BAM.

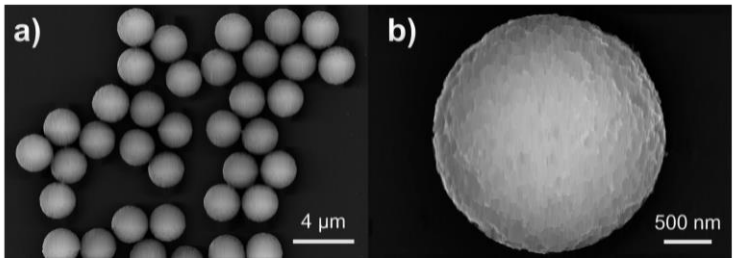

Figure A 7 "SEM images of protein G modified beads used for the immunomagnetic assay **a)** at low magnification and **b)** at high magnification. For both images an acceleration voltage of 20 kV was applied." (Figure and caption reproduced from Höfs et al.[51]).[m]

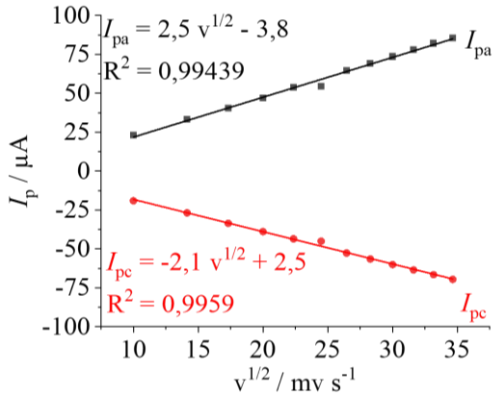

Figure A 8 "Peak currents vs. square root of the scan rate obtained from cyclic voltammetry with TMB depicted in Figure 14 a. Experiments were performed in 500 µM TMB at pH 1 in 150 mM sodium citrate buffer with 300 mM H_2SO_4 at a screen-printed gold electrode with scan rates ranging from 0.1 – 1.2 V s^{-1}." (Figure and caption reproduced from Höfs et al.[51]).

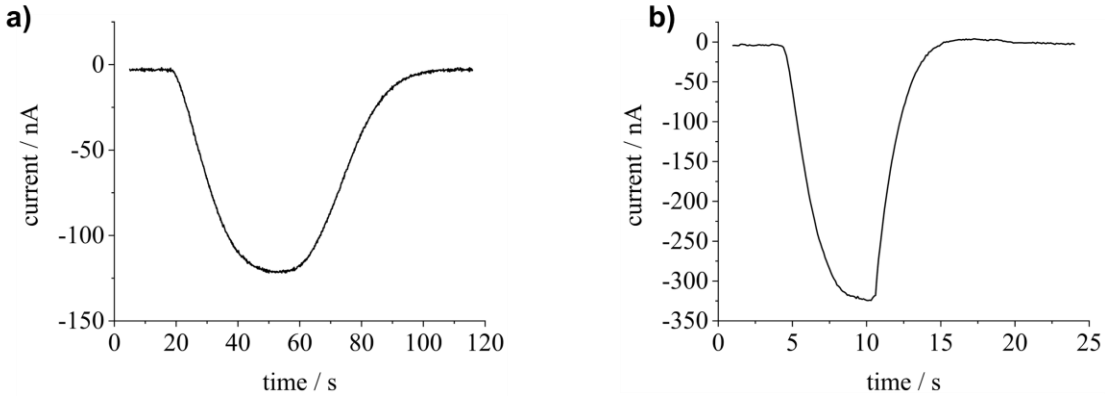

Figure A 9 "Amperometric current signals obtained with the flow injection system and screen-printed gold electrodes at 0 V vs. Ag/AgCl for the injection of 300 µL 10 µM potassium ferricyanide in 100 mM potassium phosphate buffer with 100 mM KCl (pH 7) and a flow rate of **a)** 0.5 mL min^{-1} and **b)** 4 mL min^{-1}." (Figure and caption reproduced from Höfs et al. [56]).

[m] SEM was conducted by Sigrid Benemann and Deniz Hülagü, BAM.

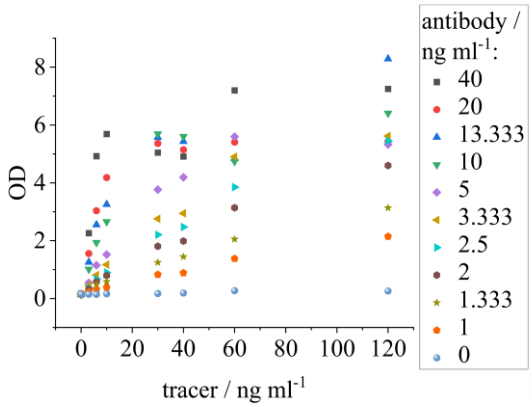

Figure A 10 "OD-Signals obtained with different tracer and antibody concentrations in the plate-based ELISA (without the addition of ergometrine) for the optimization of the assay." (Figure and caption reproduced from Höfs et al. [56]).

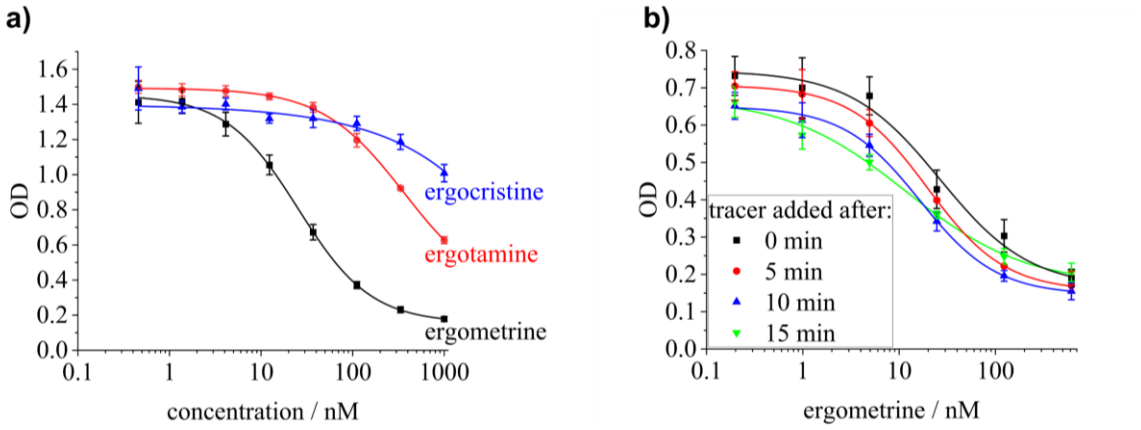

Figure A 11 "**a)** ELISA calibration curves for ergometrine, ergotamine or ergocristine. Obtained cross-reactivities were 100% for ergometrine ($C_{ergometrine}$ = 25.5 ± 0.8 nM (8.3 ± 0.3 µg L^{-1})), 7% for ergotamine and <0.1% for ergocristine; **b)** Ergometrine ELISA calibration curves with different tracer incubation times. The ergometrine standards were incubated in total for 30 min with the antibody-coated microplate and the tracer was added immediately after the standards or after 5 min, 10 min or 15 min of pre-incubation with standard. The obtained C-values were $C_{0\ min}$ = 26 ± 9 nM (9 ± 3 µg L^{-1}), $C_{5\ min}$ = 19.8 ± 0.1 nM (6.43 ± 0.05 µg L^{-1}), $C_{10\ min}$ = 16 ± 1 nM (5.3 ± 0.3 µg L^{-1}), and $C_{15\ min}$ = 12 ± 3 nM (3.8 ± 0.8 µg L^{-1})." (Figure and caption reproduced from Höfs et al. [56]).

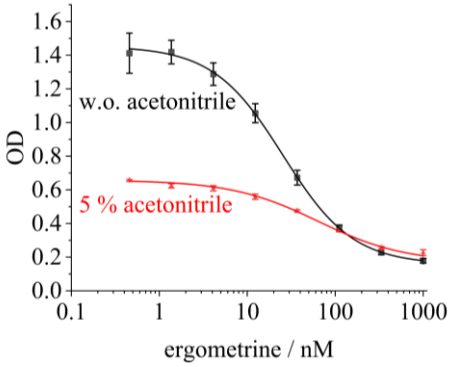

Figure A 12 " ELISA calibration curves for ergometrine in absence and in the presence of 5% acetonitrile, $C_{w.o.\ acetonitrile}$ = 26 ± 9 nM (9 ± 3 µg L^{-1}), $C_{5\%\ acetonitrile}$ = 63 ± 9 nM (21 ± 3 µg L^{-1})." (Figure and caption reproduced from Höfs et al. [56]).

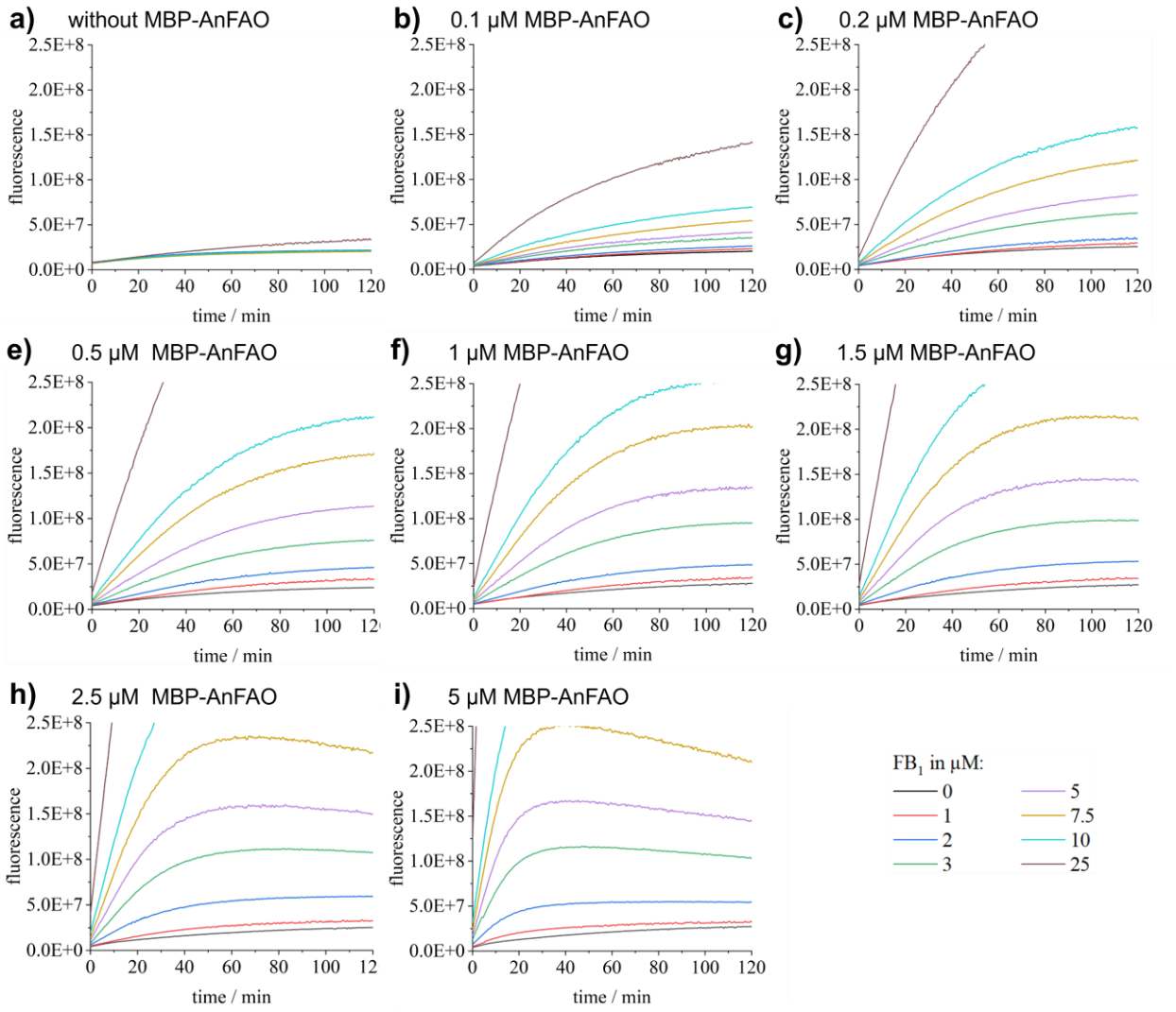

Figure A 13 - Results of the Amplex Red H_2O_2/HRP fluorescence assay at different MBP-AnFAO and FB_1 concentrations. Fluorescence detection was performed at 560 nm excitation and 590 nm emission and the assay was performed at 37°C.

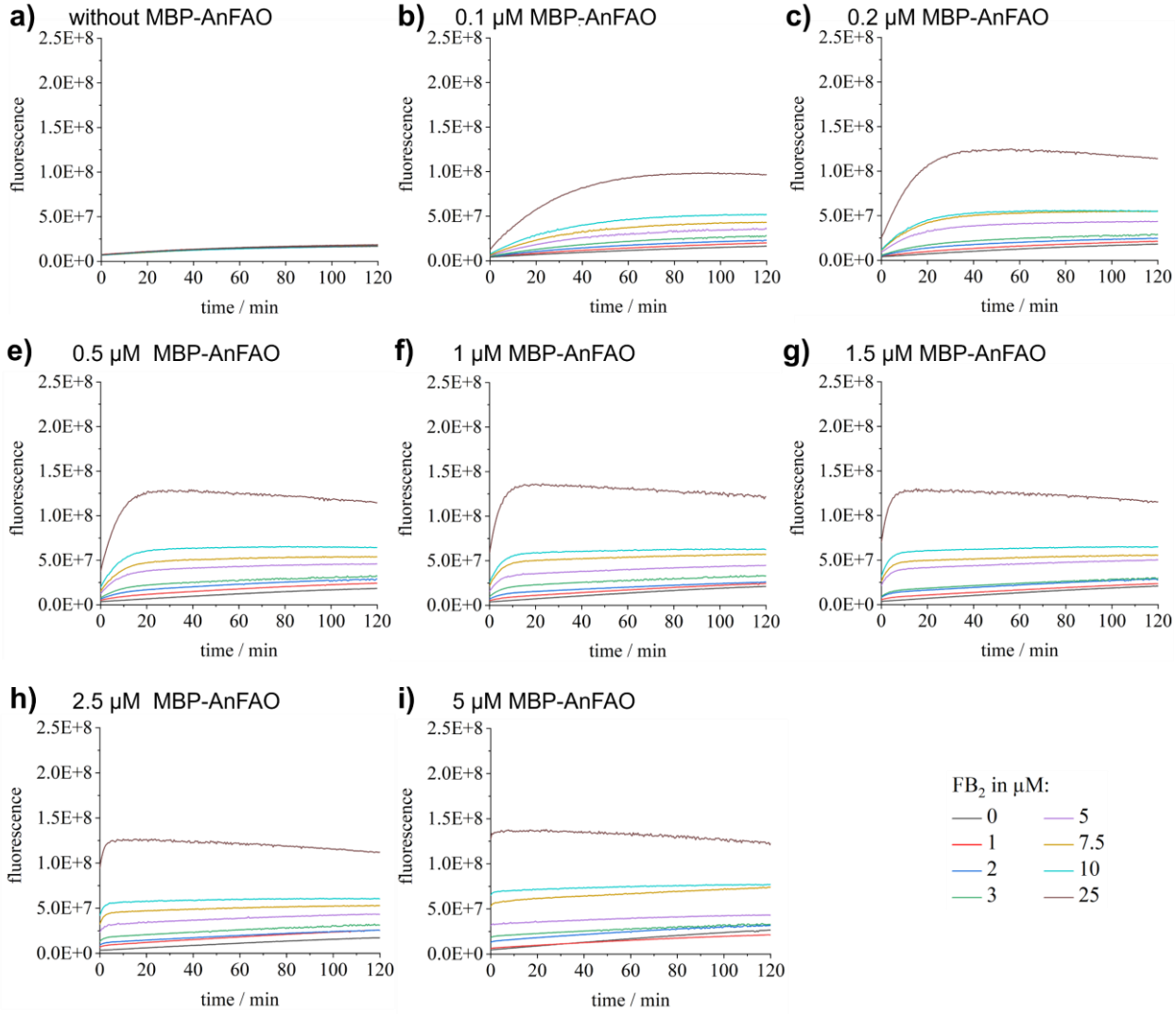

Figure A 14 - Results of the Amplex Red H_2O_2/HRP fluorescence assay at different MBP-AnFAO and FB_2 concentrations. Fluorescence detection was performed at 560 nm excitation and 590 nm emission and the assay was performed at 37°C.

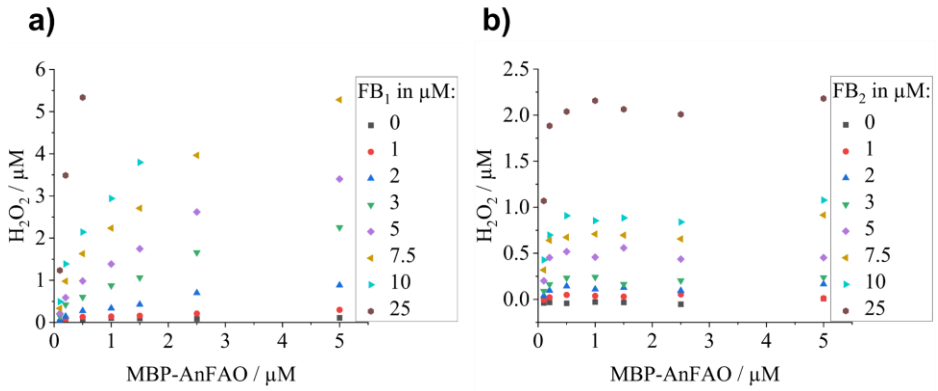

Figure A 15 - Enzymatically produced H_2O_2 at different MBP-AnFAO concentrations and **a)** with different FB_1 or **b)** with different FB_2 concentrations. The assay was performed at 37°C.

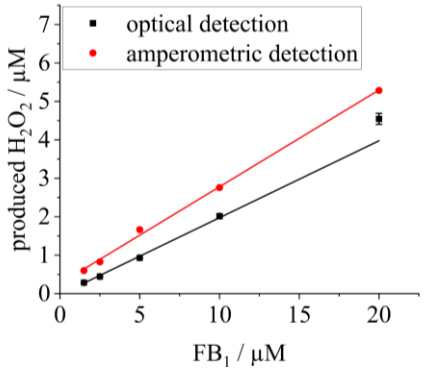

Figure A 16 - Enzymatically produced H_2O_2 at different FB_1 concentrations determined with optical (Amplex Red H_2O_2/HRP fluorescence assay) and amperometric detection.

Wissenschaftliche Leistungen

Publikationen (peer-reviewed)

Höfs, S.; Jaut, V.; Schneider, R. J., Ergometrine sensing in rye flour by a magnetic bead-based immunoassay followed by flow injection analysis with amperometric detection. *Talanta* **2023,** *254*, 124172.

Singh, C.; **Höfs, S.**; Konthur, Z.; Hodoroaba, V.-D.; Radnik, J.; Schenk, J. A.; Schneider, R. J., Functionalized Ti3C2Tx nanosheets based biosensor for point-of-care detection of SARS-CoV-2 antigen. *ACS Applied Engineering Materials* **2023,** *1* (1), 495-507.

Höfs, S.; Hülagü, D.; Bennet, F.; Carl, P.; Flemig, S.; Schmid, T.; Schenk, J. A.; Hodoroaba, V. D.; Schneider, R. J., Electrochemical immunomagnetic ochratoxin A sensing: Steps forward in the application of 3,3',5,5'-tetramethylbenzidine in amperometric assays. *ChemElectroChem* **2021**, 8 (13), 2597-2606.

Höfs, S.; Greiner, T.; Göbel, G.; Talke, A.; Lisdat, F., Activity determination of human monoamine oxidase B (Mao B) by selective capturing and amperometric hydrogen peroxide detection. *Sensors and Actuators B: Chemical* **2021,** *328*, 129020.

Riedel, M.; **Höfs, S.**; Ruff, A.; Schuhmann, W.; Lisdat, F., A tandem solar biofuel cell: harnessing energy from light and biofuels. *Angewandte Chemie International Edition* **2021,** *60* (4), 2078-2083.

Publikationen (in preparation)

Höfs, S.; Bayram, R.; Döring, S.; Schneider, R. J.; Konthur, Z., Fumonisin sensing by Aspergillus niger fumonisin amine oxidase (AnFAO) and amperometric hydrogen peroxide detection

Vorträge

Höfs, S.; Hülagü, D.; Bennet, F.; Carl, P.; Flemig, S.; Schmid, T.; Schenk, J. A.; Hodoroaba, V. D.; Schneider, R. J.; Application of 3,3',5,5'-tetramethylbenzidine (TMB) in amperometric immunoassays for mycotoxin detection, 73rd Annual Meeting of the ISE 2022.

Höfs, S., How to trace a *cereal* killer?, Bionnale, online, 2021.

Höfs, S.; Hülagü, D.; Bennet, F.; Carl, P.; Flemig, S.; Schmid, T.; Schenk, J. A.; Hodoroaba, V. D.; Schneider, R. J.; Immunomagnetic ochratoxin A assay with electrochemical 3,3',5,5' tetramethylbenzidine detection, 23rd JCF-Frühjahrssymposium (GDCh), online, 2021.

Höfs, S.; Greiner, T.; Göbel, G.; Talke, A.; Lisdat, F., Enzyme activity determination of human monoamine oxidase B (Mao B) by amperometric hydrogen peroxide detection, European Biosensor Symposium, online, 2021.

Höfs, S.; Schneider, R. J.; An ELISA-inspired electrochemical detection system for the quantification of ochratoxin A, Interdisziplinäres Doktorandenseminar des AK Prozessanalytik (GDCh), online, 2020.

Posterbeiträge

Höfs, S.; Bayram, R.; Döring, S.; Schneider, R. J.; Konthur, Z., Tracing toxic fumonisins - Fumonisin sensing by *Aspergillus niger* Fumonisin Amine Oxidase (AnFAO) and amperometric hydrogen peroxide detection, Posterschau des Adlershofer Forschungsforums, Berlin, 2022.

Höfs, S.; Hülagü, D.; Bennet, F.; Carl, P.; Flemig, S.; Schmid, T.; Schenk, J. A.; Hodoroaba, V. D.; Schneider, R. J.; Steps forward in the application of 3,3',5,5'- tetramethylbenzidine (TMB) in amperometric assays, Electrochemistry, Berlin, 2022.

Höfs, S.; Hülagü, D.; Bennet, F.; Carl, P.; Flemig, S.; Schmid, T.; Schenk, J. A.; Hodoroaba, V. D.; Schneider, R. J.; Smartphone-based amperometric detection of 3,3',5,5'-tetramethylbenzidine (TMB) – An immunomagnetic Ochratoxin A assay, European Biosensor Symposium, online, 2021.

Höfs, S.; Schneider, R. J.; Ochratoxin A detection by an immunomagnetic assay and smartphone-based amperometry, Rapid Methods Europe, online, 2021.

Höfs, S.; Carl. C., Schneider, R. J.; Immunomagnetic ochratoxin A assay with smartphone-based amperometric detection, SALSA Make and Measure, online, 2020.

Eidesstattliche Erklärung

Hiermit versichere ich, dass ich die vorliegende Arbeit ohne Hilfe Dritter und ohne Zuhilfenahme anderer als der angegebenen Quellen und Hilfsmittel angefertigt habe. Die den benutzten Quellen wörtlich oder inhaltlich entnommenen Stellen sind als solche kenntlich gemacht. Die Dissertation ist bisher keiner anderen Prüfungsbehörde vorgelegt worden.

_____

Ort, Datum, Unterschrift